

SOIL-PILE INTERACTION IN SOFT SOILS



Jakub Gabriel Kania

ISBN: 978-87-7507-481-5
DOI: 10.7146/aui.380

SOIL-PILE INTERACTION IN SOFT SOILS

PhD Dissertation

Jakub Gabriel Kania

March 2020

cp test a/s



AARHUS
UNIVERSITY
DEPARTMENT OF ENGINEERING

Dissertation submitted: March, 2020

PhD supervisors: Professor (Docent) Dr. Kenny Kataoka Sørensen
Department of Engineering, Aarhus University

Managing Director Per Grud
cp test a/s, Vejle, Denmark

PhD co-supervisor: Operations Manager Rune Tranborg Tuxen
cp test a/s, Vejle, Denmark

3rd party PhD supervisors: Senior Geotechnical Design Engineer
Anders Tovsig Andersen
Per Aarsleff A/S, Viby J, Denmark

Managing Director Lars Gøttrup Christensen
Centrum Pæle A/S, Vejle, Denmark

PhD Series: Faculty of Technical Sciences, Aarhus University

Department: Department of Engineering

Dla mojej żony Joanny, córki Zofii
oraz Rodziców
za cierpliwość i wyrozumiałość

ACKNOWLEDGEMENTS

This study has been financially supported by cp test a/s, DMT Gründungstechnik GmbH, Per Aarsleff A/S and a grant from the Innovation Fund Denmark.

I would like to thank my supervisors: Professor (Docent) Dr. Kenny Kataoka Sørensen, Managing Director Per Grud, Operations Manager Rune Tranborg Tuxen, Senior Geotechnical Design Engineer Anders Tovsig Andersen and Managing Director Lars Gøttrup Christensen for their support, valuable technical discussions and guidance during the project. Also, to Head of Design and Engineering at Per Aarsleff A/S Søren Viborg Kristensen for his support and contribution to the project.

I would like to thank Professor Martin Kristensen and Associate Professor Martijn Heck for providing expert knowledge on fibre optics in general at the beginning of the project.

The help, support and goodwill of Per Aarsleff A/S, Centrum Pæle A/S, Randers Havn, and Danish Stevedore A/S is gratefully acknowledged.

I would like to express great appreciation for the advice and invaluable critique given by Dr. Tech., P. Eng. Bengt H. Fellenius throughout the final period of this project.

I would like to thank my colleagues at cp test a/s, Centrum Pæle A/S, Per Aarsleff A/S and my fellow PhD-students at Aarhus University, Jannie, Thomas, and Michael, for fruitful discussions and a stimulating working environment.

PREFACE

In the past, as a graduate geotechnical engineer, I was mainly responsible for pile testing. During the collaboration with my colleague PhD Andrzej Słabek from Professor Kazimierz Gwizdała's research group, I have noticed that conventional pile head-down static loading tests provide very limited information. Therefore, I have started investigating the state-of-the-art in the instrumentation of piles. I have found fibre optic systems as a very promising tool to facilitate my objective. In the first trials, conducted with my colleague PhD Arkadiusz Grzywa, we used Fiber Bragg Grating (FBG) sensors and they were partly successful. One trial, completely unsuccessful at that time, employed distributed fibre optic sensing (DFOS) technology. However, it was the DFOS technology which brought to my attention.

Among many e-mails I have sent to the universities and companies around Europe, Dr. Kenny Kataoka Sørensen replied and organized a meeting with Per Grud. This research project started from the meeting on a Saturday at the Burger King restaurant in Aabenraa.

I am grateful to the persons mentioned above.

ABSTRACT

When piles are installed through soft, subsiding soils, a drag force is developed in the piles. The consolidation induced by e.g. lowering of the groundwater table or placing the fill around the piles causes settlements and thus a relative movement between the pile and the soil. As a consequence, negative skin friction develops in the upper part of the pile, which is resisted by positive shaft resistance in the lower part of the pile and the toe resistance. This phenomenon should be considered in the design of pile foundations.

Previous studies on the development of negative skin friction have mainly been performed on driven piles installed in marine clay. Driven piles installed in gyttja, a typical of Denmark, have received little attention. Consequently, there is still insufficient documentation for the effect of bitumen coating in reducing the shear force between the pile and the soil in such ground conditions. Additionally, all the test piles in the reported studies were instrumented with spot sensors giving information only at discrete points. Therefore, the full distribution of strain along the piles was not possible to obtain.

The present thesis investigates the soil-pile interaction in soft, subsiding soils using a distributed fibre optic sensing system, which provided a high spatial resolution. The development of and the controlling factors behind negative skin friction along uncoated and bitumen coated piles were of special focus. These objectives were obtained through a program of full-scale field tests, supplemented by laboratory soil-pile interface shear tests.

This PhD study has shown that the development and magnitude of negative skin friction was a function of effective stress and settlement. The soil-pile interface type had an impact on the magnitude of the shear stress in both full-scale and laboratory tests. The bitumen coating significantly reduced negative skin friction and its efficiency is related to the shearing rate. Finally, driven piles can be successfully instrumented with distributed fibre optic sensors providing continuous distribution of strain along piles.

RESUMÉ

Når pæle nedsættes i bløde, indsynkende jordlag, vil en trækraft udvikle sig i pælen. Konsolidering, fremkaldt ved f.eks. sænkningen af grundvandsspejlet eller anvendelsen af sedimentfyld omkring pælene, medfører sætning og hermed en relativ bevægelse mellem pælen og jorden. Som en konsekvens deraf vil en negativ overflademodstand udvikle sig i den øverste del af pælen, hvilket modvirker den positive overfaldemodstand fra den nederste del af pælen samt spidsmodstanden. Denne mekanisme bør medregnes i designet af pælefundamenter.

Tidligere studier omkring udviklingen af negativ overfaldemodstand er hovedsageligt foretaget med rammede pæle nedsat i marint ler. Der har været mindre fokus på rammede pæle nedsat i gytje; en karakteristisk lithologi i Danmark. Som følge deraf, er der stadig begrænset dokumentation for effekten af bitumenbelægning ift. at reducere forskydningsstyrken mellem pælen og jorden under sådanne jordforhold. Derudover er alle pælene i det rapporterede studie udstyret med sensorer, som giver information fra enkelte punkter langs pælen. Det giver derfor ikke det samlede billede af hele belastningen langs pælen.

Nærværende studie undersøger sammenspillet mellem jorden og pælen i bløde, indsynkende jordlag ved anvendelse af et system af fiberoptiske sensorer, hvorved en høj spatial opløselighed opnås. Udviklingen af, og de kontrollerede bagvedliggende faktorer for, en negativ overflademodstand langs pæle hhv. med og uden bitumenbelægning anses som studiets hovedfokus. Denne målsætning blev opnået gennem gennemgående feltarbejde, suppleret med laboratorieforsøg, hvor grænsefladen mellem jorden og pælen testes mht. forskydningsstyrke.

Dette ph.d.-studie har demonstreret, at udviklingen og omfanget af den negative overflademodstand er en funktion af det effektive stress og indsynkningen. Typen af interaktion mellem pælen og jorden viste sig at have indflydelse på graden af forskydningsstyrke; både i felten og ved laboratorieforsøg. Bitumenbelægningen viste sig ligeledes at reducere den negative overfaldemodstand betydeligt, og effektiviteten er relateret til forskydningsraten. Endeligt kan rammede pæle udstyres med et system af fiberoptiske sensorer og med succes opnå kontinuerlig fordeling af belastningen langs pælen.

LIST OF PUBLICATIONS

- Journal Paper 1 Kania, J.G., Sørensen, K.K., and Fellenius, B.H., 2020. Application of distributed fibre optic cables in piles. *Geotechnical Engineering Journal of the SEAGS and AGSSEA*, March 51(1) 94-102.
- Journal Paper 2 Kania, J.G., Sørensen, K.K., and Fellenius, B.H. Analysis of a static loading test on an instrumented cased CFA pile in silt and sand. *ISSMGE International Journal of Geoenvironment Case Histories*. Submitted on December 2019. Revised and resubmitted on March 2020.
- Journal Paper 3 Kania, J.G., Sørensen, K.K., and Fellenius, B.H. The development of unit shaft resistance along driven piles in a subsiding soil. Planned for a journal submission.
- Conference Paper 1 Kania, J.G. and Sørensen, K.K., 2018. A static pile load test on a bored pile instrumented with distributed fibre optic sensors. 10th International Symposium on Field Measurements in Geomechanics, Rio de Janeiro, Brazil, July 17-20, 9 p.
- Conference Paper 2 Kania, J.G. and Sørensen, K.K., 2019. A case study of soil-pile interaction in soft soils. XVII European Conference on Soil Mechanics and Geotechnical Engineering, Reykjavik, Iceland, September 1-6, 8 p.
- Conference Paper 3 Kania, J.G., Sørensen, K.K., and Fellenius, B.H., 2020. Driven piles installed in soft soils subjected to vertical and lateral soil movements. The 73rd Canadian Geotechnical Conference, Calgary, Canada, September 13 - 16. Planned for the conference submission (manuscript has been prepared).
- Conference Paper 4 Kania, J.G., Sørensen, K.K., and Fellenius, B.H., 2020. Shear stress between a soft soil and various pile materials. The 73rd Canadian Geotechnical Conference, Calgary, Canada, September 13-16. Planned for the conference submission (manuscript has been prepared).
-

TABLE OF CONTENTS

ACKNOWLEDGEMENTS	vii
PREFACE	ix
ABSTRACT	xi
RESUMÉ	xiii
LIST OF PUBLICATIONS	xv
TABLE OF CONTENTS	xvii
Chapter 1. Introduction	1
1.1. Objectives	4
1.2. Outline of the thesis	5
Chapter 2. Application of distributed fibre optic sensors in piles	7
2.1. Introduction	7
2.2. Assessment of the applied methodologies	8
2.3. Summary of the results	9
2.4. Critical review	9
2.5. PhD student's contribution	10
2.6. Conference Paper 1	11
2.7. Journal Paper 1	23
Chapter 3. Soil-pile interaction analysed from a static loading test	35
3.1. Introduction	35
3.2. Assessment of the applied methodologies	35
3.3. Summary of the results	35
3.4. Critical review	36
3.5. PhD student's contribution	36
3.6. Journal Paper 2	37
Chapter 4. Laboratory interface shearing tests	51
4.1. Introduction	51
4.2. Assessment of the applied methodologies	51
4.3. Summary of the results	51
4.4. Critical review	52
4.5. PhD student's contribution	52
4.6. Conference Paper 4	53
Chapter 5. Distribution of strain due to installation of piles and soil movement	67
5.1. Introduction	67
5.2. Assessment of the applied methodologies	67
5.3. Summary of the results	68
5.4. Critical review	68
5.5. PhD student's contribution	69

5.6. Conference Paper 2.....	71
5.7. Conference Paper 3.....	81
Chapter 6. Soil-pile interaction in a subsiding soil.....	99
6.1. Introduction	99
6.2. Assessment of the applied methodologies.....	99
6.3. Summary of the results	100
6.4. Critical review	100
6.5. PhD student's contribution	101
6.6. Journal Paper 3	103
Chapter 7. Conclusions	131
Chapter 8. Further work	133
COMPLETE LIST OF REFERENCES.....	135

CHAPTER 1

INTRODUCTION

The design of piled foundations in soft, subsiding soils is a complex soil-pile interaction problem. As presented in Figure 1, soil settlement will develop negative skin friction along the upper length of a pile and positive shaft resistance along the lower length. At a depth called “neutral plane”, a force equilibrium exists between the sum of the sustained load on the pile plus the force accumulated due to negative skin friction (drag force) and the sum of the positive shaft resistance and the mobilised toe resistance. The neutral plane is also the settlement equilibrium between the pile and the soil, i.e. there is no relative movement. A transition zone develops above and below the neutral plane, at which the unit shaft resistance changes from a negative to a positive direction of shaft resistance. The length of the transition zone depends on the relative movement between the pile and the soil (Fellenius 2020).

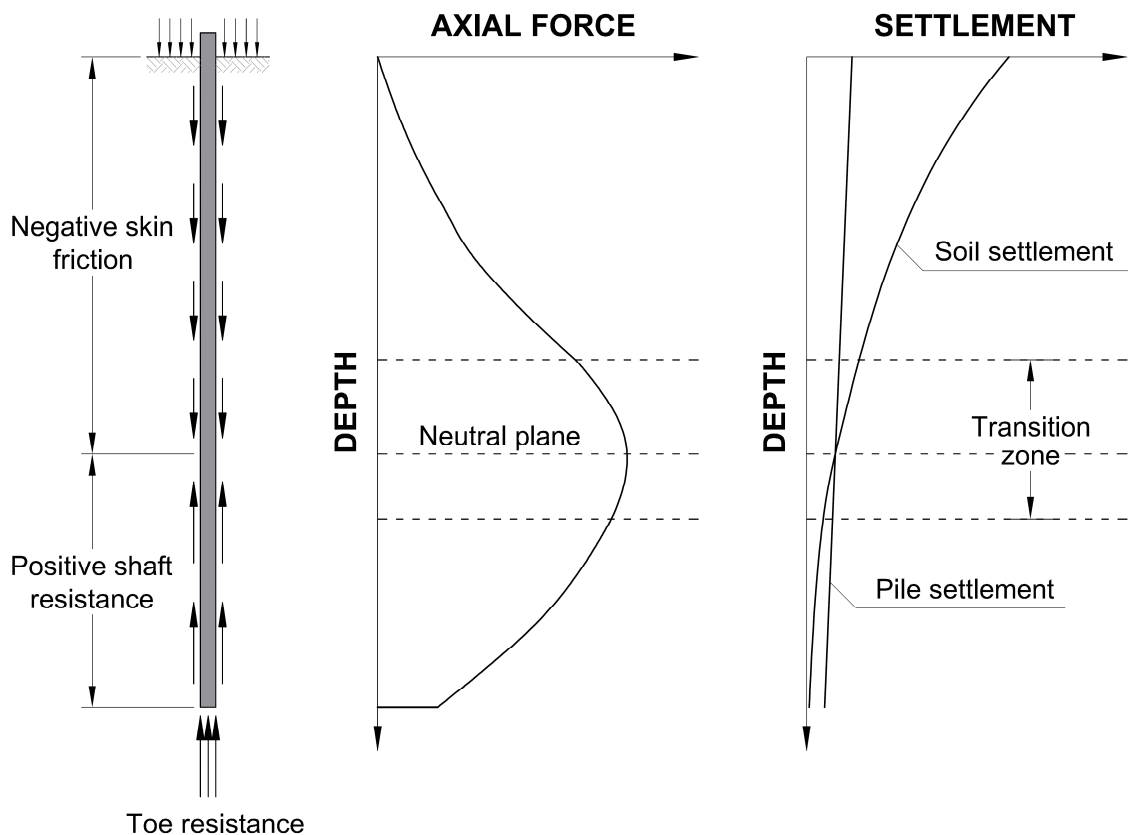


Figure 1. Soil-pile interaction in soft soils (a concept without the sustained load)

The magnitude of negative skin friction can be analysed using either a total or an effective stress method. The total stress method applies an empirical coefficient, α , to the undrained shear strength of the soil, c_u (Tomlinson 1957), and the negative skin friction can be calculated according to the following equation:

$$q_n = \alpha \cdot c_u \quad (1)$$

The effective stress method applies an empirical coefficient, β , to the effective overburden stress (Burland 1973), and the negative skin friction can be calculated using the equation:

$$q_n = \beta \cdot \sigma'_v = K \cdot \tan \delta \cdot \sigma'_v \quad (2)$$

where K is the earth pressure coefficient, and δ is the effective angle of friction between the remoulded clay due to installation and the pile. The author assumed that the failure takes place in the remoulded soil, so the interface angle of friction, δ , can be taken as the remoulded effective angle of friction of the soil, ϕ_d . Additionally, the earth pressure coefficient, K , after driving the pile, can be greater than the earth pressure coefficient at rest, K_0 ; therefore assuming K equal to K_0 will provide lower values of unit shaft resistance.

Both coefficients depend on the soil and the pile type. For soft soils, Tomlinson (1957) proposed the value of α coefficient close to 1.0, and Burland (1973) proposed the value of β coefficient equal to 0.25 (as the upper limit).

According to Terzaghi et al. (1996) the location of the neutral plane can be assumed at the depth of the bearing stratum. For loaded end-bearing piles, Tomlinson (2008) proposed the location of the neutral plane at the depth of 0.9 H from the ground surface, where H is the thickness of fill or compressible soil.

The development and understanding of the controlling mechanism behind negative skin friction on piles has interested many in the past. Johannessen and Bjerrum (1965) reported the results from a full-scale field test setup investigating negative skin friction on 55 m long, 470 mm diameter steel piles driven through a soft marine clay to rock. The placing of a 10 m thick fill caused about 1.2 m consolidation of the clay. The piles, instrumented with telltales, were monitored for 2 years and experienced shortening due to drag force. The authors concluded that negative skin friction is likely to be governed by the effective stress distribution, and that the ultimate beta-coefficient for soft marine clay is about 0.2.

Unfortunately, telltales can provide strain data only after driving. Therefore, the influence of pile installation was not defined. Fellenius (1971, 2006) established a full-scale test setup consisted of two 55 m long, 300 mm diameter, precast concrete, hexagonal cross section piles driven through 40 m of sensitive marine clay into a 15 m thick layer of silty sand. The piles were instrumented with load-cells (Fellenius and Haagen 1969), which provided the effects of the pile installation (Fellenius and Broms 1969). The soil-pile interaction was studied during the reconsolidation of the soil after driving, after adding a load to the pile head and after placing a 2 m high fill. Monitoring of the site has last for

more than 14 years. The beta coefficient obtained in this study for soft marine clay ranged from 0.14 to 0.18.

Endo et al. (1969) investigated negative skin friction on four 43 m long (two inclined) and one 31 m long, strain gauge instrumented, closed and open-ended steel piles installed in silty sand and silt. In order to minimize the group effect, the spacing between the test piles was about 10 m. Negative skin friction developed due to pumping of water from the sand below 43 m depth. The test site was monitored for more than 2 years. During the observations, the location of the neutral plane moved upwards with time and fell within a range from 0.73 to 0.78 of the pile embedment in the compressible soil. The authors reported that the values of the alfa and beta coefficient were 0.5 and 0.2-0.35, respectively. The study concluded that the development of negative skin friction was not related to the decreasing rate of relative movement between the soil and the pile.

Walker and Darvall (1973) presented results from full-scale field tests performed on two 760 mm steel piles installed through silty sand deposited on stiff silty clay followed by sandy silt on top of dense sand and gravel. One of the piles was bitumen coated. Soil settlement was induced by placing a 3 m high fill. The test piles were instrumented with strain gauges. The placement of the fill caused an initial increase in pore water pressure by about 25 kPa and the remain stable during the monitoring period of about 230 days. It was concluded that the development of negative skin friction is a function of ground settlement.

Bozozuk (1972) documented negative skin friction on a 39 m long, 300 mm diameter, telltale instrumented steel pile installed through marine clay. The development of negative skin friction caused by the placement of a 9 m high fill was monitored during 5 years. The author concluded, that the unit shaft resistance is comparable with the remoulded strength when large relative movement (between a pile and a soil), and excess pore water pressure occur. In contrast, the unit shaft resistance approaches the drained strength, if the relative movement is small and excess pore water pressure has dissipated. The author carried out a static loading test on the same pile 10 years later (Bozozuk 1981) and demonstrated the change from the negative to a positive direction of shear in the upper part of the pile. The author concluded, that a pile subjected to negative skin friction can carry a transient load up to twice the magnitude of the long-term drag force.

Indraratna et al (1992) compared the results of negative skin friction from long-term measurements and short-term pullout tests (quick maintained loading test) on precast concrete driven piles installed in soft clay. One of the test piles was bitumen coated. The piles were instrumented with load cells and telltales. The long-term behaviour of the test piles was investigated for a period of 9 months by adding a 2 m high fill. The authors have found that both alfa and beta coefficients obtained from short- and long-term measurements are in general agreement. The authors concluded that negative skin friction is a function of relative displacement between the pile and the soil.

The magnitude of negative skin friction can be reduced by e.g. electroosmosis or coating the pile with bitumen. Bozozuk and Labrecque (1969) reported the use of electroosmosis

on an 82 m long steel pile filled with concrete installed in marine clay to temporarily neutralize the shaft resistance. Unfortunately, the authors could not determine the effectiveness of the method, because the pore water pressure gauges were damaged prior to the experiment. However, negative skin friction has started to build up immediately after the application of electroosmosis. In contrast, the bitumen coating is considered the most suitable method for reducing negative skin friction. Several laboratory tests (Fellenius 1970, Baligh 1978, Khare and Gandhi 2009) and full-scale field tests (Bjerrum et al. 1969, Walker and Darvall 1973, Clemente 1981, Indraratna et al. 1992) have been carried out to investigate the effect of bitumen on the development of shear stress. In the reported full-scale tests, the bitumen coating reduced negative skin friction from 30 to more than 90 % (comparing to the unit shaft resistance on the similar uncoated pile). The lower values were obtained during short-term pullout tests conducted at different time (and ground temperature) of a year (Hutchinson and Jensen 1968). The findings from full-scale tests were in agreement with laboratory tests, that the effectiveness of bitumen coating mainly depends on shearing rate, temperature and thickness of the bitumen coating layer.

The distributed fibre optic sensing (DFOS) technology has previously been applied to monitor geotechnical structures such as: tunnels (Mohamad et al. 2010), slopes (Nöther et al. 2008), pipelines (Inaudi and Glisic, 2010) and bored piles (Klar et al. 2006, Pelecanos et al. 2018, Kechavarzi et al. 2019). Those studies employed Brillouin-based DFOS interrogators. So far, however, little attention has been paid to the use of Rayleigh-based DFOS systems in piles (Monsberger et al. 2016, Bersan et al. 2018). No research has been found that investigated the development of negative skin friction using distributed fibre optic sensing technology.

1.1. OBJECTIVES

The overall objective of this PhD project was to extend the current knowledge of the soil-pile interaction in soft, subsiding soil. The objectives were formulated as follows:

- to investigate how various ground conditions and pile materials influence the soil-pile interaction in soft, subsiding soils.
 - to investigate and document the effect of bitumen coating on the development of shear forces along piles.
 - to investigate the application of distributed fibre optic sensors for determining the strain and stress distribution in piles.
 - to make general guidelines and recommendations for use in the design of piled foundations.
-

1.2. OUTLINE OF THE THESIS

This dissertation is formed as a paper-based thesis. It includes a number of scientific manuscripts or papers in different stages of completion as outlined in List of Publications. There are three manuscripts prepared for a journal submission and four manuscripts prepared for conference proceedings. Journal paper 1 has been published in the Geotechnical Engineering Journal of the SEAGS and AGSSEA on March 2020. Journal paper 2 has been submitted to the ISSMGE International Journal of Geoengineering Case Histories on December 2019 and it is currently (March 2020) under re-review. Journal paper 3 is planned for a journal submission. Conference paper 1 and 2 have been published in the conference proceedings. Conference paper 3 and 4 have been written with the purpose of submitting them to the 73rd Canadian Geotechnical Conference held in Calgary, Canada on September 13 – 16, 2020. The abstract of Conference paper 3 and 4 has been accepted by the conference committee on February 15, 2020.

The main body of this thesis is divided into 8 chapters.

Chapter 1 presents the theoretical background of the project, lists the objectives and provides the outline of the thesis.

Chapter 2 focuses on the application of the distributed fibre optic sensing system used in this study, describes its components and installation methods of distributed fibre optic cables in piles. Furthermore, it presents methods of recorded data interpretation and comparison between conventional strain sensors and the distributed fibre optic sensors. Journal paper 1 and Conference paper 1 are introduced.

Chapter 3 presents the step-by-step analysis of the results obtained from an instrumented static loading test. It highlights the effects of the testing programme on the strain records and further data interpretation. Finally, it proposes the pile load-transfer functions for the shaft and toe resistance of the tested pile. Journal paper 2 is introduced.

Chapter 4 investigates the shear stress between soft soil samples collected from one of the test sites and various pile materials. The effect of the interface type and the shearing rate is studied. The influence of bitumen coating on the development of the shear stress is elaborated. Conference paper 4 is introduced.

Chapter 5 presents the results obtained from the full-scale test setups established on construction sites during this PhD project. The influence of pile installation method and construction activities, causing lateral and vertical soil movement, on the strain measurements along the piles are discussed. Conference paper 2 and 3 are introduced.

Chapter 6 analyses the results of the third full-scale test setup established during the project. The test site, within a certain area, was solely used for research purposes. The development of unit shaft resistance along uncoated and bitumen-coated driven piles is presented and discussed. The full-scale results are supported with the obtained laboratory data. Journal paper 3 is introduced.

Chapter 7 provides general conclusions drawn from the laboratory and full-scale tests carried out in the present study.

Chapter 8 gives recommendations for further research work based on the outcome of this PhD project.

CHAPTER 2

APPLICATION OF DISTRIBUTED FIBRE OPTIC SENSORS IN PILES

2.1. Introduction

The first research questions were: the choice of a relevant distributed fibre optic sensing system for the objective PhD project, its application in piles and agreement with conventional strain monitoring system. The description of the chosen DFOS system, its application in piles and some lessons learnt are presented in Journal Paper 1. The agreement between the chosen DFOS system and the conventional strain monitoring system is presented in Conference Paper 1.

A DFOS system is composed of two main elements: a fibre optic spectrum analyser and a fibre optic cable. Among the available DFOS analysers, two main types were considered in this PhD project: Brillouin- and Rayleigh-based systems. The Brillouin-based analysers are widely used to monitor civil and geotechnical engineering structures (Kechavarzi et al. 2016, Ravet et al. 2017). However, the Rayleigh-based analysers have received little attention (Monsberger et al. 2016). The main practical difference between those two analysers are: the sensing range and the spatial resolution. The sensing range of Brillouin analysers is typically from 50 to 100 km and the spatial resolution is typically about 0.5 m. In contrast, the Rayleigh analysers in general have a sensing range of 20-80 m (can be up to 2 km divided into 80 m sections) and the spatial resolution of a few millimetres. The precision and repeatability of both systems are comparable according to the data sheets. As sensors i.e. fibre optic cables, bare fibres or specially designed cables can be used. An example of a bare fibre is presented in Figure 2 and an example of a fibre optic strain cable is shown in Figure 3.

It should be noted that the PhD student prepared all the DFOS sensors from several components by himself for the purpose of this PhD project.

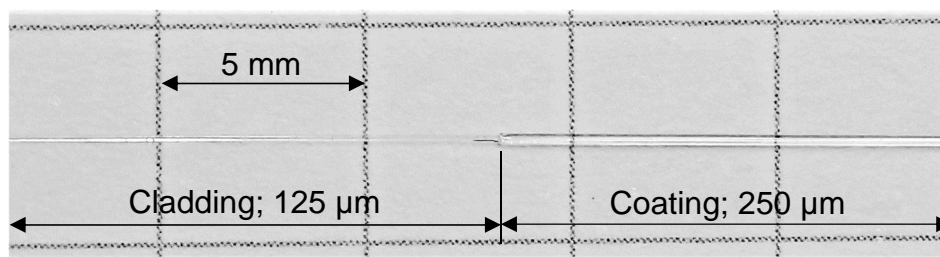


Figure 2. An example of a bare fibre.

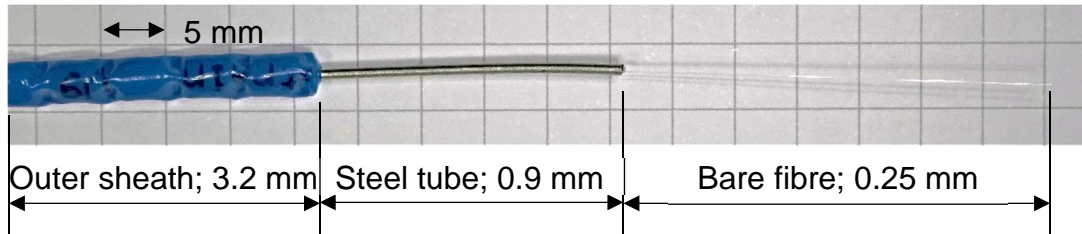


Figure 3. An example of a strain cable.

The installation of DFOS in various structures has been described in detail by Kechavarzi et al. (2016). Even though it is well described, a successful installation of fragile DFOS sensors in a structure, as presented in Figure 2 and Figure 3, is a challenging task. Additionally, the DFOS systems are based on light scattering, which is sensitive to any micro- and macrobends. These distortions, together with contaminated connectors and unnecessary splices, cause an optical power loss and affect the performance of the monitoring system.

In general, the test piles in the objective project were instrumented with two strain monitoring systems. The DFOS system was considered as the main system for strain and temperature data. Vibrating wire strain gauges (VW) were used as a backup system. However, in some cases it was difficult to install both systems. Therefore, the agreement between the two systems needed to be investigated.

2.2. Assessment of the applied methodologies

The Rayleigh-based analyser has been chosen based on the literature review, preliminary experiments conducted at Aarhus University, Norwegian University of Science and Technology and Centrum Pæle A/S and research visits at Cambridge University and NBG Fiber Optics using both DFOS systems during the first year of the PhD study. The main parameter in the decision-making process was the high spatial resolution. It allowed to obtain extremely dense distribution of strain and temperature data points. During the first full-scale use of the chosen DFOS system (during the static loading test), the analyser could not identify most of the connected DFOS sensors. Identifying the connected sensor was crucial for long-term monitoring. This issue was solved afterwards by re-keying the sensor and enabled long-term measurements.

The BRUsens V9 strain cable and the BRUsens temperature 85°C cable have been used in the objective PhD project. The selection of the DFOS cables was done similarly to the choice of the analyser. The treatment of the chosen cables to make a sensor (i.e. stripping and splicing the connectors) was relatively simple. The performance of the strain cable was satisfying. In contrast, the performance of the temperature cable installed in driven steel and precast concrete piles was poor. Therefore, it was not possible to use the temperature data from these cables to thermally correct the strain data.

A preliminary, DFOS instrumented, steel and precast concrete driven test pile was tested at Per Aarsleff's workshop yard in Hasselager. The instrumentation survived harsh driving conditions and confirmed the proposed installation method. The instrumentation of the main test piles (both driven and bored) consisted of at least a pair of opposite mounted gauges. In most cases, the DFOS system was supported with the traditional VW gauges. Such instrumentation layout was appropriate, since all the test piles during short- and long-term monitoring experienced bending. Additionally, the temperature data obtained from the VW gauges were used for the thermal correction of the strain DFOS data.

The agreement between the two monitoring systems was tested in the field during the static loading test. It would be beneficial to check the agreement in more controlled laboratory conditions.

2.3. Summary of the results

The chosen Rayleigh-based DFOS system successfully provided long-term measurements of strain and temperature distribution with a few millimetres spatial resolution. It was revealed that the chosen temperature DFOS cable installed in driven piles experienced mechanical strain and could not be used for the temperature correction of the strain data.

The DFOS sensors can be successfully installed in bored and driven piles. At least one pair of opposite mounted strain DFOS sensors is needed to provide useful information about the soil-pile interaction. The installation of strain DFOS cables on the side surfaces of precast concrete driven piles is prone to concrete cracks due to driving.

The strain measurements obtained from the DFOS and the VW gauges during the static loading test were in agreement.

2.4. Critical review

For this PhD project the most state-of-the-art DFOS analyser has been chosen. The selection of it should be based not only on literature review, research visits and some preliminary experiments, but based on preliminary full-scale tests, similar to those considered during the objective project.

During the preliminary full-scale tests at Hasselager, a more scattered strain distribution along precast concrete than steel pile was noted, however, at that time, the origin of it was not recognized. The issue with the temperature DFOS cable was also not recognized. These results should be in-depth analysed, and some precautions implemented to the main test piles.

The documented existence of cracks on the sides of precast concrete driven piles, questions the results obtained from the instrumented precast concrete piles with strain sensors (especially spot sensors) placed close to the side surfaces of the pile.

In this PhD project, standard values of strain and temperature conversion coefficients were used. Both strain and temperature DFOS cables should be calibrated, and the obtained actual coefficients should be used during the measurements.

The findings from the preparation and full-scale installation of the DFOS sensors in piles were used during the PhD student's co-operation with a manufacturer in the field of fibre optic telecommunication and resulted in manufacturing of the entire DFOS sensors. Such DFOS sensors were successfully used by a further Industrial PhD student at Aarhus University.

2.5. PhD student's contribution

The PhD student's contribution to Conference Paper 1 includes preparation of the DFOS sensors, instrumentation of the test pile, collecting data from the VW and the DFOS sensors, analysing the data and writing the paper (proportional contribution).

The PhD student contributed to Journal Paper 1 in the research and writing phase in a major way. All the presented data in the paper were obtained and analysed from the test sites prepared by the PhD student.

CONFERENCE PAPER 1

Kania, J.G. and Sørensen, K.K., 2018. A static pile load test on a bored pile instrumented with distributed fibre optic sensors. 10th International Symposium on Field Measurements in Geomechanics, Rio de Janeiro, Brazil, July 17-20, 9 p.

Status: published



A Static Pile Load Test on a Bored Pile Instrumented with Distributed Fibre Optic Sensors

Jakub Kania

cp test a/s and Aarhus University, Vejle / Aarhus, Denmark, jakub@cptest.dk / jgk@eng.au.dk

Kenny Kataoka Sørensen

Aarhus University, Aarhus, Denmark, kks@eng.au.dk

SUMMARY: This paper presents a case study of a static pile load test on an instrumented 630 mm diameter cased CFA pile installed in sand at a site located in Viborg, Denmark. The test was conducted to obtain the load-movement relationship, the distribution of strain and stresses along the pile and to compare the readings from conventional strain gauges and distributed fibre optic sensors for measuring internal pile strains. For this purpose, the pile was instrumented with vibrating wire sister bar strain gages in addition to fibre optic strain and temperature cables along the full length of the pile. The pile was loaded incrementally at the pile head in two loading cycles. It was found that the distributed fibre optic sensors gave strain measurement in good agreement with those obtained from conventional strain gauges and that they can provide detailed information of stress and strain distribution along the full length of a pile.

KEYWORDS: static pile load test, bored pile, field instrumentation, distributed fibre optic sensing

1 INTRODUCTION

One of the most reliable test to assess a bored pile capacity is a static pile load test. Unfortunately, during the test only the movement of a pile head subjected to a given load is measured. More comprehensive results can be obtained with dedicated pile instrumentation. Traditionally, bored concrete piles have been instrumented with simple telltales to achieve a measurement of pile deformation relative to the pile head (Dunncliff, 1993) or in recent decades more commonly with spot measurement using vibrating wire (or electrical) embedded or sister bar strain gauges (Dunncliff, 1993, Fellenius, 2002, Siegel and McGillivray, 2009). The typical gauge length of single point strain gauges range from around 50 mm to 250 mm. Recent developments in the field of distributed fibre optic sensors have shown the possibility of implementing low cost distributed fibre optic sensors in civil engineering for obtaining high resolution strain measurements in structures. While the majority of reported studies are based on measurements from distributed fiber optic sensors taken using interrogators based on Brillouin scattering (Kechavarzi et al., 2016, Mohamad et al., 2017), only a small number of studies have so far focused on the application of interrogators based on Rayleigh back scattering (Monsberger et al., 2016). Using Rayleigh back scattering it is possible to obtain practically continuous high resolution data of strain and temperature inside a pile with a spatial resolution of only a few millimetres, while the spatial resolution is around 0.5 m using Brillouin scattering. The use of distributed fibre optic sensing in connection to pile testing as

compared to spot measurements makes it possible to achieve a previously unseen high degree of detail and increased reliability in the strain measurement and hence a much greater insight into the development and distribution of shaft resistance.

The purpose of this paper is to compare the strain measurements obtained from obtained from Vibrating Wire Strain Gauges (VWSG) and Distributed Fibre Optic Sensors (DFOS) based on Rayleigh back scattering, and to document the use of DFOS for strain measurements in a bored pile.

The paper firstly gives details of the test site conditions and the instrumentation of the pile. The presentation and discussion of results will focus on the correlation between spot and distributed sensors and the distribution of strains in the pile cross section and over the full length of the pile.

2 MATERIALS AND METHODS

2.1 Site conditions

The static pile load test was carried out at a construction site in Viborg, Denmark. The test pile has the same dimensions as the production piles which were designed to support a 6-storey building with parking basement at the lower level.

The boring and CPT profile nearest to the test pile indicate a soil profile consisting of 3.8 m sandy clay fill underlain by a 1.2 m thick layer of buried soft organic sandy clayey top soil on top of sorted late glacial meltwater sand, cf. Figure 1. The meltwater sand continues well below the pile toe and increases in coarseness with depth. Based on the measured cone resistance, q_c from CPT testing, the sand can be classified as medium to very dense. The groundwater table is located at level 19 m ASL (above mean sea level) around 2.7 m above the toe of the test pile.

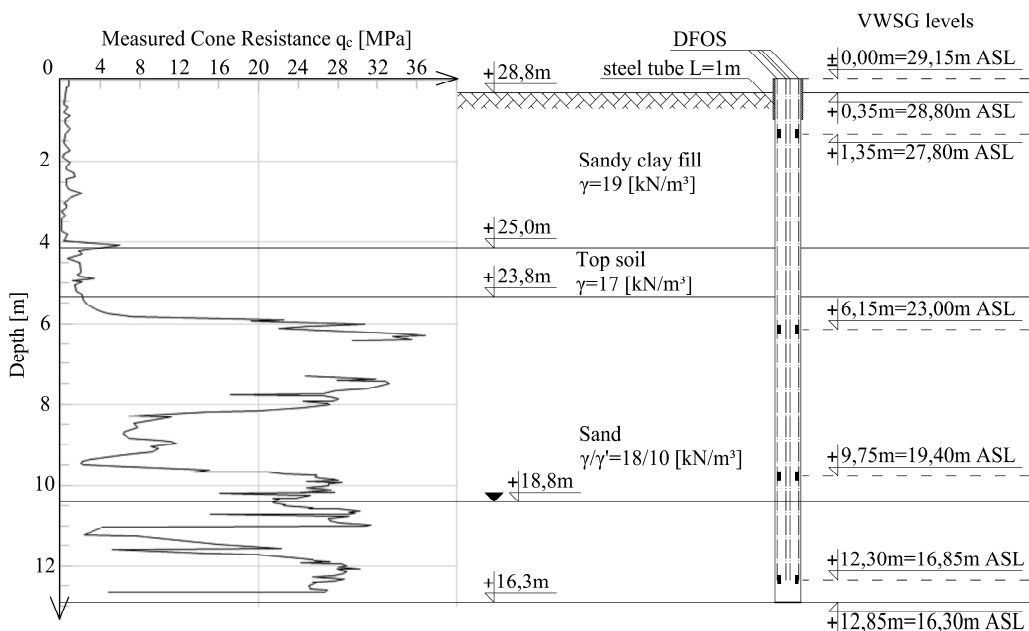


Figure 1. Soil profile and the test pile.

2.2 Test pile

An instrumented, 630 mm diameter, 12,5 m long, cased CFA pile was drilled from a working platform at 28,80 m ASL. The pile head and toe level was 29,15 m ASL and 16,30 m ASL as shown in Figure 1. C35/45 class of concrete was used for the test pile. The 470 mm outer diameter reinforcing cage

consisted of twelve 20 mm diameter main reinforcing bars and 12 mm diameter spiral reinforcement with 150 mm spacing. The bottom 1 m long section of the reinforcing cage was narrowed down to 320 mm diameter using an additional six 20 mm diameter, 1.8 m long main reinforcing bars at the bottom end. The reinforcing cage had additional stiffening rings every 970 mm consisting of 6x60 mm flat bar.

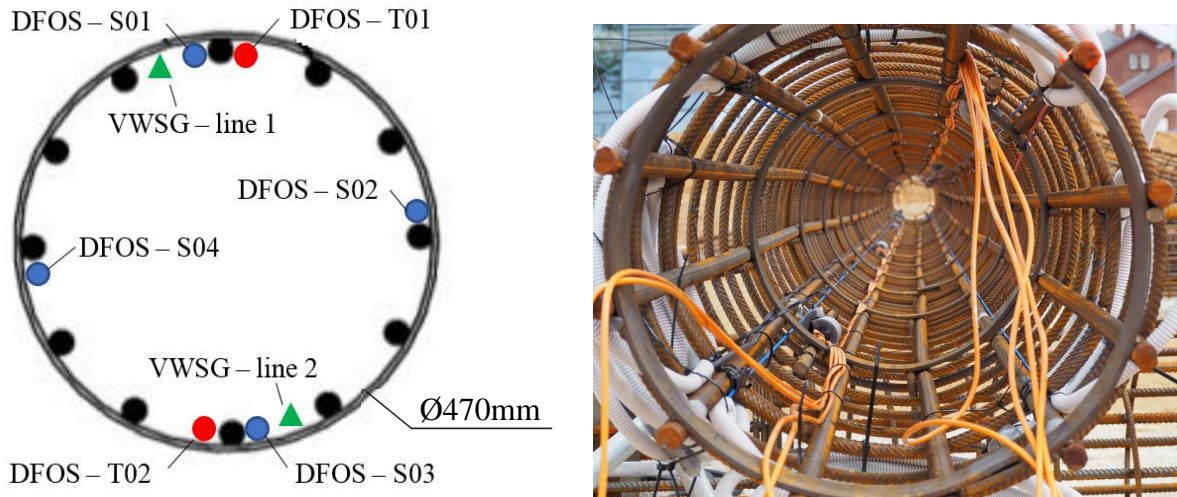


Figure 2. Cross-section of the reinforcement cage showing instrumentation.

Figure 2 shows a photo and illustration of the cross-section of the test pile. As shown in Figure 2 the test pile was instrumented with four lines of strain and two lines of temperature distributed fibre optical sensors (DFOS). A BRUsens V9 strain cable, a BRUsens temperature cable and a standard loose tube gel-filled fibre optical cable (temperature sensor) was used in this case study. The fibre optical sensing cables were fixed to the main reinforcing bars from the pile head to the pile toe. All of strain distributed optical fibre sensing cables were pre-stained to about $700\mu\epsilon$ (cf. Figure 3). Temperature sensing cables were attached on diametrically opposite sides alongside the strain cables as presented in Figure 2. To measure strain and temperature changes, an optical reflectometer based on Rayleigh back scattering was used. The interrogation unit provides data with resolution of about $\pm 1,0\mu\epsilon$ for strain and about $\pm 0,1^\circ\text{C}$ for temperature measurements. A spatial resolution was set to 2,6 mm. Detailed description of Rayleigh-based distributed fibre-optical sensing techniques was presented by Palmieri and Schenato (Palmieri and Schenato, 2013).

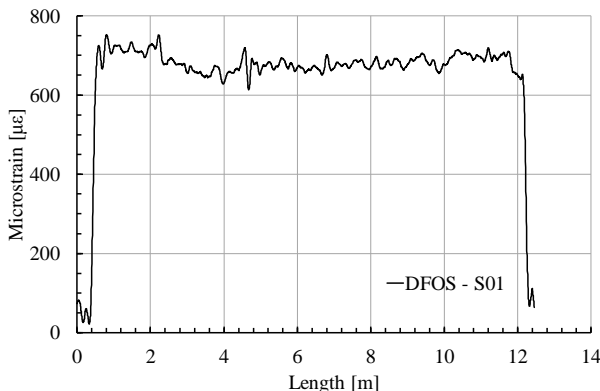


Figure 3. Pre-straining of the fibre optical cable - DFOS-S01.

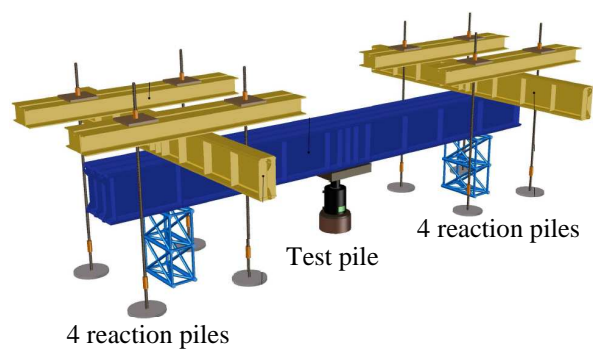


Figure 4. Illustration of the static pile load test setup (Aamann-Svale and Møller, 2017).

In addition to distributed fibre optic sensors, the test pile was instrumented with more traditional 16 mm diameter sister bar vibrating wire strain gauges (VWSG) with a resolution of $0,6\mu\epsilon$ and 50 mm gauge length (shown connected using orange cables in Figure 2). As illustrated in Figure 1 and in the cross-section in Figure 2, two sets of VWSG were installed on diametrically opposite sides at four depths in the pile: 1.35, 6.15, 9.75 and 12.3 m respectively.

2.3 Static pile load test

A static pile load test was performed on the test pile 14 days after installation. Figure 4 illustrates the test setup which makes use of eight reaction piles, four on either side of the test pile and a stiff cross beam. Loads were applied by a computer controlled single hydraulic jack and measured with a load cell. The pile head movement was measured by three displacement transducers attached to a reference frame.

The test was performed as a maintained load (ML) test in which the load is increased in stages to a maximum load with the time/movement curve recorded at each stage of loading and unloading (Tomlinson and Woodward, 2008). As presented in Figure 6, two load cycles were performed. In the first load cycle, the load was applied from initial 0 kN to 1000 kN in 4 increments of each 250 kN and subsequently unloaded in 2 steps of 500 kN. In the second cycle, the load was applied in 9 steps of 250 kN or 500 kN until reaching 4000 kN, and then the pile was unloaded in 2 steps of 2000 kN. The load was maintained for 10 min at each load step before reaching the maximum load in each cycle and maintained for 5 min after each unloading step. After reaching the maximum load in cycle 1 and 2, the load was maintained for 15 min and 30 min respectively.

3 RESULTS

3.1 Static pile load test result

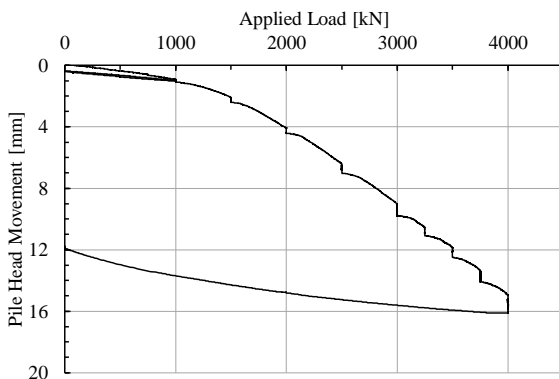


Figure 5. Load-movement curve of the pile head (Aamann-Svale and Møller, 2017).

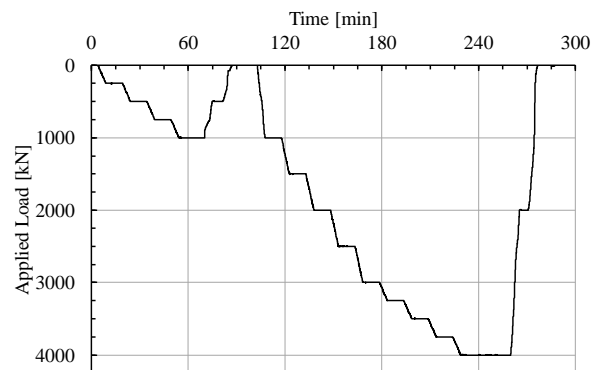


Figure 6. Schedule of the test (Aamann-Svale and Møller, 2017).

Figure 5 shows the load-movement curve at the pile head level. The maximum applied load was 4000kN and the pile head movement at this load was 16 mm, corresponding to around 2.5% of the pile diameter. The load-movement curve does not indicate impending failure/mobilisation of full capacity in the test. The load-movement response is seen to be very stiff in the first load cycle for loads up to 1000 kN with limited plastic strain generated.

3.2 Measured strain distribution

Figure 7 and Figure 8 present the development in measured strain distribution along the test pile for four selected load steps from 500 kN to 4000 kN obtained from the two sets of sensors that were

placed on diametrically opposite sides; (VWSG-line 1 and DFOS-S01) and (VWSG-line 2 and DFOS-S03) respectively.

Stress free conditions have for simplicity been assumed at the start of the load test. To smoothen the strain profile, a moving average of 40 consecutive reading was used to present data obtained from DFOS (giving a virtual gauge length of roughly 10 cm). The temperature data obtained from VWSG did not indicate any significant change in temperature during the test ($\pm 0,1^{\circ}\text{C}$) thus the obtained strain profiles were not thermally compensated.

During the first loading cycle all the DFOS sensors where connected to the interrogation unit through a multi-channel switch. During the second loading cycle only one sensor was directly connected to the interrogator. The more fibre optical connectors are used, the poorer (more scattered) signal can be obtained. To minimize the scatter in the obtained strain measurement in the second load cycle, a new baseline was taken at the end of the first load cycle, and the accumulated strain profile after first load cycle (averaged over 400 readings) was subsequently added to all subsequent readings.

Comparison of strain measurements using DFOS and VWSG

From Figure 7 and Figure 8 a very high correspondence is observed between strain measurements from the vibrating wire strain gauges (VWSG) and distributed fibre optic sensors (DFOS) at the locations of the VWSG. The correspondence of strain measurements is further illustrated in Figure 10 for measurement taken during all load steps.

However, it is also clearly illustrated that distributed fibre optic sensors provide a much more detailed strain profile, which is not possible to obtain from interpolation between the spot measurements using VWSG. For example, it is seen that the soft soil layer located above the sand layer between a depth of 4.1 m and 5.3 m appears to be distinguished from DFOS measurements (constant strain). Furthermore, from Figure 7 the strain profile is shown to yield sharply in the lower part of the test pile (VWSG-line 1 and DFOS-S01) and the exact depth at which it occurs can be clearly seen from the strain profile obtained from DFOS, while the spot measurements only indicate an approximate level.

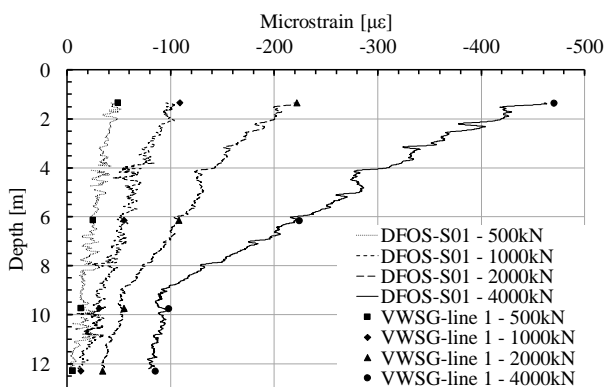


Figure 7. Measured strain distribution of the test pile for selected load steps obtained from VWSG-line 1 and DFOS-S01.

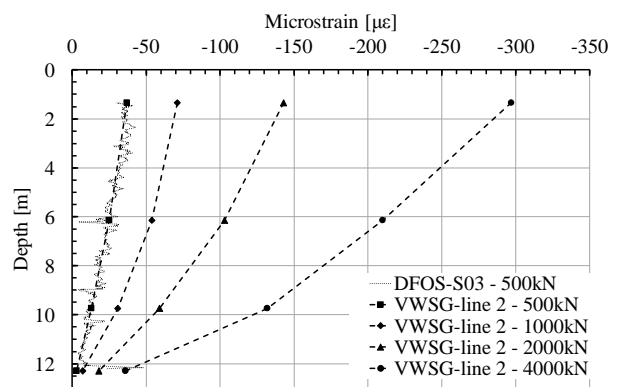


Figure 8. Measured strain distribution of the test pile for selected load steps obtained from VWSG-line 2 and DFOS-S03.

Cross-sectional variation in strain

As shown in Figure 7 and Figure 8, the measured strain profiles may differ significantly depending on the location of a strain sensors set. At the maximum load of 4000 kN VWSG-line 1 and DFOS-S01 sensors recorded around 470 $\mu\epsilon$ at the pile head, while VWSG-line 2 sensor showed around 300 $\mu\epsilon$.

The percentage difference between those two readings is 44%. The more surprising difference was recorded in the lower part of the test pile. VWSG-line 1 and DFOS-S01 sensors indicate an almost vertical strain profile at the bottom of the test pile with very little change with increasing applied load. In contrast, the strain profile obtained from VWSG-line 2 on the opposite side of the pile is showing significant changes in inclination with increasing loads.

The non-uniformity of strain measurement in different cross-sectional locations and at different levels under the same applied load at the pile head is further illustrated in Figure 9. Although, the strains are non-uniform in the cross section and varies with depth, it is found that if the average strain of opposing strain measurement are compared, then the strain measurements are in very good agreement; e.g. average of VWSG-line 1 and VWSG-line 2 vs. average of DFOS-S02 and DFOS-S04.

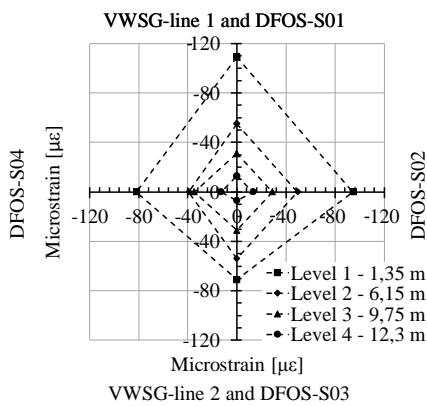


Figure 9. Cross-sectional distribution of strains at four different levels under the pile head load of 1000 kN.

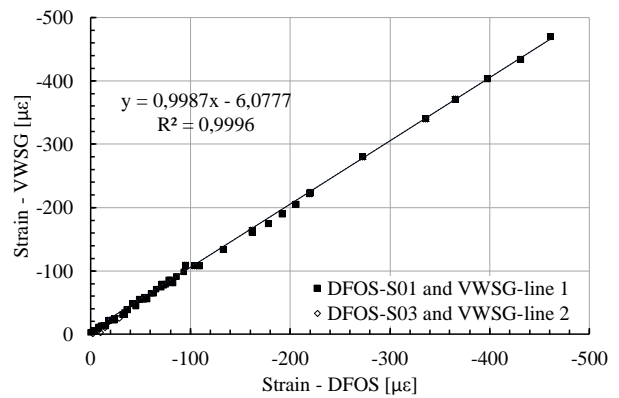


Figure 10. Agreement of strain measurement between VWSG and DFOS sensors located at the same depths

3.3 Back calculated concrete modulus and conversion of strains to axial load

The concrete modulus was back calculated assuming that the load at the first layer of VWSG (1,35m below the pile top) and DFOS was equal to the applied load at the pile head. Furthermore, it is assumed that the concrete modulus is uniform along the pile length. It has not been possible to back calculate the concrete modulus using the tangent method from the lower levels of the pile from the test results, as full shaft resistance may not have been mobilised.

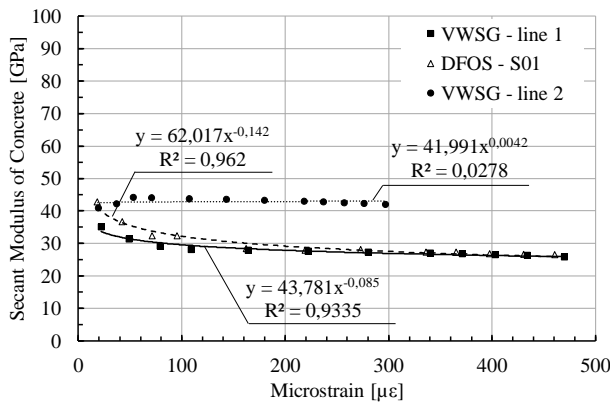


Figure 11. Back-calculated secant modulus of concrete.

In Figure 11 the back calculated secant modulus of concrete from VWSG-line 1, VWSG-line 2 and DFOS-S01 strain measurements are plotted against microstrain. It is found that the back calculated secant modulus of concrete from VWSG-line 1 and DFOS-S01 strain measurements are in good agreement, specially at strains above 150 $\mu\epsilon$. The secant modulus of concrete is seen to reduce from around 35-45 GPa at 20 $\mu\epsilon$ to around 29 to 30 GPa at 150 $\mu\epsilon$. Above 150 $\mu\epsilon$ the modulus is seen only to reduce slightly with increasing strain. The evolution of the secant modulus with strain may with good precision be described by a power function, as shown in Figure 11, as given by the following equations:

$$\text{DFOS-S01: } y=62,017 \cdot x^{-0,142} \quad (1)$$

$$\text{VWSG-line 1: } y=43,781 \cdot x^{-0,085} \quad (2)$$

In contrast, the back calculated secant modulus of concrete from VWSG-line 2 strain measurements give a more or less constant value of secant modulus of 41-44 GPa independent of strain magnitude.

The measured strains were converted to axial load using the equation:

$$F=\varepsilon \cdot (E_c \cdot A_c + E_s \cdot A_s) \quad (3)$$

where: F – axial load, ε – strain reading, E_c – concrete modulus, A_c – cross-sectional area of concrete, E_s – steel modulus, A_s – cross-sectional area of steel reinforcement.

3.4 Mobilised shaft resistance

Figure 12 and Figure 13 shows the average mobilised unit shaft resistance along the test pile in each sublayer derived from the VWSG and DFOS strain data under the maximum applied load of 4000 kN at the pile head.

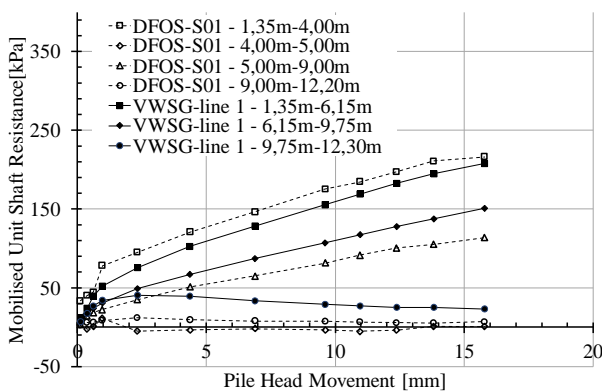


Figure 12. Average mobilised unit shaft resistance in selected sublayers obtained from VWSG-line 1 and DFOS-S01.

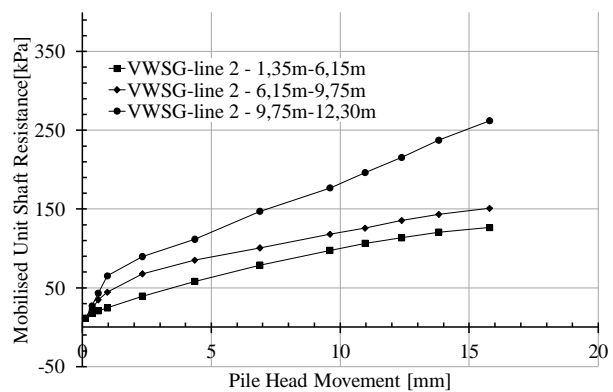


Figure 13. Average mobilised unit shaft resistance in selected sublayers obtained from VWSG-line 2.

From the VWSG data it is only possible to get an average mobilised shaft resistance between the measurement points (three layers), while the DFOS data allows for division into more sensible sublayers based on the characteristics of the strain profile. For the DFOS data a division into four sublayers was chosen.

Based on VWSG-line 1 and DFOS-S01 (Figure 12) it can be seen that strain mobilisation in the lower part is very limited and does not evolve with increasing load. The upper part of the test pile on the other hand show a significant mobilisation of shaft resistance with continues to increase with increasing load. In contrast, based on VWSG-line 2 (Figure 13) the situation is very different especially at the lower end of the pile, where significant shaft resistance is clearly mobilised with increasing load.

4 DISCUSSION AND CONCLUSIONS

In this paper, the results are shown assuming ideal stress-free conditions at the start of the test. This is very likely not the case, as residual forces may arise after pile installation resulting from soil disturbance during pile installation and concrete curing, as discussed by (Mascarucci et al., 2013, Fellenius, 2015). Since the stress conditions at the start of test is very uncertain and due to the measured existence of significant stress non-uniformity in the cross-section of the pile, no attempts have been made in this paper to further interpret the test results and to derive the actual mobilised shaft resistance and end bearing of the test pile.

This study document the use of distributed fibre optic sensors based on Rayleigh scattering for detailed internal strain measurement in a concrete bored pile installed in sand. The strain measurements confirm a high agreement between vibrating wire sister bar gauges strain and distributed fibre optic sensors.

Unlike telltales, the distributed fibre optic sensors can be the primary measurement system because they are installed before pile installation. As opposed to spot sensors, using the distributed fibre optic sensors an engineer does not have to specify the final depths of sensors, because they can measure along its entire length. Owing to this fact, interpolation between sensing points is not needed. The distributed fibre optic sensors based on Rayleigh scattering gives a very detailed strain profile and were able to distinguish internal pile strain variation in different soil layers due to the high spatial resolution of the unit.

The results of this study furthermore highlight the importance of having several sensing points located in the cross section of the pile as strains may be non-uniformly distributed.

ACKNOWLEDGEMENTS

The authors would like to thank cp test a/s, Per Aarsleff A/S, DMT Gründungstechnik GmbH and Innovation Fund Denmark for proving funding for this study and Per Aarsleff A/S for providing data and for installing the instrumented test pile.

REFERENCES

- Dunnicliff, J. (1993) *Geotechnical instrumentation for monitoring field performance*. John Wiley & Sons.
- Fellenius, B. H. (2002) 'Determining the true distributions of load in instrumented piles', *Deep Foundations 2002: An International Perspective on Theory, Design, Construction, and Performance*, pp. 1455-1470.
- Fellenius, B. H. (2015) 'Static tests on instrumented piles affected by residual load', *DFI Journal-The Journal of the Deep Foundations Institute*, 9(1), pp. 11-20.
- Kechavarzi, C., Soga, K. B., Battista, N. d., Pelecanos, L., Elshafie, M. Z. E. B., Mair, R. J. and Cambridge Centre for Smart Infrastructure and Construction. (2016) *Distributed fibre optic strain sensing for monitoring civil infrastructure : a practical guide*. London: ICE Publishing, a division of Thomas Telford Ltd.
- Mascarucci, Y., Mandolini, A. and Miliziano, S. (2013) 'Effects of residual stresses on shaft friction of bored cast in situ piles in sand', *Journal of Geo-Engineering Sciences*, 1(1), pp. 37-51.

- Mohamad, H., Tee, B. P., Chong, M. F. and Ang, K. A. 'Investigation of shaft friction mechanisms of bored piles through distributed optical fibre strain sensing'. *19th International Conference on Soil Mechanics and Geotechnical Engineering*, Seoul.
- Monsberger, C., Woschitz, H. and Hayden, M. (2016) 'Deformation measurement of a driven pile using distributed fibre-optic sensing', *Journal of Applied Geodesy*, 10(1), pp. 61-69.
- Palmieri, L. and Schenato, L. (2013) 'Distributed optical fiber sensing based on Rayleigh scattering', *The Open Optics Journal*, 7(1).
- Siegel, T. C. and McGillivray, A. 'Interpreted residual load in an augered cast-in-place pile'. *Annual DFI Conference*, Kansas City.
- Tomlinson, M. and Woodward, J. (2008) *Pile design and construction practice*. Abingdon: Taylor & Francis.
- Aamann-Svale, R. and Møller, O. (2017) *Midtbyens Gymnasium, Viborg. Statisk prøvebelastning (222.437)*.

JOURNAL PAPER 1

Kania, J.G., Sørensen, K.K., and Fellenius, B.H., 2020. Application of distributed fibre optic cables in piles. Geotechnical Engineering Journal of the SEAGS and AGSSEA, March 51(1) 94-102.

Status: published

Application of Distributed Fibre Optic Cables in Piles

Jakub G. Kania¹, Kenny Kataoka Sorensen² and Bengt H. Fellenius³

¹PhD student, Department of Engineering, Aarhus University, Aarhus, Denmark and cp test a/s, Vejle, Denmark

²Associate Professor, Department of Engineering, Aarhus University, Aarhus, Denmark

³Consulting Engineer, Sidney, BC, Canada, V8L 2B9

¹E-mail: jakub@cptest.dk

²E-mail: kks@eng.au.dk

³E-mail: bengt@fellenius.net

ABSTRACT: A high spatial resolution distributed fibre optic sensing system for measuring strain and temperature was used to instrument fourteen single piles subjected to general subsidence. Thirteen piles were driven (six steel and seven precast concrete) and one was a cased continuous flight auger pile, CFA. The CFA pile was subjected to a static loading test. The distributed fibre optic analyser measured the spectral shift in the fibre Rayleigh scatter to obtain strain and temperature data. The seasonal temperature changes in the surficial soil layers showed to influence the strain records. Several lessons were learnt from the application of distributed fibre optic sensors in piles, such as installation methods, influence of temperature, and performance of fibre optic cables.

KEYWORDS: Instrumented piles, Distributed fibre optic sensing, Rayleigh scattering, Temperature effect, Strain gauges

1. INTRODUCTION

Instrumentation of piles are used to provide detailed information about soil-pile interaction, necessary for optimizing the design of a piled foundation, e.g., determine distribution of shaft resistance and measure the pile toe load-movement response. Conventionally, piles have been instrumented by means of telltales and strain gages placed along the pile to determine the force distribution caused by a load applied to the pile head or an axial force induced by subsiding soils. In recent years, there has been an increasing interest in the using distributed fibre optic sensing (DFOS) systems for monitoring strain in geotechnical structures. The DFOS technology employs light scattering along an optical fibre (Culshaw and Kersey 2008). Owing to the vast measurement range of the DFOS (tens of kilometres), they were primarily used for pipeline monitoring projects (Inaudi and Glisic 2010, Ravet et al. 2017). The development in fibre optic analysers, mainly in terms of spatial resolution and accuracy, allowed to use the technology also in geotechnical applications, e.g., tunnels (Mohamad et al. 2010), slopes (Nöther et al. 2008), and piles (Klar et al. 2006, Pelecanos et al. 2018, Kechavarzi et al. 2019). Most of the early studies employed Brillouin-based DFOS systems, whereas Rayleigh-based DFOS systems in piles has received little attention (Monsberger et al. 2016, Bersan et al. 2018).

This paper focuses on lessons learnt from employing a Rayleigh-based DFOS system to monitor strain in piles, describing the components of the DFOS system and methods of installing distributed fibre optic (FO) cables in piles, as well as presenting method of analysis of the records, and observed performance.

2. DISTRIBUTED FIBRE OPTIC ANALYSER AND CABLES

A DFOS system is composed of two main elements: a fibre optic spectrum analyser and an FO cable. The subject study of measuring strain and temperature changes in piles, a Luna ODISI-B system was used. The system comprises an interrogation unit (IU), a stand-off cable, and a remote module (see Figure 1). The IU uses swept-wavelength interferometry to measure the spectral shift in the Rayleigh backscatter (Luna 2017). The maximum sensing length of the unit employed in the subject test was 20 m and the spatial and sampling resolutions were 5.2 and 2.6 mm, respectively. The spatial resolution is a length over which the IU calculates a single strain or temperature data point. The sampling resolution is the distance between two data points. FO cable sensors, standard telecommunication bare fibres or commercially available coated strain and temperature sensing cables can be used. The subject study

employed a FO cable connected to the IU through the remote module and stand-off cable.

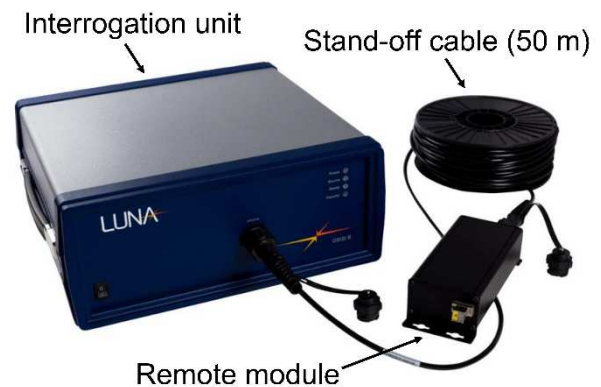


Figure 1 ODISI-B measurement system (Luna 2017)

Figure 2(a) shows a bare fibre glued to the reinforcement bar and Figure 2(b) shows FO strain and temperature cables attached to the reinforcement cage. The FO strain cable must transfer the applied strain without any slippage between the coatings. Thus, bare fibres would appear to be most suitable. However, bare cables are brittle and unsuitable in a harsh environment, such as a pile. Therefore, strain sensing cables with a coating to serve as a protection layer have been developed. It is important that the coating and any glue (epoxy) for affixing the sensor to a construction unit is free of shrinkage and creep to avoid imposing extraneous strain in the cable. In contrast to the FO strain cable, the FO temperature cable should allow slippage between the protective layers to eliminate all strain influencing the temperature records. In this study, a BRUsens V9 strain cable and a BRUsens temperature 85°C cable were used.

The IU used in this study requires a distributed FO cable to have an LC/APC connector to connect the sensor to the IU (through a remote unit and stand-off cable). The fibre-end termination should ensure a greater than -65dB return loss (no back reflection). This can be achieved by splicing a coreless fibre or a commercially available no-reflection terminator to the fibre end. An alternative method is to terminate the fibre with a few (5 to 6) small diameter (about 2 mm) loops. In this study, the termination was made by making small diameter loops.

In using an IU type Luna ODISI-B, each FO cable must have a sensor key (Luna 2017). The sensor key is a file containing the

characteristic spectral shift for a given FO cable and is used for its identification. The unit is using an algorithm along the first 200 mm of the connected sensor to identify it (Luna 2017). Therefore, it is important to relieve this part of the FO sensor from any strain and temperature gradients. This can be done by placing a protective tube or shaping the fibre into a loop along this part. If a FO sensor is damaged, and repaired, or not identified by the IU, all its characteristics must be re-keyed, i.e., sensor name, strain, temperature coefficients, and start and end locations of the sensing section along the fibre.

To validate the re-keying procedure, an identified FO sensor was re-keyed. The standard deviation between strain measurement obtained from identified and re-keyed sensor was $\pm 2 \mu\epsilon$. The sensor key can be provided by the manufacturer of the unit or can be created by the user.

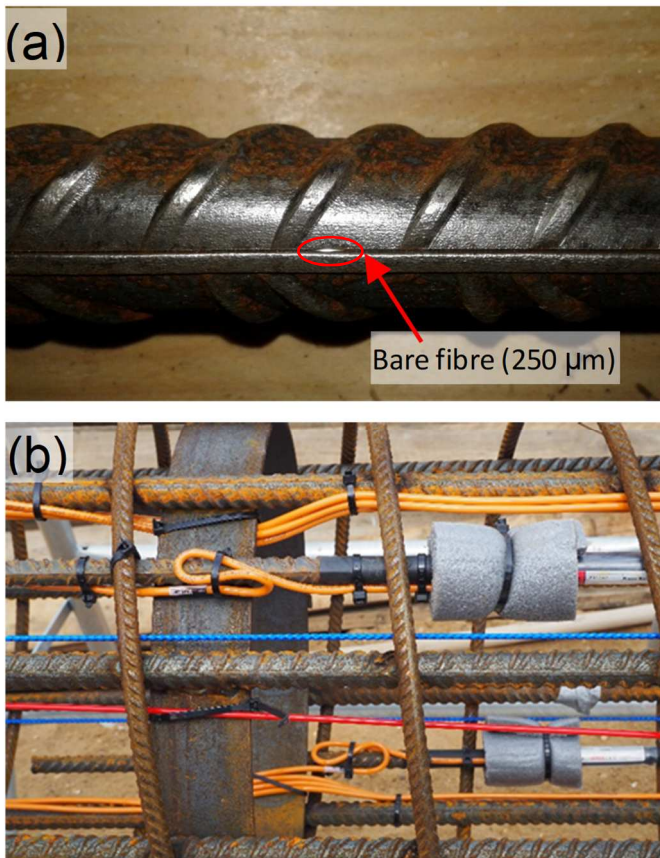


Figure 2 An example of (a) a bare fibre glued to the reinforcement bar along the longitudinal rib and (b) FO strain (blue) and temperature (red) cables attached to the reinforcement cage. The "250 µm" label refers to the thickness of the fibre cable

The IU records spectral shift in the fibre. This shift (frequency or wavelength) is proportional to change of temperature or strain in proportion to the properties of the fibre as calibrated in the laboratory for response to frequency shift for a known temperature or strain change (Kreger et al. 2006, Monsberger et al. 2016). For standard telecommunication fibres the value of the coefficients may vary around 10 % (Luna 2017). In this study, the temperature and strain coefficients of $0.634 \text{ }^\circ\text{C}/\text{GHz}$ and $-6.67 \mu\epsilon/\text{GHz}$ were used, respectively.

According to the manufacturer, the accuracy of the IU used in this study was $\pm 25 \mu\epsilon$ (Luna 2017). The measurements were compared to NIST traceable extensometer measurements measuring over the range of 0 to 10,000 $\mu\epsilon$. An accuracy of 0.25 % is similar to the accuracy of commercially available vibrating wire (VW) strain gages.

According to the VW data sheet (from Geosense) the accuracy of VW gauges is 0.1-0.5% FS (where the FS is $3000 \mu\epsilon$).

3. INSTALLATION OF FIBRE OPTIC CABLES IN PILES

A distributed FO cable usually combines two sections; one for sensing and one for routing. The sensing section provides strain or temperature data. The routing section links the sensing section with the IU (Kechavarzi et al. 2016). A robust FO cable should be used as routing section, since it is placed outside the monitored structure. The two sections are connected by a fusion splice or by a fibre optic adapter. The former entails lower optical loss than the latter, but safe fusion splicing could be difficult to achieve on site. Either connection is likely the weakest spot of the distributed FO cable. Therefore, it should be well protected. One method of protection is to keep them outside the monitored element, e.g., in a protective box or sleeve. Another is to embed them in the monitored element. The advantage of placing them outside is the accessibility to repair. In this study, the connections were kept outside for the CFA pile and were embedded for the steel or precast concrete driven piles. Both methods worked well.

Figure 3 shows a typical cross-section layout of an instrumented (a) steel pile and (b) a reinforcement cage of a bored pile. It is good practice to install at least one pair of opposite mounted strain sensors, because it is very likely that the pile will be subjected to bending. Installing two pairs will ensure a back-up redundancy in case of damage to the FO cable, or provide a valuable independent verification (confirmation) of unexpected results. Because the FO system provides continuous measurements, the location of sensors with depth is not an issue.

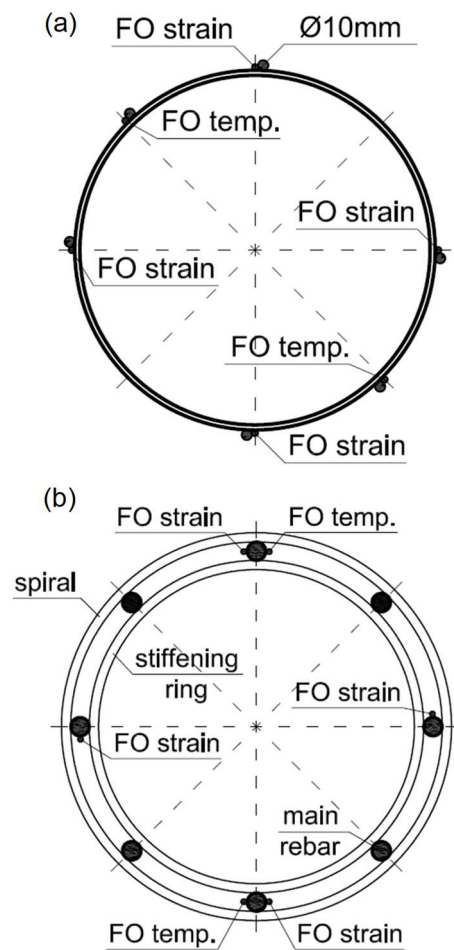


Figure 3 Typical cross-section layout of FO cables attached to (a) a steel pile and (b) a bored pile

A FO installation can either be fully bonded or installed between fixed points. In the fully bonded condition, the FO cable is continuously attached to the structure. In the fixed-point method, the FO cables provide intermittent strain information, i.e., only between the fixed points (Kechavarzi et al. 2016). In piles, the fully bonded method is preferable and the FO cables are entirely glued or embedded in the structure. Figure 4a shows an installation of a FO cable on the surface of a steel pile. An additional steel rebar was welded to the pile (one side only) as a guide and protection for the FO cable. Close to the pile toe, the bar was bent around to protect the cable end during the driving of the pile. Before attaching the FO cable to the pile, the steel surface was polished, cleaned from dust, and degreased. The FO cable was glued to the pile surface and covered using an epoxy component.

Figure 4b shows FO cables installed in a precast concrete pile. The FO cables were inserted into grooves (cleaned from dust and primed before placing the cables) and fixed with an epoxy glue. Figure 4c shows epoxy-coated FO cables installed on a reinforcement cage. The cables were installed affixed the main reinforcement bars, as shown in Figure 4d. A rubber pad was placed around each FO strain cable-tie to avoid localised point stress from cable ties. The FO temperature cables were installed without rubber pads. The cables can also be attached using specialised cable clamps (Kechavarzi et al. 2016). To avoid the flow of wet concrete affecting a FO cable, it is recommended to place the FO cables (strain and temperature) close

to the reinforcement along the whole length of the sensing section. It can be done by placing the cable ties at close spacing, e.g., at every 1.0 m. It is necessary to record strains immediately after placing in the pile (in the reinforcing cage) and before pouring the concrete, as well as after pouring because the heating and cooling involved in the hydration process will impose differential strain in the concrete and reinforcement. Such strain has no relation to the interaction between the pile and the soil and must be considered in the data analysis (Fellenius et al. 2009).

Before the FO strain cables are affixed to the structure, it is good practice to pre-tension the cable to an amount larger than the expected compressive strain (Kechavarzi et al. 2016). An example of pre-tensioning of a FO strain cable is shown in Figure 5. A pre-tensioning between two known points along the element can help align the length scale of the FO cable. Once a FO cable is attached to a structure, the locations of interest (e.g., pile head, specific depths, and pile toe) should be established, for example, by pressing or heating/cooling the FO cable at the location of interest and recording the signal at the same time.

It is important to avoid sharp bends along the FO cables to avoid loss of signal. An area where a bend easily occurs is where the cable exits from a structure. Figure 6 presents FO and VW cables exiting from a pile head. The FO cables were additionally sleeved using plastic tubes.

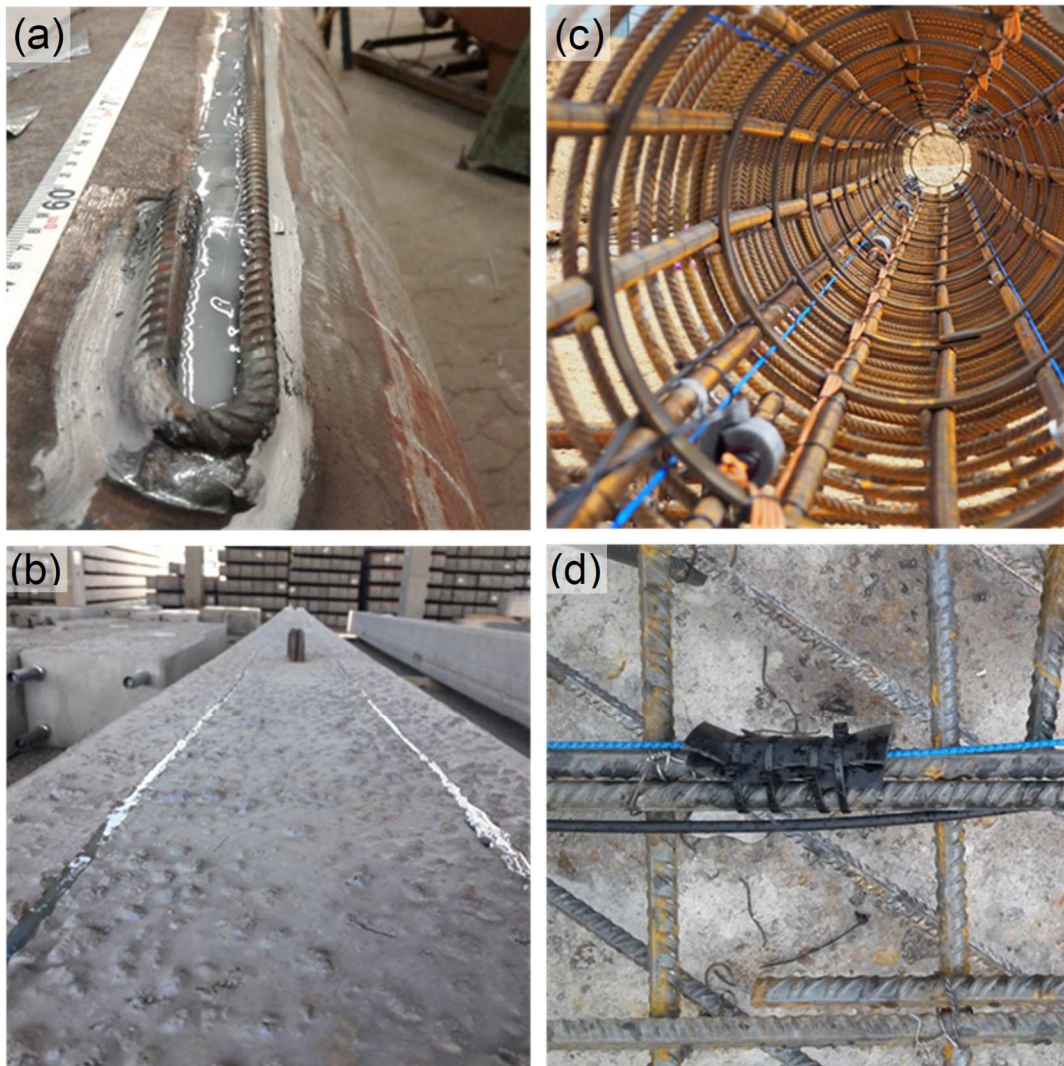


Figure 4 FO cable installation in piles: (a) glued to a steel pile, (b) glued in a groove cut along a precast concrete pile, (c) attached to a reinforcement cage, (d) attached to a rebar

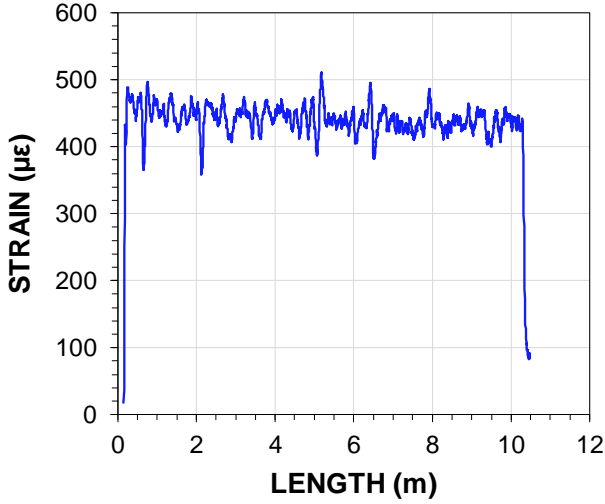


Figure 5 Pre-tension strain of a FO strain cable



Figure 6 A pile head and the sleeved FO cables at the exit points

4. DATA ANALYSIS

The measurements are always referenced to an initial state of strain (or temperature) in the cable. Therefore, it is important to establish a reliable reference reading (initial reading) to the measurements. The initial reading is actually several readings, each one taken when a change is made in the construction process from initial placement to start of a test or monitoring a development over time. Moreover, each such should be recorded over a brief period of time to eliminate any effect of a mistake or disturbance during the recording.

4.1 Influence of Temperature

The distributed FO sensors are sensitive to strain and temperature changes (Kreger et al. 2006). Thus, to obtain the mechanically induced strains the measured strains must be thermally compensated in case of any temperature changes. Because the stiffness of all the materials making up the FO cable is much smaller than the stiffness of the host structure (e.g., steel and/or concrete), it can be assumed that the FO cable undergoes the same thermal expansion as the host structure (Kechavarzi et al. 2016). However, the temperature change will still shift the spectrum of light scattered in the fibre (Luna 2014). Therefore, the thermal expansion of the host structure and the temperature effect on the scattered light in the fibre must be considered in order to obtain thermally-compensated strains. As mentioned before, strain and temperature conversion coefficients are used to convert the spectral shift into strain or temperature data.

For example, a coefficient of $1 \text{ GHz} = -0.634 \text{ }^\circ\text{C} = -6.67 \text{ } \mu\epsilon$ will show a temperature effect on the FO sensor of about $10 \text{ } \mu\epsilon/^\circ\text{C}$. The mechanical strain can be calculated using Eq. 1 (Luna 2014):

$$\epsilon_m^z = \Delta v_S^z \cdot k_\epsilon - (0,95 \cdot \Delta v_T^z \cdot k_\epsilon + \Delta v_T^z \cdot k_T \cdot \alpha_L) \quad (1)$$

where ϵ_m^z = mechanical strain at depth z
 Δv_S^z = spectral shift in a strain FO cable at depth z
 Δv_T^z = spectral shift in a temperature FO cable at depth z
 k_ϵ = strain conversion factor (strain/frequency)
 k_T = temperature conversion factor ($^\circ\text{C}/\text{frequency}$)
 α_L = thermal expansion coefficient of a monitored element

4.2 Strain Data Interpretation

The axial strain should be determined from Eq. 2 using the average of the records of a pair of strain FO cables placed at opposing diameters and at equal distance from the center of the pile.

$$\epsilon_a^z = \frac{1}{2}(\epsilon_1^z + \epsilon_2^z) \quad (2)$$

where ϵ_a^z = averaged axial mechanical strain at depth z
 ϵ_1^z and ϵ_2^z = mechanical strain of two opposite FO strain cables at depth z

The axial force can be calculated by multiplying the processed mechanical strains with the pile stiffness (EA/L , $L=1$). The stiffness of the concrete pile can be calculated using tangent or secant stiffness (Fellenius 2013; 2019).

The mechanical strain data of two opposite FO cables can be used to calculate: curvature, gradient (change of curvature), lateral displacement, bending moment, and shear force according to Eqs. 3 through 7.

$$\kappa^z = \frac{1}{d}(\epsilon_1^z - \epsilon_2^z) \quad (3)$$

$$\phi^z = \int_0^z \kappa \, dz + A \quad (4)$$

$$u^z = \int_0^z \phi \, dz + B \quad (5)$$

$$M^z = EI\kappa^z \quad (6)$$

$$Q^z = \frac{d}{dz} EI\kappa^z \quad (7)$$

where κ^z = curvature at depth z
 d = distance between two FO sensors
 ϕ^z = gradient at depth z
 u^z = lateral displacement at depth z
 M^z = bending moment at depth z
 E = the Young's modulus of the element
 I = moment of inertia
 Q^z = shear force at depth z
 A and B = integration coefficients as determined by the boundary conditions.

4.3 Smoothing and Filtering of Data

For the subject project, the IU was set to record five times (one record per second) and the average was determined. To smoothen the distributed fibre optic data, a moving average was then calculated. For the steel pile, the moving length was 0.26 m and for the precast piles it was 1.0 m. For a concrete pile, it is necessary to check that the moving average has not become affected by a sudden change of stiffness (cross section) or a fissure.

Figure 7 shows an example of raw and average FO strain records. Outlier data points were removed before averaging.

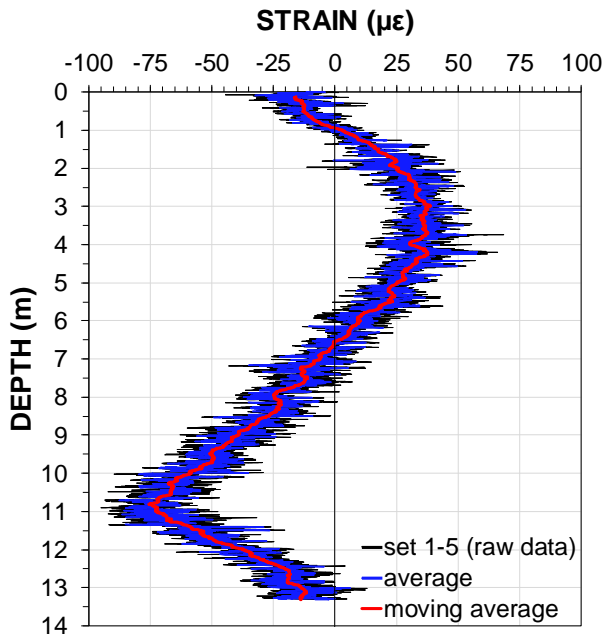


Figure 7 An example of raw and smoothed strain data obtained from an individual strain FO cable

5. PERFORMANCE OF FIBRE OPTIC CABLES IN PILES

5.1 Distribution of Strain along A Driven Steel Pile after Driving

The magnitude of strain introduced by the pile construction must be known and considered in the analysis of the strain records. Figure 8 shows the distributions of thermally corrected strain in four individual FO strain cables and the average (black line) obtained on November 13, 2017 immediately after driving a 11.5 m long 273-mm diameter, closed-toe steel pile. Negative values denote compression. One individual FO cable (S0013) reported a compression peak at 9.0 m depth, whereas its companion (S0011) did not show a similar peak. The records of this pair were removed from the average of the two pairs over the length between 8.8 through 9.4 m depth.

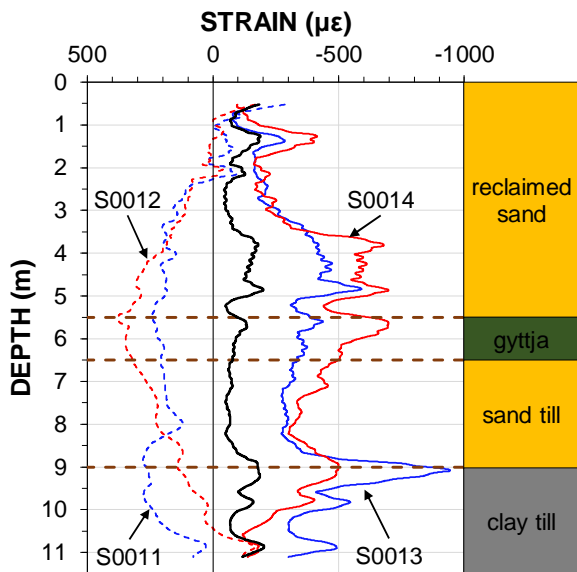


Figure 8 Distribution of strains along individual strain FO cables mounted on a driven steel pile

5.2 Performance of FO Strain Cables in Concrete Piles

5.2.1 Influence of non-uniform concrete pile stiffness

Figure 9 shows the strain distributions from an individual strain FO cable obtained for twelve load increments applied in a static loading test on the CFA pile. The small circles show the strains determined at the four VW gage levels for the last load increment (maximum load) applied to the pile. The strains measured by the two systems agree well.

The dashed horizontal lines show the depths of the stiffening rings of the reinforcement cage. The rings were size 6x60 mm and located every 0.97 m along the cage. It can be seen from the graph that a local strain reduction was observed in the FO cable at the locations of stiffening rings. This finding is in agreement with observations of Bersan et al. 2018, who investigated detection of highly localized small strains using a Rayleigh-based interrogation unit, Luna OBR4600. Kania and Sorensen (2018) reported the test setup and compared the two systems.

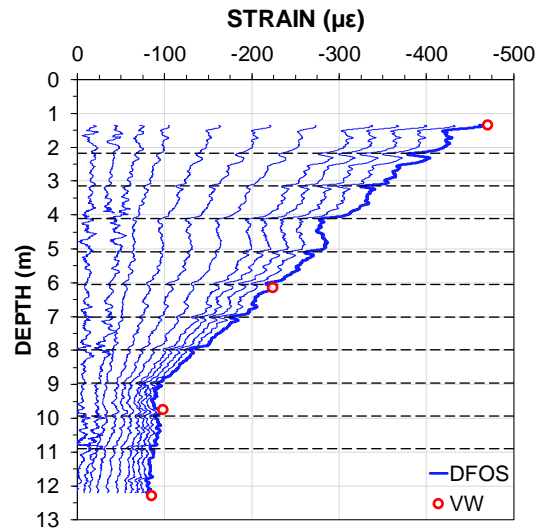


Figure 9 Strain distributions obtained from FO (all load increment) and VW sensors (the last load increment). The dashed, black lines indicate the location of stiffening rings (every 0.97 m)

5.2.2 Influence of cracks in precast concrete driven piles

Cracks and fissures may occur in driven precast concrete piles and even a fissure can distort the FO strain measurements. Figure 10 presents raw strain profiles between 9 and 10.2 m depth obtained from one of the FO strain cables mounted on the side surfaces (c.f., Figure 4b). of one of the precast concrete piles. The strains were measured at the listed selected days after placing the fill. Positive strain values denote compression. As can be seen from the data, numerous peaks of compression and tension appeared along the test pile. The peaks made the smoothing of the strain data difficult. For discussion of the ability to detect cracks in concrete piles using a Rayleigh based IU, see Monsberger et al. (2016)

5.3 Short- and Long-Term Influence of Temperature on Strain Fibre Optic Cables

The temperature considerations are important during short-term (e.g., during the process of pile installation) and long-term measurements for shallow depths where the ground temperature changes seasonally (Alberdi-Pagola 2018). Figure 11 shows the soil temperature on selected days at the test site. The temperature data were recorded from the VW gages installed on one of the driven steel piles. The graph shows that the ground temperature span was about 8 °C at 1 m depth and no more than 0.4 °C at 5.9 m. The temperature at about 10 m depth is equal to the mean annual air temperature at the site. The VW gages mounted on the other test piles indicated similar temperature profiles.

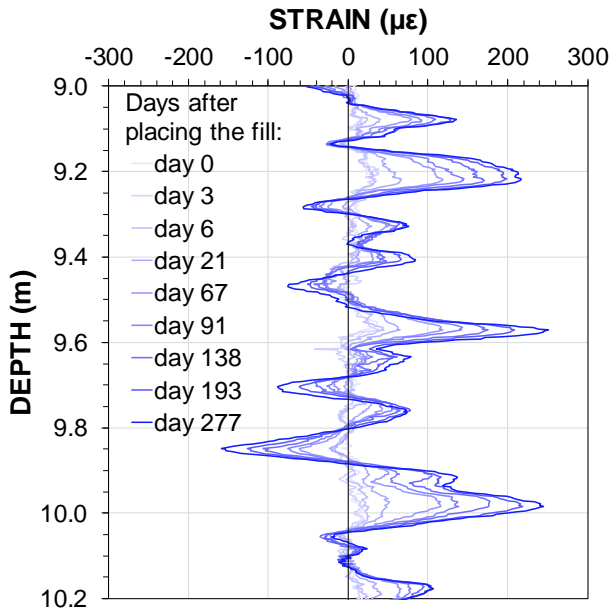


Figure 10 Evolution of cracks along precast concrete pile (raw strain from one of the strain FO cable mounted on the pile)

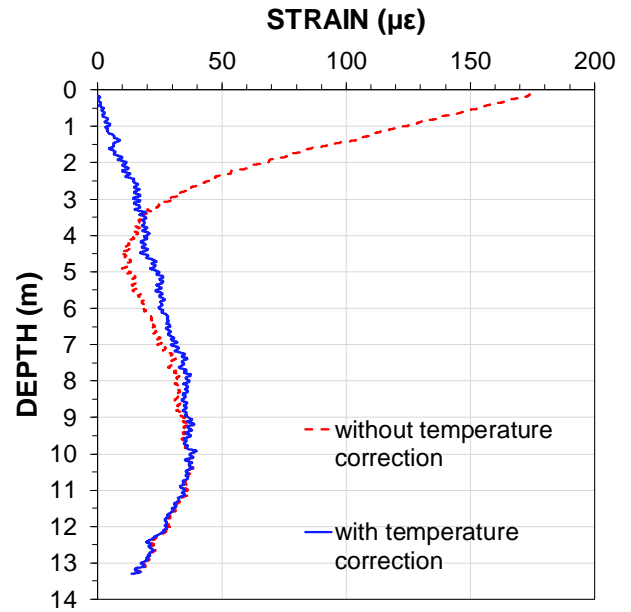


Figure 12 An example of the influence of temperature on the change of strain measured as average of two pairs of FO cables between Sep. 6, 2018 and Jan. 30, 2019

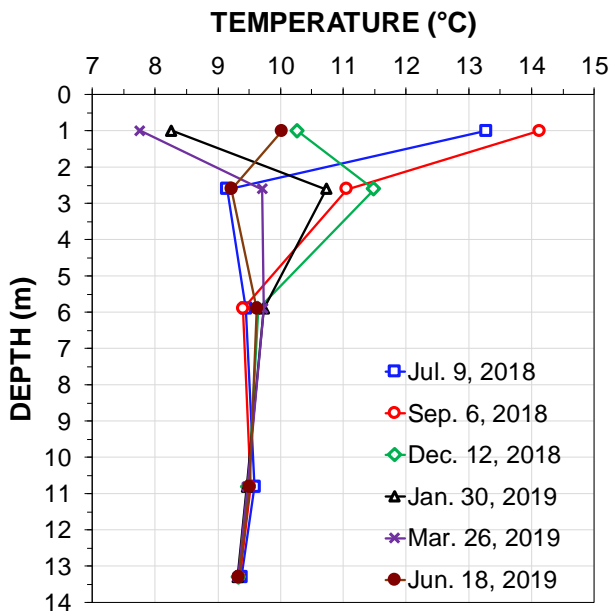


Figure 11 Soil temperature at selected days at the test site

Figure 12 presents the distribution of the average change of strain of two FO cable pairs between September 6, 2018, and January 30, 2019, due to development of negative skin friction, as measured by FO strain cables mounted on one of the steel piles. The records are shown with and without temperature correction. Positive strain values denote compression of the pile. As expected, a significant temperature correction was needed in the upper part of the pile, where the temperature changed by about 6 °C over initial through the final readings (see Figure 11). Below 9 m depth, the strain distribution with and without the temperature correction are the same, because the seasonal temperature change did not go deeper than that depth at the site (the temperature-corrected curve shows the strain change due to the development of negative skin friction along the pile after placing the fill at the site, resulting in increase of axial strain as the drag force built up and, then, the decrease as the positive shaft resistance reduced the axial force in the pile below a force equilibrium at about 10 m depth).

Figure 13 shows an example of the influence of daily temperature variations on the individual strain FO sensor mounted on the same steel pile. Negative strain values denote elongation of the pile. The initial reading was taken on September 6, 2018 at 06:30h and the figure shows the change of strain at 9:00h and 15:00h. It is very unlikely that mechanically induced strains would have influenced the strain measurements in the test pile during that 8.5-hour period. Therefore, the change above 1.0 m depth is related to temperature changes in the test pile (the spectral shift has changed in the fibre due to both the thermal expansion of steel and the refractive index of the fibre).

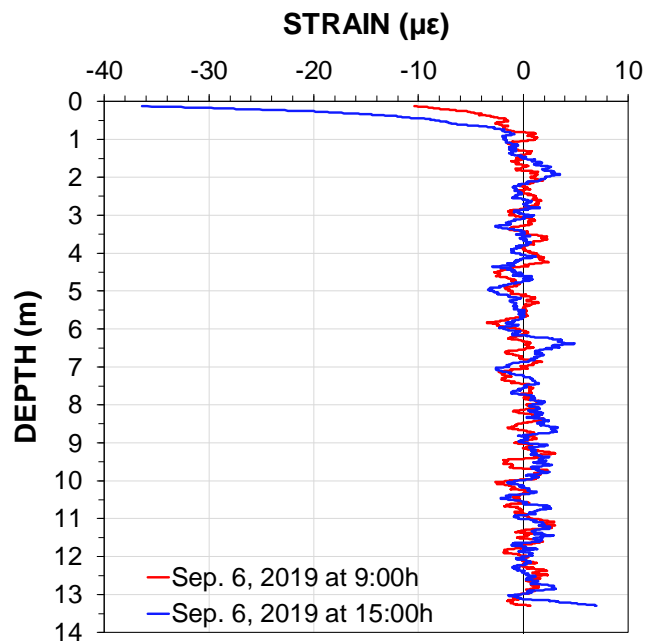


Figure 13 An example of the influence of daily ground temperature changes on the individual FO strain cable on Sep. 6, 2018 from an initial reading taken the same day at 06:30h

5.4 Performance of Gel-Filled Temperature Fibre Optic Cables

Loose tube gel-filled FO temperature cables were installed on the driven piles at the test site. Previous studies have reported the use of loose tube gel-filled FO cables as temperature sensors (Klar et al. 2006, Soga et al. 2015, Pelecanos et al. 2018). However, the findings of the current study show that the loose-tube gel-filled cables installed on driven piles might be influenced by mechanical strains. Figure 14 shows the temperature change between the reference reading recorded on Sep. 6, 2018 and the data recorded immediately after placing the 2.0 m thick fill on Sep. 14, 2018. The presented data were obtained from the VW and temperature FO sensors mounted on the steel test pile. As expected, both opposite mounted VW recorded only small temperature variations at the pile head (at 1.0 m depth) and no temperature change with depth during these 8 days between the reference and the first reading after placing the fill. The temperature change obtained from both opposite mounted VW were in agreement. In contrast, the temperature change profiles obtained from the individual FO temperature cables showed mirrored S-shape curves. Note that an increase and decrease in relative temperature indicates elongation and compression of a FO cable, respectively. The individual FO strain cables mounted close to the temperature DFOS-T0010 and temperature DFOS-T0012 showed similar S-shape compression and elongation respectively with similar S-shape curves. This finding suggests that the gel-filled temperature FO cables, used in this study, were affected by bending of the driven test piles after placing the fill.

5.5 Influence of lateral forces

In order to investigate the influence of lateral forces on a steel driven pile deflected due to one-sided surcharge loading, the data from two individual FO strain cables were compared. To determine the integration coefficients (cf. Eqs. 4 and 5), initial readings were taken after driving a pile and it was also assumed that the pile works as a cantilever beam fixed at the pile toe. Figure 15 shows the strain profiles obtained 126 days after driving the pile from the two individual FO strain cables (S1 and S2). Positive strain values denote elongation (tension). The strain profiles were smoothed using a moving average over 100 strain data spaced every 2.6 mm. Based on the presented strain data the curvature, gradient, and lateral displacement of pile were calculated using the Eqs. 3 - 5.

Figure 16 shows the (a) lateral displacement, (b) the gradient, and (c) the curvature of the steel test pile 126 days after driving. It can be seen from the data that the pile bent due to lateral soil movement at the boundary between the bottom sand layer and the soft soil layer (about 7.5 m depth). The pile head was displaced by about 50 mm.

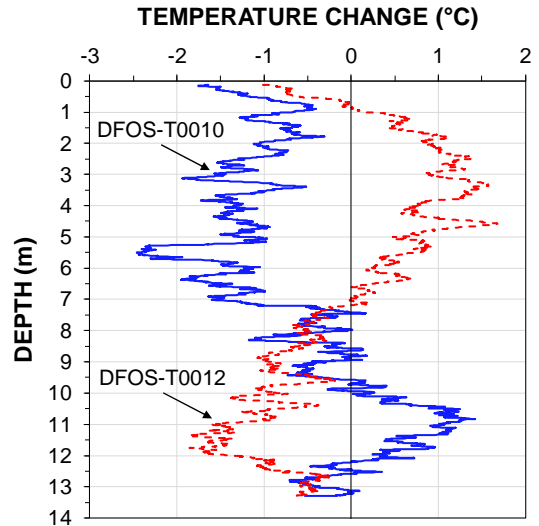


Figure 14 Temperature change obtained from the individual FO temperature cables immediately after placing the fill (Sep. 14, 2018) in reference to the initial reading of Sep. 6, 2018

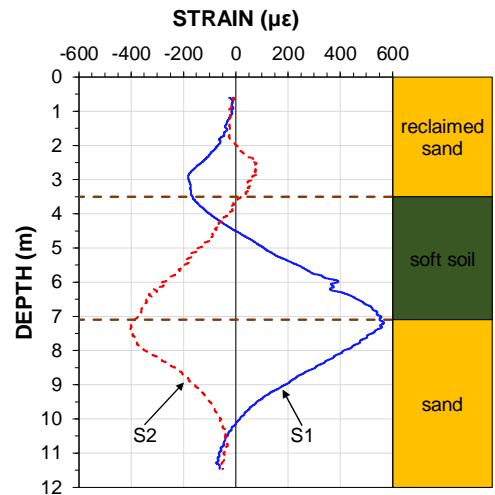


Figure 15 Strain profiles measured in the steel test pile 126 days after driving (the initial reading was recorded immediately after driving the pile)

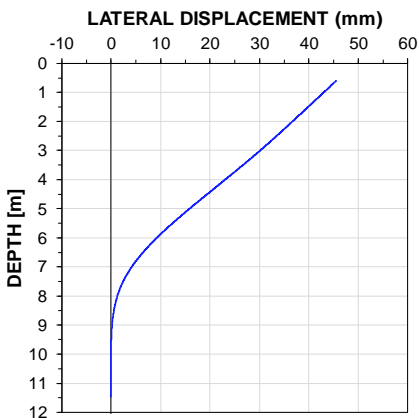


Figure 16 (a) Lateral displacement of the steel test pile recorded 126 days after driving

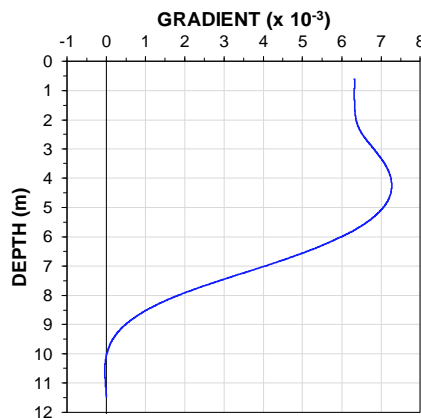


Figure 16 (b) gradient of the steel test pile recorded 126 days after driving

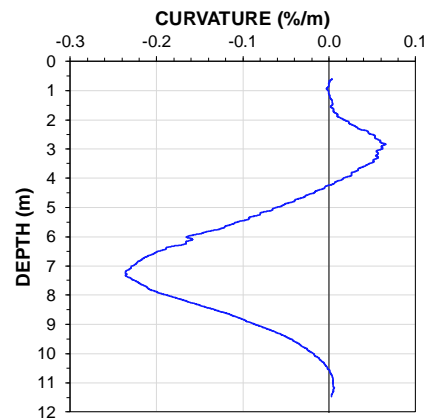


Figure 16 (c) curvature of the steel test pile recorded 126 days after driving

Figure 17 shows the bending moment and shear forces of the test pile due to lateral soil movement from strain change recorded 126 days after driving (the initial reading was recorded immediately after driving the pile). The bending moment and shear force were calculated using the Eqs. 6 and 7, respectively. As recommended by Mohamad et al. (2011), the strain records were smoothed and averaged before differentiation. The moving average was over 200 data points and 2.6 mm length. The shear force acting on the test pile at about 7.5 m depth (the boundary between sand and soft soil layer) was calculated to about 100 kN. Mohamad et al. (2011) highlighted difficulties with estimating shear forces based on the FO strain cable records due to the spatial resolution of the BOTDR analyser used in their study (approximately 1 m spatial resolution spaced every 50 mm). However, as mentioned before, the analyser used in this study had 5.2 mm spatial resolution and 2.6 mm sampling resolution.

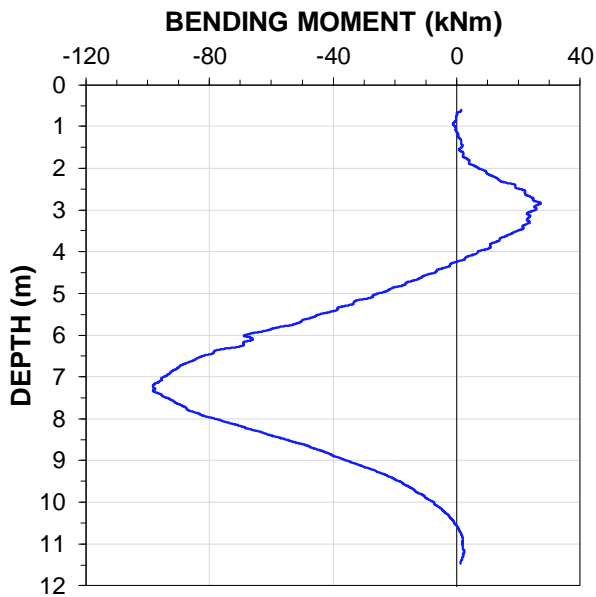


Figure 17 (a) Bending moment diagram

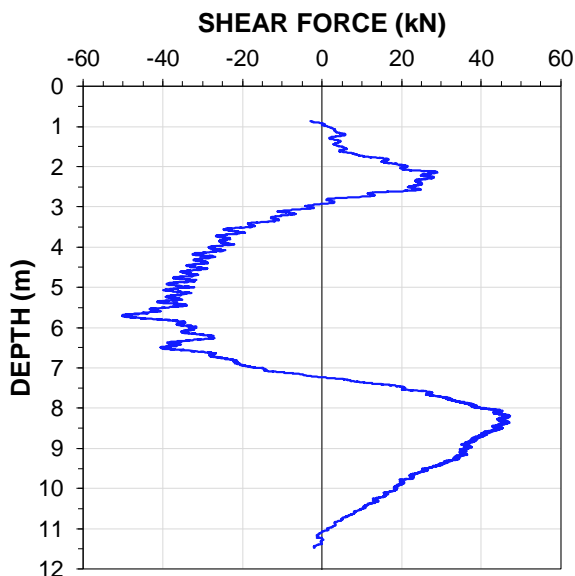


Figure 17 (b) shear force diagram

6. CONCLUSION

Prior studies have reported agreement between VW strain gages and distributed FO strain cables in piles (Mohamad et al. 2017, Pelecanos et al. 2018). This study confirms the agreement between the two instrumentation systems.

FO systems have the advantage over the conventional intermittent measurements (VW strain gages or retrievable extensometers) due to their providing continuous strain and temperature records. The Brillouin-based analysers have the spatial resolution of 0.5-1.0 m and sampling resolution of few centimetres. Such spatial resolution makes it difficult to detect local strain changes, e.g., due to concrete cracks (Zhang and Wu 2008). The Rayleigh-based analyser (Luna ODiSI B) used in this study has the spatial resolution of 5.2 mm and the sampling resolution of 2.6 mm. Therefore, it was possible to detect cracks in concrete (Figure 10) or local changes in pile stiffness (Figure 9).

A temperature change will always affect the FO cable regardless the pile material it is attached to. This is mainly due to temperature dependence of refractive index of the fibre core (Kersey et al. 1997, Luna 2014). In contrast, if the steel vibrating wire (inside a VW strain gage) and the steel or concrete pile has the same thermal expansion coefficient, temperature correction is not needed.

Driven and bored piles can be successfully instrumented with distributed FO cables. The FO cables can be glued directly on the surface or embedded in the piles. Placing the FO cables on the surface of a precast concrete pile will expose the cable to concrete cracks induced during driving.

Distributed FO cables are sensitive to both: temperature and strain changes, therefore, it is necessary to correct the records for temperature changes.

Loose tube gel-filled temperature FO cables used in this study were not suitable for driven piles since they were shown to be sensitive to mechanical strain. Owing to the spatial resolution of the interrogation unit used in this study, it was possible to detect highly localized strain changes due to fissures or change of pile cross section (stiffness).

The data can be smoothed by averaging over time or length. However, with smoothing over length, caution must be applied, as it might disguise local changes.

When two opposite strain FO cables are mounted in a pile, the information about axial and lateral deformation can be obtained. The DFOS can supplement the benefits of inclinometers installed in a pile.

7. ACKNOWLEDGEMENT

The authors would like to thank cp test a/s, Per Aarsleff A/S, Centrum Pæle A/S, DMT Gründungstechnik, GmbH and Innovation Fund Denmark for providing funding for this study and Per Aarsleff A/S for installing the instrumented test piles.

8. REFERENCES

- Alberdi-Pagola, M., 2018. Design and performance of energy pile foundations. PhD thesis. Aalborg University.
- Bersan, S., Bergamo, O., Palmieri, L., Schenato, L., and Simonini, P., 2018. Distributed strain measurements in a CFA pile using high spatial resolution fibre optic sensors. *Engineering Structures*, 160, pp. 554-565.
- Culshaw, B. and Kersey, A., 2008. Fiber-optic sensing: A historical perspective. *Journal of lightwave technology*, 26(9), pp. 1064-1078.
- Fellenius, B.H., 2013. Capacity and load-movement of a CFA pile: A prediction event. *GeoInstitute Geo Congress San Diego*, March 3-6, 2013, Honoring Fred H. Kulhawy—Foundation Engineering in the Face of Uncertainty, ASCE, Reston, VA, James L. Withiam, Kwok-Kwang Phoon, and Mohamad H. Hussein, eds., *Geotechnical Special Publication, GSP 229*, pp. 707-719.
- Fellenius, B.H., 2019. Basics of foundation design—a textbook. Electronic Edition, www.Fellenius.net, 484 p.
- Fellenius, B.H., Kim, S.R., and Chung, S.G., 2009. Long-term monitoring of strain in instrumented piles. *ASCE Journal of Geotechnical and Geoenvironmental Engineering*, 135(11), pp. 1583-1595.

- Inaudi, D. and Glisic, B., 2010. Long-range pipeline monitoring by distributed fiber optic sensing. *Journal of Pressure Vessel Technology*, 132, 011701.
- Kania, J.G. and Sørensen, K.K., 2018. A static pile load test on a bored pile instrumented with distributed fibre optic sensors. 10th International Symposium on Field Measurements in Geomechanics. Rio de Janeiro.
- Kechavarzi, C., Pelecanos, L., and Soga, K., 2019. Distributed fibre optic sensing for monitoring reinforced concrete piles. *Geotechnical Engineering Journal of the SEAGS & AGSSEA*, 50(1).
- Kechavarzi, C., Soga, K.B., Battista, N.D., Pelecanos, L., Elshafie, M.Z.E.B., Mair, R.J., 2016. Distributed fibre optic strain sensing for monitoring civil infrastructure - a practical guide, ICE Publishing, London, UK, 264p.
- Kersey, A.D., Davis, M.A., Patrick, H.J., Leblanc, M., Koo, K., Asking, C., Putnam, M., and Friebele, E.J., 1997. Fiber grating sensors. *Journal of lightwave technology*, 15, pp. 1442-1463.
- Klar, A., Bennett, P.J., Soga, K., Mair, R.J., Tester, P., Fernie, R., St John, H.D., and Torp-Peterson, G., 2006. Distributed strain measurement for pile foundations. *Proceedings of the Institution of Civil Engineers-Geotechnical Engineering*, 159, pp. 135-144.
- Kreger, S.T., Gifford, D.K., Froggatt, M.E., Soller, B.J., and Wolfe, M.S., 2006. High resolution distributed strain or temperature measurements in single-and multi-mode fiber using swept-wavelength interferometry. *Optical Fiber Sensors*. Optical Society of America, ThE42.
- Luna Inc., 2014. Distributed Fiber Optic Sensing: Temperature Compensation of Strain Measurement. Internal report.
- Luna Inc., 2017. ODiSI B. Data sheet.
- Mohamad, H., Bennett, P., Soga, K., Mair, R., and Bowers, K., 2010. Behaviour of an old masonry tunnel due to tunnelling-induced ground settlement. *Géotechnique*, 60(12), pp. 927-938.
- Mohamad, H., Soga, K., Pellew, A., and Bennett, P.J., 2011. Performance monitoring of a secant-piled wall using distributed fiber optic strain sensing. *ASCE Journal of Geotechnical and Geoenvironmental Engineering*, 137(12), pp. 1236-1243.
- Mohamad, H., Tee, B.P., Chong, M.F., and ANG, K.A., 2010. Investigation of shaft friction mechanisms of bored piles through distributed optical fibre strain sensing. 19th International Conference on Soil Mechanics and Geotechnical Engineering 2017, Seoul.
- Monsberger, C., Woschitz, H., and Hayden, M., 2016. Deformation measurement of a driven pile using distributed fibre-optic sensing. *Journal of Applied Geodesy*, 10(1), pp. 61-69.
- Nöther, N., Wosniok, A., Krebber, K., and Thiele, E., 2008. A distributed fiber optic sensor system for dike monitoring using Brillouin optical frequency domain analysis. *Smart Sensor Phenomena, Technology, Networks, and Systems 2008*. International Society for Optics and Photonics, 6933, pp. 69330T.
- Pelecanos, L., Soga, K., Elshafie, M.Z., De Battista, N., Kechavarzi, C., Gue, C.Y., Ouyang, Y., and Seo, H.J., 2018. Distributed fiber optic sensing of axially loaded bored piles. *ASCE Journal of Geotechnical and Geoenvironmental Engineering*, 144(3), pp. 04017122.
- Ravet, F., Niklès, M., and Rochat, E., 2017. A decade of pipeline geotechnical monitoring using distributed fiber optic monitoring technology. *ASME 2017 International Pipeline Geotechnical Conference 2017*. American Society of Mechanical Engineers.
- Soga, K., Kwan, V., Pelecanos, L., Rui, Y., Schwamb, T., Seo, H., and Wilcock, M., 2015. The role of distributed sensing in understanding the engineering performance of geotechnical structures. *XVI European Conference on Soil Mechanics and Structures*.
- Zhang, H. and Wu, Z., 2008. Performance evaluation of BOTDR-based distributed fiber optic sensors for crack monitoring. *Structural Health Monitoring*, 7(2), pp. 143-156.

CHAPTER 3

SOIL-PILE INTERACTION ANALYSED FROM A STATIC LOADING TEST

3.1. Introduction

The proposed research question was the soil-pile interaction analysed from an instrumented static loading test on a bored pile. Even though the soil profile did not consist of soft, subsiding soils, the development of residual force, presented in the manuscript, is similar to the development of drag force during long-term measurements. Disturbance due to installation of a bored pile will develop negative skin friction along the upper part of the pile and positive shaft resistance along the lower part of the pile (Fellenius 2015).

This chapter includes Journal Paper 2.

3.2. Assessment of the applied methodologies

The static loading test procedure (including the magnitude of the final load) was proposed by the contractor. It included two loading cycles with uneven load increments and time intervals. These events affected the analysis of the pile stiffness. The proposed maximum load was too little to fully mobilize the shaft resistance.

The stiffness of the pile was not assumed as a constant value, but was back-calculated as a function of induced strain. The back-calculated pile stiffness in Journal Paper 2 was presented as a linear function and not as an exponential function as presented in Conference Paper 1. Based on the mathematical relations (Fellenius 1989, 2001), the method used in Journal Paper 2 was more appropriate.

The load distribution based on measured strain suggested that the unit shaft resistance in the upper part of the pile is much greater than the unit shaft resistance in the middle and lower part of the pile. The obtained distribution of the unit shaft resistance was unexpected. Therefore, the existence of residual force was considered in the analysis.

3.3. Summary of the results

The main finding was that the best simulated function for the shaft and toe resistance appeared to be Gwizdała function (ratio function) with a different function coefficient for

the shaft and toe resistance. This means that the soil response was strain-hardening. The strain-hardening response of the pile toe is very common. However, it is not typical for the pile shaft resistance. It also means that for strain-hardening soil-pile interaction an ultimate resistance is hard to achieve despite of the induced movement.

3.4. Critical review

The maximum applied load was too small to fully mobilize the pile shaft resistance and achieve a failure movement criterion.

The analysis assumed the existence of residual force and did not provide any on site measurements that could support this assumption. A tension test performed after the compression test could support the existence of the residual forces. Placing some of the strain sensors in so-called no stress-strain enclosers (Geokon 2017) could help estimate the magnitude of concrete shrinkage before conducting the static loading test, and thus, quantify residual forces.

3.5. PhD student's contribution

The PhD student's contribution to Journal Paper 2 includes instrumentation of the test pile, collecting data from the VW sensors, analysing the data (proportional contribution) and writing the paper (proportional contribution).

JOURNAL PAPER 2

Kania, J.G., Sørensen, K.K., and Fellenius, B.H. Analysis of a static loading test on an instrumented cased CFA pile in silt and sand. ISSMGE International Journal of Geoengineering Case Histories. Submitted on December 2019.

Status: submitted on December 2019 to ISSMGE International Journal of Geoengineering Case Histories, revised and resubmitted on March 2020



Analysis of a static loading test on an instrumented cased CFA pile in silt and sand

Jakub G. Kania, Industrial PhD student, cp test a/s / Aarhus University, Vejle/Aarhus, Denmark; email: jakub@cptest.dk

Kenny Kataoka Sørensen, Associate Professor, Department of Engineering, Aarhus University, Aarhus, Denmark; email: kks@eng.au.dk

Bengt H. Fellenius, Consulting Engineer, Sidney, BC, Canada, V8L 2B9; email: bengt@fellenius.net

ABSTRACT: A static loading test was performed on an instrumented 630-mm diameter, 12.5 m long, cased CFA pile. The soil at the site consisted of a 4.0 m thick layer of loose sandy and silty fill layer underlain by a 1.6 m thick layer of dense silty sand and sand followed by dense sand to depth below the pile toe level. The instrumentation comprised vibration-wire strain-gages at 1.0, 5.8, 9.4, and 12.0 m depth. The pile stiffness (EA) was determined by the secant and tangent methods and used in back-calculating the distributions of axial load in the pile. A t - z / q - z simulation of the test was fitted to the load-movement distributions of the pile head, gage levels, and pile toe. The load-movement response for the shaft resistance was strain-hardening. The records indicated presence of residual force. Correction for the residual force gave a more reasonable shaft resistance distribution and indicated an about 600 kN residual toe force.

KEYWORDS: Soil-pile interaction, load-transfer functions, beta-coefficient, residual force, vibrating wire strain gage

SITE LOCATION: [Geographic Database](#) (requires Google Earth)

INTRODUCTION

This paper presents results from a static loading test on an instrumented cased CFA pile embedded in silt and sand. The pile type is somewhat new to the Danish practice which mostly uses driven precast concrete piles. Only little local experience is available on bored piles, notably, continuous flight auger piles. However, the bored pile is widely used internationally (e.g., Touma and Reese 1972, Gwizdała 1984) and Platzek and Gerressen (2010) describe the cased continuous flight auger pile.

In regard to piled foundations, the Danish practice is regulated and mandated by National Annex to the Eurocode (DS/EN 1997-1 DK NA:2015), which limits the shaft resistance of bored piles to 30 % of that for a similar driven pile and the unit toe resistance of bored piles to 1,000 kPa, unless a larger bearing resistance can be demonstrated. This principle was introduced in the Danish code for foundations in 1977 with some adjustments in 1984 and 1998 (Knudsen et al. 2019). The restriction limits the use of bored piles in Denmark.

The paper presents a case study of the response of cased CFA piles in silt and sand. The results support modifying the rules in regard to bored piles constructed as cased CFA piles in the National Annex to the Eurocode.

MATERIALS AND METHODS

Soil profile

The construction site was located in Viborg, Denmark. Prior to the pile test, the site was excavated to between 2 to 3 m depth over a 50 by 120 m area. The test pile was installed at 3m distance from the nearest excavation slope, 1-1.5(H):1(V). Figure 1 shows the results of a CPT sounding pushed 8 m from the test pile. Figure 2 shows the CPT soil classification chart according to the Eslami-Fellenius method (Eslami 1996). The classification is also indicated in the soil profile at the right of Figure 1.

Info to be filled by Journal formatting staff. Do not move this box from the first page and do not change its size

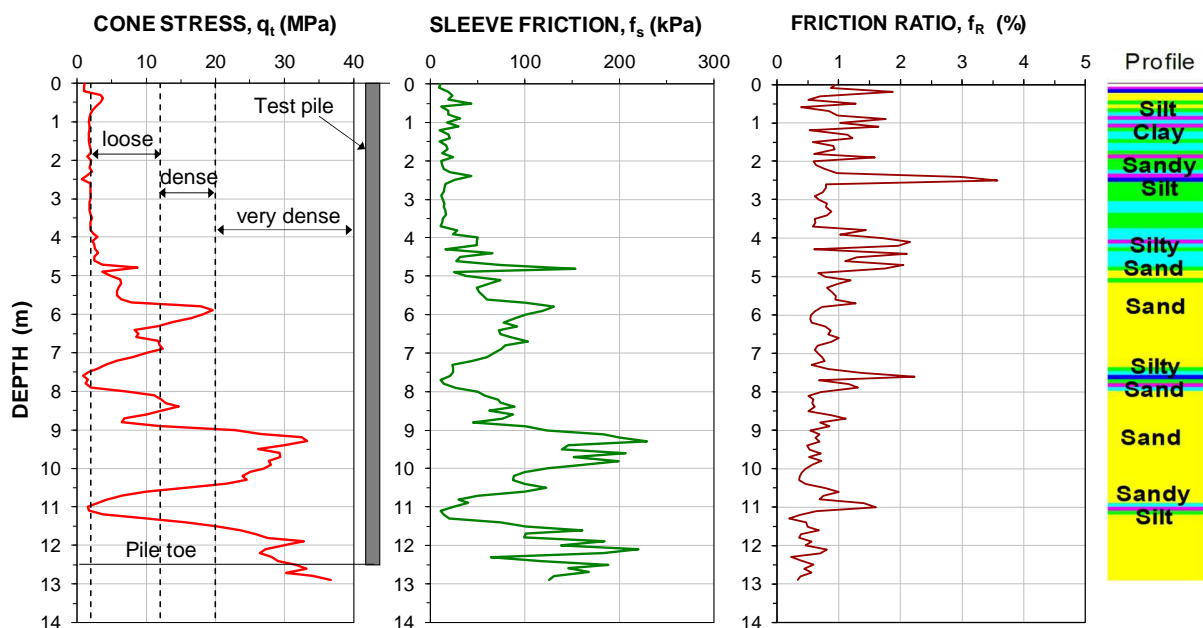


Figure 1. Results of a CPT sounding pushed 8 m from the test pile.

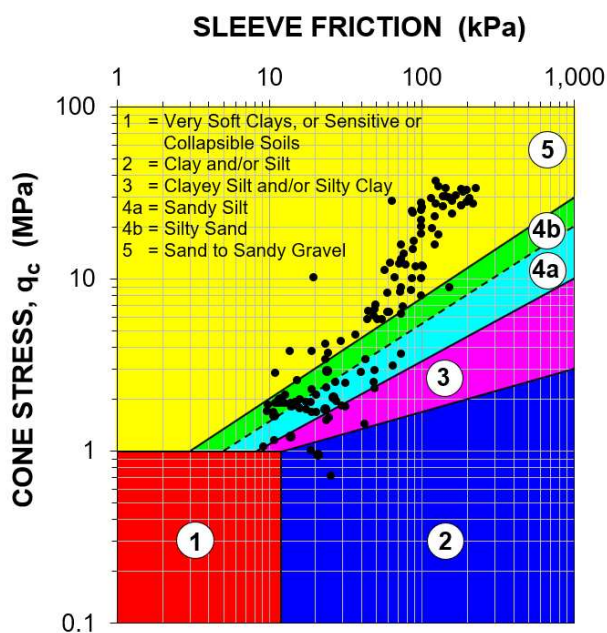


Figure 2. CPTU soil classification chart according to the Eslami-Fellenius method (Eslami 1996).

The soil profile below the excavation level consists of three layers, as follows:

- Sandy and silty fill to about 4.0 m
- Silty sand and sand to 5.6 m
- Sand to the end of the CPTU sounding at 13 m depth with a zone of silty sand at sandy silt.

The sand between 5.6 and 9 m depth is loose, but for a 0.8 m thick dense zone at 6 m depth and an almost very loose zone of silty sand at about 7.7 m depth. Below 9 m depth, the sand is dense to very dense, but for an about 0.3 m thick zone of loose sandy silt at 11 m depth.



Figure 3a shows the soil profile and water content distribution (the distances to the test pile location are indicated in the figure caption). The water content was determined on relatively intact samples considered to have neither gained nor lost water due to the sampling process. The average water content to 5.4 m depth was about 14 %. The water content of the sand layer was about 3 % at 5.7 m depth increasing to about 15 % at 12.7 m depth with an intermediate 25 % silty layer at 8.7 m depth. The groundwater table was at about 9.7 m depth (measured June 30, 2016). The unit densities, according to the geotechnical report (GEO 2016), were on average 1,900, 1,700, and 1,800 kg/m³ of the fill, silty sand and sand, and sand layers, respectively. Figure 3b shows the undrained shear strength obtained from field vane test and calculated from CPT profile using N_k equal to 15, as conventionally recommended. The shear strength of the fill layer obtained from the field vane test is similar to the distribution of the vertical effective stress. The shear strength obtained from the CPT (using $N_k=15$) is about three times greater than the one obtained from the field vane test.

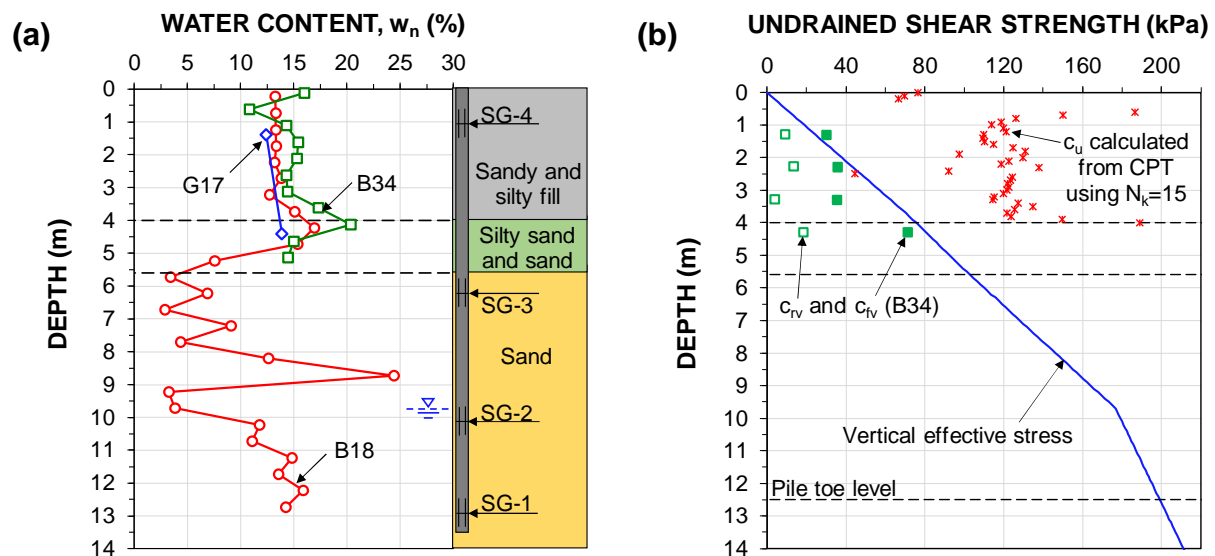


Figure 3. (a) Soil profile and distribution of water content. Data are from three soil borings: B34 (performed in October, 1989; 13 m from the test pile), B18 (performed in December, 2014; 27 m from the test pile), and G17 (performed in June, 2016; 8 m from the test pile); (b) undrained shear strength determined from the field vane test (peak, c_{fv} , and remolded, c_{rv}) and CPT and the distribution of vertical effective stress.

Test pile

The test pile was a nominal 630 mm diameter, cased CFA pile drilled to a depth of 12.5 m on July 13, 2017. After augering to the final depth, the concrete was pumped through the hollow stem of the auger while withdrawing the auger with the casing. When the casing end was withdrawn to about 7 m depth, the supply of concrete was unintentionally stopped and the concreting process interrupted. Within less than 3 hours after the interruption of the initial concreting process, the pile was re-augered to the required depth (i.e. 12.5 m). The concreting process was then restarted and successfully finished. The pile head was encased with a 630-mm diameter, 1,000 mm long pipe. The pile stick-up (height above the ground surface) was 300 mm. Accidentally, the 1,000-mm pipe was placed 30-mm off center with the reinforcing cage.

Vibrating wire (VW) sister-bar strain gages (SG) were installed at four depths (one opposite mounted pair at each level): 12.0 m (SG-1), 9.4 m (SG-2), 5.8 m (SG-3), and 1.0 m (SG 4). The gages were mounted on a 470 mm diameter reinforcement cage placed centrally in the pile. Thus, the nominal thickness of the concrete cover was 80 mm. The cage consisted of twelve 20 mm diameter main reinforcing bars and 12 mm spiral reinforcement on 150 mm spacing. Additionally, the reinforcing cage had 6x60 mm flat bar stabilizing rings spaced every 970 mm. The 1 m long lowermost section of the cage was tapered to 320 mm diameter and consisted of six 20 mm diameter, 1.8 m long reinforcing bars (0.8 m overlap).

The test setup is presented in Figure 4. Before constructing the test pile, two groups of four piles of reaction piles were installed to 12.5 m depth. The free distance between the test pile and the closest reaction pile was 2.9 m (4.6 pile diameters). Each reaction pile was connected via a Dywidag bar to a system of reaction beams. A steel reference frame was anchored about 2.5 m from the test pile and the nearest reaction piles, covered by a tarp to protect it from sunshine. Details about the test setup are reported in Kania and Sørensen (2018). No telltales were installed.



Figure 4. The test setup.

Test procedure

A static pile loading test was carried on July 27, 2017, on the 14th day after the concreting of the test pile. The pile load was applied by a single hydraulic jack centered to the steel-pipe encased pile head and operated by an automatic load-holding pump. The load applied to the pile was measured with a load cell connected to a data logger. The pile head movement was monitored with three inductive displacement transducers also connected to the data logger.

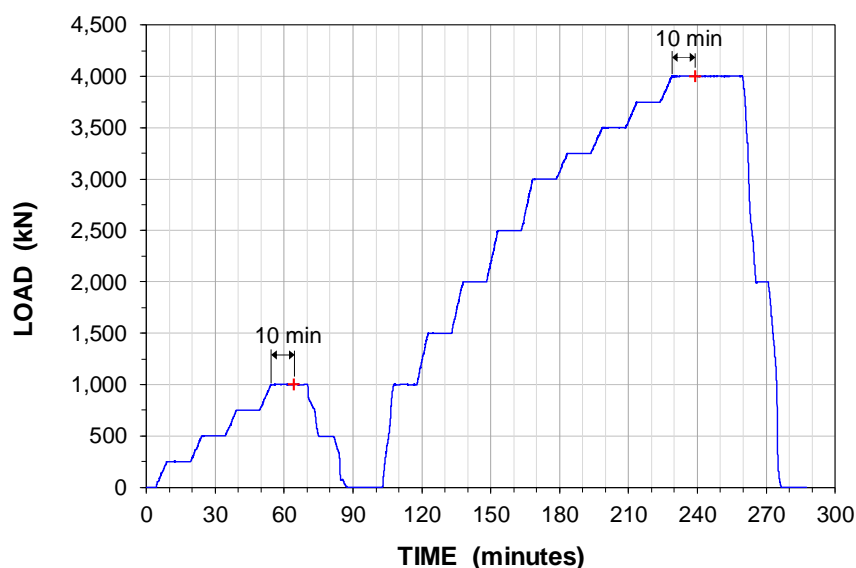


Figure 5. Load-time schedule (Data from Aamann-Svale and Møller 2017).

All gages and sensors were recorded at 1-second intervals. The test schedule is presented in Figure 5. The loading schedule comprised two loading stages. During the first stage, the load was increased to 1,000 kN in four 250-kN increments. Adding each increment took about 5 minutes and, afterward, the load levels were maintained for about 10 minutes. The 1,000-kN maximum load was maintained for 15 minutes, whereupon the pile was unloaded in two 500-kN steps with the half-load value maintained for 5 minutes. After a 15-minute wait, the pile was re-loaded to 1,000 kN in one step. Then, 500-kN load increments were applied to a total load of 3,000 kN. Beyond 3,000-kN load, the load increments were 250 kN. The final load was 4,000 kN. After 30-minutes load-holding, the pile was unloaded in two 2,000 kN load steps. Each unloading step took 5 minutes and the half-load was maintained for 5 minutes.



TEST RESULTS

Pile-head load-movement

Figure 6a shows the pile-head load-movement records and demonstrates that the load-holding device functioned well. At the 4,000-kN maximum load, the movement for the 5 minutes of adding load and the following 10-minute load-holding resulted in a 2.1 mm pile-head movement. The movement over the then following 20-minute extended load-holding was only 0.4 mm. The maximum pile-head movement amounted to 16 mm. Figure 6a shows that after reaching each intended load level, only small additional movement was recorded. The average movement rate calculated for the last 5 minutes at any load-holding ranged from 0.00 to 0.05 mm/min. The fast stabilization of movement is typical for piles in cohesionless soils.

Strain measurements

Figure 6b shows the strains measured at each gage of the four gage-level pairs. The uppermost gage-pair (SG-4A and SG-4B at 1.0 m depth) showed that bending occurred at the gage level, presumably due to the mentioned off-center placement of the short steel pipe at the ground surface. Bending was less pronounced for the other three gage levels. The axial force in the piles was determined from the average of the strain-gage pair at each gage level and the bending did not affect the evaluated axial loads.

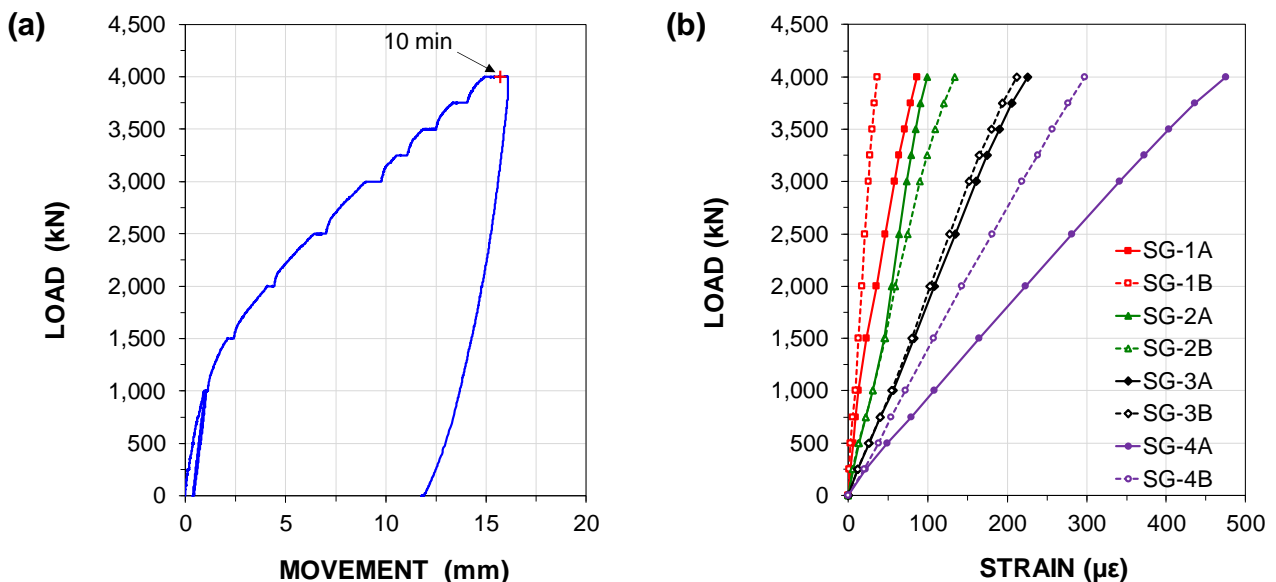


Figure 6. (a) Load-movement records of the test (Data from Aamann-Svale and Møller 2017); (b) strains measured at last reading for each gage level.

ANALYSIS

Pile stiffness

Figure 7 shows the measured load-strain records (average between two opposite strain gages) for Gage Levels SG-1 through SG-4. Generally, for gage levels at depths where the pile section between the gage level and the pile head is affected by a perfectly plastic-response shaft-resistance, the load-strain lines first rise steeply and become parallel when the resistance along the length above the strain gage location has been fully mobilized (Fellenius 2020). The slope of the straight portion of the lines then represents an approximate value of the pile stiffness. However, although the lines from the subject test results are straight, none of the lines indicates a change that would suggest full mobilization of shaft resistance and the lines are not parallel. This is an indication that the soil at the imposed movement has not develop a perfectly plastic response, but instead the soil response continues to be strain-hardening. Moreover, the linear regression of the line for SG 4, the gage level that was essentially unaffected by shaft resistance, does not extend to the origin, but shows an approximately 50-kN force in the pile. This could be due to the combined effect of the bending induced by the off-center relation of the jack in relation to the



reinforcing cage at the pile head not making the gage pair average occur at the pile center, the stiffness difference between the pile portion encased by the steel pipe and the portion without steel pipe with the change occurring 300 mm above SG-4, the unloading-reloading, and/or a small contribution of shaft resistance along the 1,000-mm length from ground surface to SG-4. The conditions combine to make the direct secant modulus less precise.

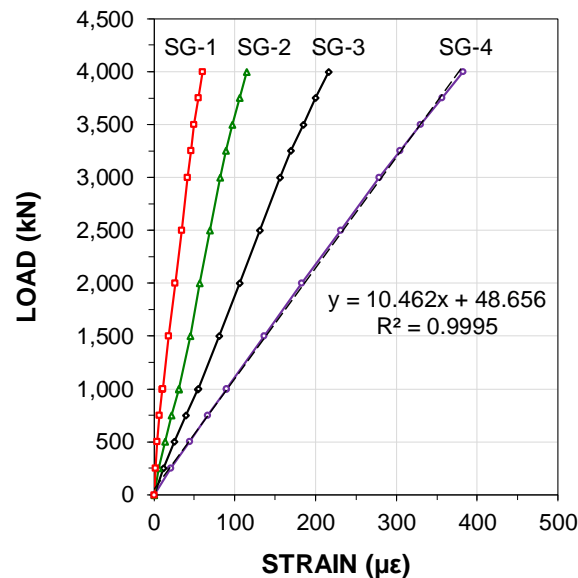


Figure 7. Load-strain from strain-gage levels SG-1 to SG-4 (last reading at each load-level).

The E-modulus of a concrete pile is often not a constant over the range of the applied loads, but reduces for increasing load (stress). Moreover, for cast-in-situ piles, the pile cross sectional area can differ from the nominal area along the pile. However, the pile axial stiffness, EA/L (the length, L , is usually set to 1 m), at a gage level usually shows a linear relation to the imposed strain. The stiffness can be determined directly from the test records (Fellenius 1989). The procedure provides a relation between the line showing tangent stiffness, $E_t A$, and the line showing secant stiffness, $E_s A$, as functions of the slope, a , and ordinate intercept, b , where $E_t A = \epsilon a + b$ and $E_s A = 0.5\epsilon a + b$. The tangent-modulus method does not depend on accurately knowing the zero reference of the strain records, but it does depend on having consistently well-established records unaffected by occasionally prolonged load-holding and unloading and reloading events. In contrast, the direct secant-modulus method is strongly affected by an error in the zero reference of the strain records as well as any prolonged load-holding and unloading and reloading events (Fellenius 2012; 2020).

Figure 8a shows the tangent modulus stiffness line for the subject test. The solid line with filled symbols shows the records for the reloading of the pile. The dashed line of with open symbols shows the records for the virgin loading. For the records from SG-4, where essentially no shaft resistance occurs, a relation for the tangent stiffness, $E_t A$, line could be determined. However, for the gage levels down in the soil, no linear tendency was established. Yet, the movement between the pile relative to the soil was well larger than 5 mm, a movement at which it is usually considered that the shaft resistance is fully mobilized (Fellenius 2020). For example, Nguyen and Fellenius (2013) reported a case with full mobilization of shaft resistance along 1,800-mm diameter, bored piles occurring at movements of 3 to 5 mm.

Possibly, the tangent modulus line for SG-3 could have developed a straight-line tendency had the test continued beyond the 16 mm maximum movement. However, that line would have been located much above the line for SG-4. The delayed establishment of the tangent modulus lines and the non-equal location of the lines is an indication that the soil at the site is strain hardening (Fellenius and Nguyen 2019).

If the instrumentation includes a gage level that has not been appreciably affected by shaft resistance along the distance between the gage and the load source (the case for SG-4), the strains measured at that gage level allow for determining the secant stiffness directly; $E_s A = Q/\epsilon$, where Q is the applied load. Figure 8b shows the secant stiffness versus strain records from SG-4, the gage level 1.0 m below the pile head. The solid line with filled symbols shows the records for the reloading of the pile. The dashed line of with open symbols shows the records for the virgin loading. The green straight-line without symbols shows the secant line converted from the tangent modulus method.

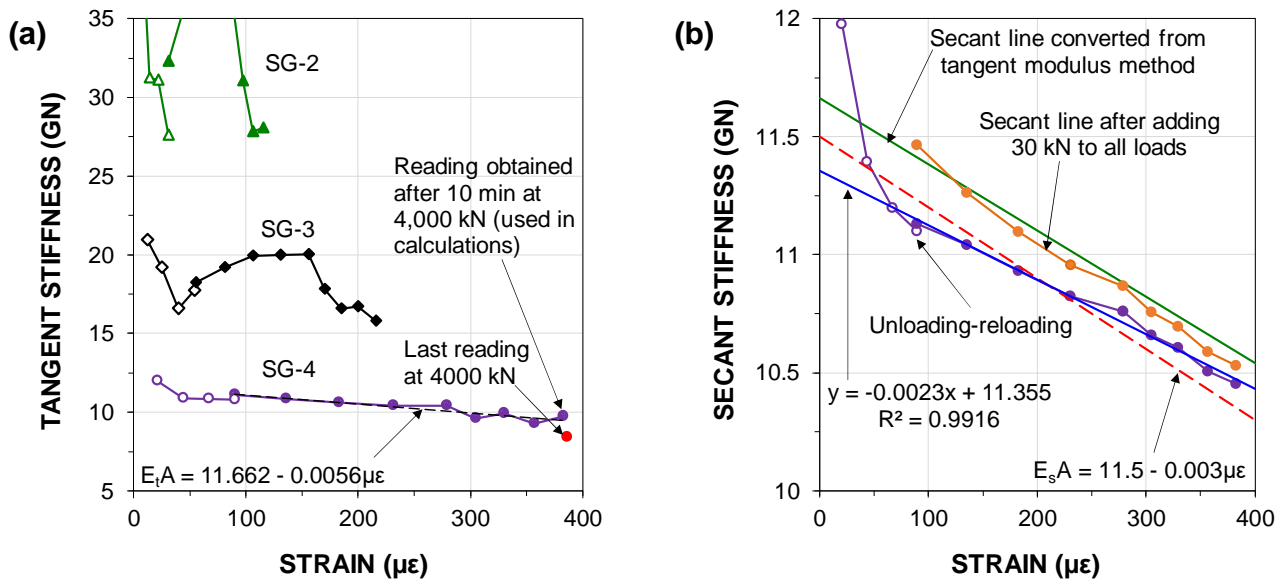


Figure 8. (a) Load-strain from strain-gage levels SG-1 to SG-4; (b) secant stiffness versus strain from SG-4.

A direct secant line may be affected by several undesirable effects, such as presence of a shaft resistance, incorrect reference to "zero-strain" (i.e., residual strain at the gage level), incorrect load values (e.g., using the pump pressure to obtain the applied load instead of an accurate load cell), differing length of load holding, and any unloading-reloading event. Normally, the secant lines determined by the direct secant and tangent methods agree (with due allowance to the larger scatter of the tangent method caused data by the differentiation). However, this is not the case here. As shown, when simulating uncertainty in the zero reference by adding a 30-kN load to each measured load value, the secant method line moves to close proximity to the tangent modulus line. The probable cause of the difference is the unloading-reloading event, although influence due to the proximity of SG-4 to the pile head (2 pile diameters) and the off-center load application cannot be ruled out. In the subsequent analysis it was decided to apply a secant line with a slope and location in-between the two plotted lines: $E_s A$ (GN) = 11.5 - 0.003 $\mu\epsilon$, as indicated by the dashed red line in the figure.

Measured and simulated load distributions

Figure 9 shows the load distributions for all loads applied in the reloading phase as converted from the measured strains using the secant stiffness. The two intermediate half-size loads employed in the test are shown as dashed lines. The 3,000-kN load that generated a 9.8 mm pile head movement was chosen as Target Load for the analysis. The red line shows the Target Load distribution.

A fit to the measured distribution of forces was first obtained by back-calculating the axial forces at Gage-Levels SG-1 through SG-4 for the 3,000-kN Target Load. The distribution of unit shaft resistance corresponding to the Target Force distribution was then correlated to the distribution of effective stress, which gave the distribution of the correlation coefficient, conventionally termed "beta (β)-coefficient". The β_{trg} coefficients that gave the fit for the shaft resistance in-between the gage levels are listed in the table to the right of the graph. The list also includes the corresponding average unit shaft resistances, r_s (kPa), for in-between the gage levels. It should be realized that the β_{trg} -coefficients simply represent the ratios between the back-calculated unit shaft resistance and the effective overburden stress as mobilized at the Target Movement.

The simulation assumed a level ground surface around the test pile. However, the area around the test pile was not fully level and the excavation slope was only about 3 m away from the test pile. Therefore, the effective overburden stress will have been somewhat larger than assumed in the simulation. A repeat analysis including the increase of the effective stress along the test pile due to load imposed by the area outside the project calculated for a wide embankment sloping 1-1.5(H):1(V) upward from a point 3.0 m away from the test pile, showed that this would reduce the β_{trg} -coefficients in the lower layers from 0.43 to 0.41, i.e., by 5% in the lower part of the pile and a difference of about 100 kN (1%) in total resistance. However, showing results to more than one decimal precision would essentially be just for "cosmetic" reason. The about 2 m elevation difference is too small to have any significant effect on the test pile response to the applied load. The calculations applied Boussinesq distribution and were performed using the UniPile5 software (Goudreault and Fellenius 2014).

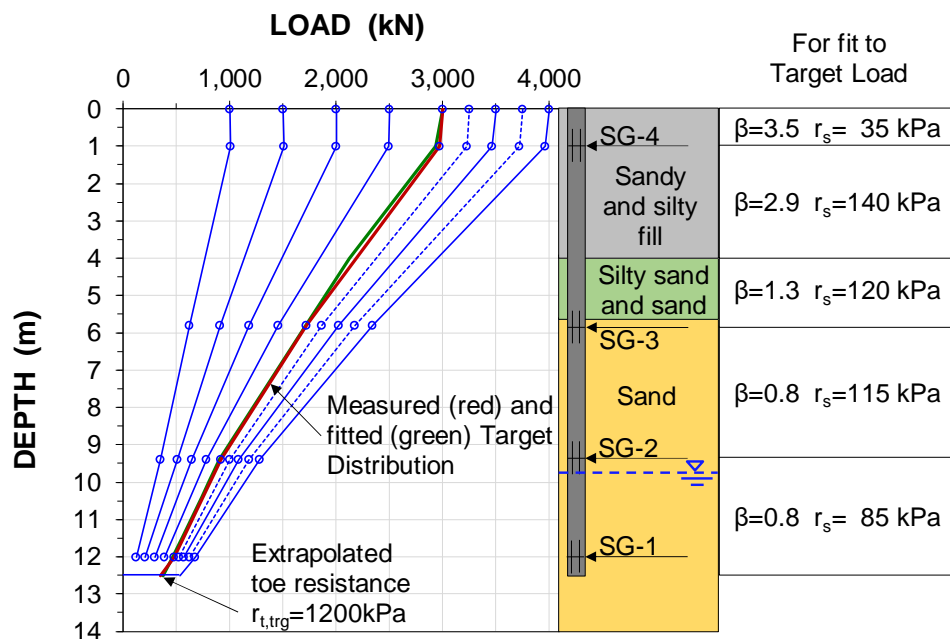


Figure 9. Measured and fitted load distributions.

Residual force and beta-coefficients

The measured unit shaft resistance for the 3,000-kN Target Load, corresponded to a β -coefficient of 3.5 at the ground surface reducing to about 0.4 at the pile toe level. Unrealistically, the unit shaft resistance back-calculated in the loose sandy and silty fill above 4 m depth was larger than that developed in the dense sand below. This is an indication that the pile was subjected to residual force, i.e., presence of axial force locked in the pile before starting the test (Mascarucci 2013, Fellenius 2015; 2020).

The residual force distribution is built up of negative direction shaft shear in the upper portion of the pile changing to positive direction along some transition length. The associated movement must be small and, presumably about the movement necessary to build up the Target resistance. In the absence of actual measurements of the distribution of axial force in the pile before the start of the static loading test, the distribution has to be estimated from the distributions induced during the test, as follows. We have assumed that down to SG-3 (≈ 6.0 m depth), the back-calculated unit shaft resistance was made-up of an equal part negative skin friction and positive shaft resistance and that between SG-3 and SG-2, the negative skin friction would start reducing and at SG-2 the shaft shear due to residual force be acting in positive direction. Moreover, because of the uniformity of the soil below 6 m depth, the beta-coefficient (ratio of the "true" unit shaft resistance to the effective overburden stress) could be assumed about constant with depth below SG-3 to the pile toe level. These assumptions resulted in the "true" distribution of axial force for the Target Load shown in Figure 10. The distribution adjusted for residual force is the green curve marked "Target Distribution w/o Residual Force". Subtracting the back-calculated distribution resulted in the red curve marked "Residual Force". After the correction for residual force, the evaluated unit shaft resistance showed to be more realistic, i.e., gradually increasing with depth, with a β -coefficient constant and equal to 0.6.

If the unit negative skin friction along the upper length would have been smaller than assumed, the "true" beta-coefficient in the lower portion of the pile would still be reducing with depth, still indicating presence of residual force. If assumed larger, this would have resulted in a larger "true" positive unit shaft resistance above the pile toe and a larger, probably overestimated, residual toe force.

After adjustment for residual force, the toe resistance would be about 970 kN (mobilized for the Target Load and the 5-mm Target Movement), as opposed to 370 kN, i.e., the residual toe force would be about 600 kN and the "true" toe stress about 3,100 kPa as opposed to 1,200 kPa. Considering the residual toe force, the toe resistance mobilized for the maximum load and the 13 mm toe-movement was about 1,100 kN as opposed to 530 kN, i.e., the "true" toe stress was about 3,500 kPa.

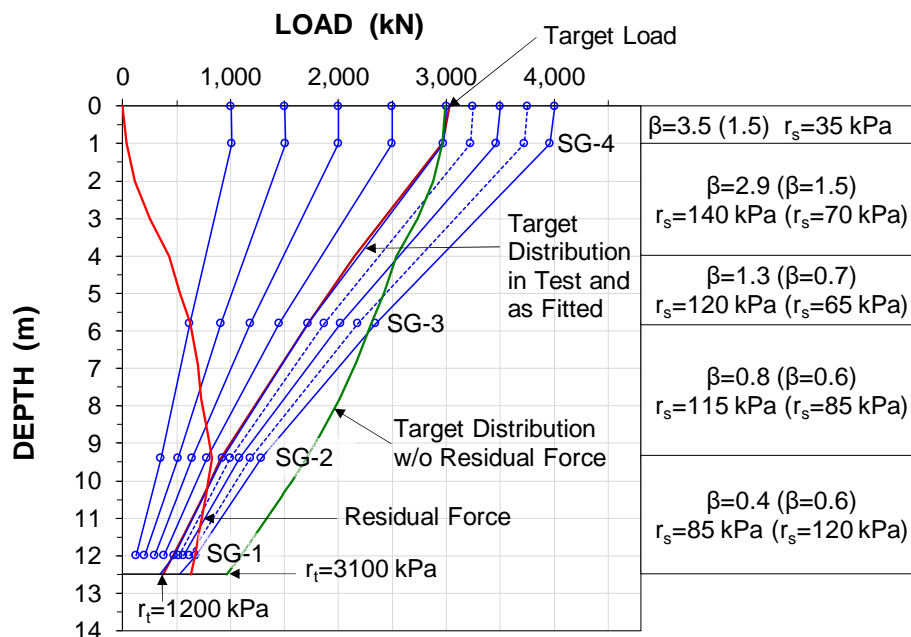


Figure 10. Back-calculated load distributions and distribution for the Target Load with and without residual force.

t-z and q-z functions

The test records show the measured load at the pile head and include the strain-determined force at the gage levels in respect to the movement measured at the pile head. The next step in the analysis of the test records was to calculate and fit load-movement curves to the measured pile-head curve and the strain-determined curve using t-z functions for the shaft response and a q-z function for the pile toe response (Fellenius 2020). Any t-z/q-z function can be made to intersect a specific load-movement point on a curve. Those points are, of course, the specific Targets for the fit to the measured loads. The process comprises choosing a suitable function, which intersects the target. Then, by adjusting the function coefficient the curve should fit the data points before and beyond the Target value. The curve-fitting analysis was performed using the UniPile5 software and proceeded by first fitting simulated t-z and q-z functions to the load-movement curve for the SG-1 level varying the input to the portion between SG-2 and the pile toe until a fit was achieved. Next, the procedure was repeated for 1.0 m long pile elements between SG-2 and SG-1, fitting the calculations to the load at SG-2 and measured pile head movement. The input for the first fit was kept intact. Afterwards, the analysis for SG-3 to SG-2, SG-4 to SG-3, and finally, for the pile head.

Of the several t-z/q-z functions available, ranging from strain-softening response through strain-hardening response, the process showed that only the strain-hardening function called "Gwizdala" function" (or "Ratio" function, or "Power" function) could be used to fit the test records (Gwizdała 1996). The function is defined by the following equation:

$$Q_n = Q_{trg} \left(\frac{\delta_n}{\delta_{trg}} \right)^\theta \quad (1)$$

where:

- Q_n = applied load
- Q_{trg} = Target Load (or unit shaft resistance)
- δ_n = movement mobilized at Q_n
- δ_{trg} = movement mobilized at Q_{trg}
- θ = function coefficient

Only two slightly different t-z function coefficients, θ , were needed. Figure 11a shows the measured load-movements curves together with the fitted curves. The latter are extrapolated to twice the actual movements. Figure 11b shows the t-z and q-z curves and the function coefficients that gave the fits.

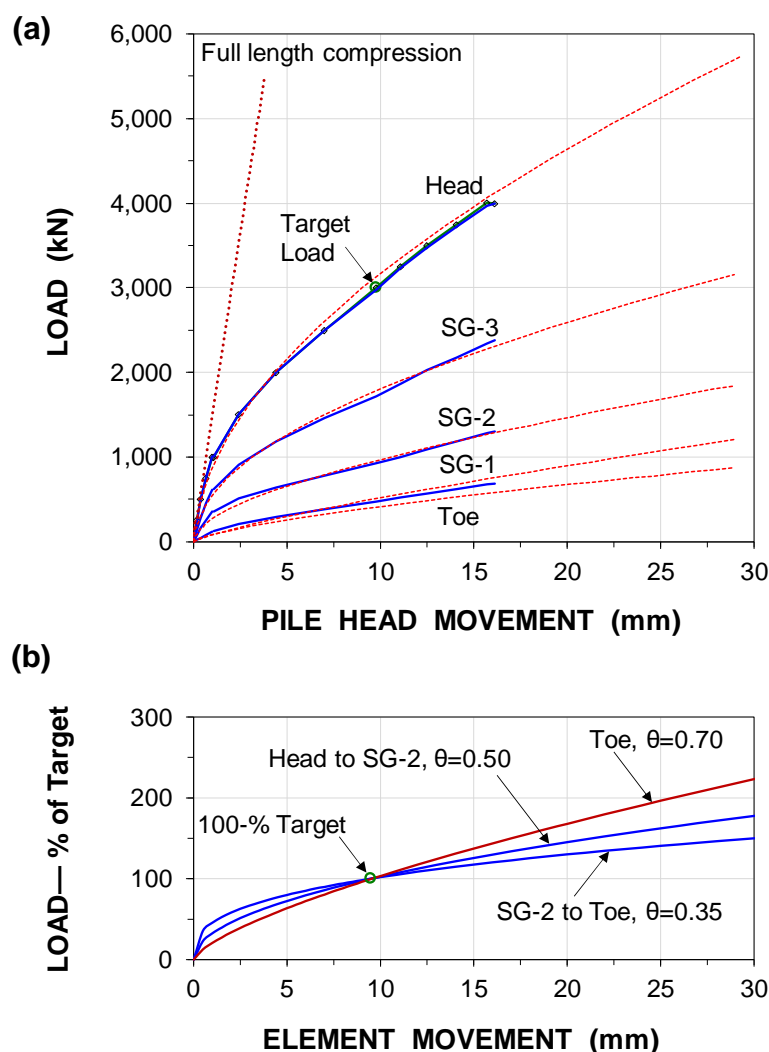


Figure 11. (a) Measured and fitted load-movement curves and (b) the associated t - z / q - z curves.

CONCLUSIONS

The analysis of the strain gage records showed that the unloading-reloading of the pile at the 1,000 kN load made the stiffness (EA) evaluated per the direct secant method less precise. By correlation to the results of the tangent method, the pile stiffness was determined to $EA \text{ (GN)} = 11.5 - 0.003 \mu \epsilon$ and this relation was applied to the strain records to calculate the axial loads in the pile at the gage levels.

The load distribution evaluated for the 3,000-kN Target Load, for which the pile head movement was 9.8 mm and pile toe movement was 7.8 mm, showed that about 370 kN reached the pile toe and the unit shaft resistance was largest at shallow depth and reduced significantly with depth. The beta-coefficients for the resistance mobilized by the Target Load were about 3.5 near the ground surface and 0.4 at the pile toe.

The back-calculations of the measured strains assumed that the pile was not affected by residual force. However, the evaluated distributions of shaft resistance indicated that residual force was indeed present in the test pile at the start of the test. The most likely distribution of residual force was determined and showed a more consistent mobilization of the pile shaft resistance as well as a 600-kN residual toe force. When adjusted for residual force, the toe resistance mobilized for the maximum load and the 13-mm toe-movement was about 1,000 kN as opposed to 530 kN, i.e., the “true” toe stress was about 3,500 kPa.



The fit to the measured load-movement curves showed that simulating the response with t - z and q - z functions per the Gwizdala method gave good fits for functions coefficients, θ , of 0.70 for the pile toe response, and 0.35 and 0.50 for the length below SG-2 (9.4 m depth) and the length above SG-2, respectively. These coefficients indicated that the soil is strain-hardening and that no ultimate resistance will develop even at movements somewhat larger than the 16-mm maximum imposed in the test.

The results show that the test pile shaft resistance is well within the range of that observed in driven piles and that already the toe resistance mobilized at the 13-mm maximum toe movement was several times larger than the 1,000-kPa limit indicated in the Danish Annex to the Eurocode. We believe that similar tests on further projects will show that the current Annex is overly restrictive in regard to CFA piles.

ACKNOWLEDGMENTS

The authors would like to thank cp test a/s, Per Aarsleff A/S, Centrum Pæle A/S, DMT Gründungstechnik, GmbH, and Innovation Fund Denmark for providing funding for this study and Per Aarsleff A/S for providing data and for installing the instrumented test pile.

REFERENCES

- Aamann-Svale, R., and Møller, O. (2017). "Midtbyens Gymnasium, Viborg. Statisk prøvebelastning". Aarsleff, Viby J, 23 p.
- Eslami, A. (1996). "Bearing capacity of piles from cone penetrometer test data". Ph. D. Thesis, University of Ottawa, Department of Civil Engineering, 516 p.
- Fellenius, B.H. (1989). "Tangent modulus of piles determined from strain data". *1989 Foundation Congress by F.H. Kulhawy*, ASCE, 1, 500-510.
- Fellenius, B.H. (2012). "Critical assessment of pile modulus determination methods. Discussion". *Canadian Geotechnical Journal*, 49(5) 614-621.
- Fellenius, B.H. (2015). "Static tests on instrumented piles affected by residual load". *Journal of the Deep Foundation Institute*, 9(1), 11-20.
- Fellenius, B.H. (2020). "Basics of foundation design—a textbook". Electronic Edition, www.Fellenius.net, 524 p.
- Fellenius, B.H., and Nguyen, B.N. (2019). "Common mistakes in static loading-test procedures and result analyses". *Geotechnical Engineering Journal of the SEAGS & AGSSEA*, 50(3), 20-31.
- GEO (2016). "Viborg Banegårds Alle. Gymnasie i 6 etager uden kælder. Geoteknisk og miljøteknisk undersøgelse.". Geo, Brabrand, 115 p.
- Goudreault, P.A., and Fellenius, B.H. (2014). "UniPile Version 5, User and Examples Manual.". UniSoft Geotechnical Solutions Ltd., [www.UniSoftGS.com], 120 p.
- Gwizdala, K. (1984). "Large diameter bored piles in non-cohesive soils". *Swedish Geotechnical Institute. Report no. 26*. Linköping, 154 p.
- Gwizdala, K. (1996). "The analysis of pile settlement employing load-transfer functions (in Polish)". *Zeszyty Naukowe Politechniki Gdańskiej, Nr 532, Budownictwo Wodne, nr 41*, Gdańsk, 192 p.
- Kania, J.G., and Sørensen, K.K. (2018). "A static pile load test on a bored pile instrumented with distributed fibre optic sensors". *10th International Symposium on Field Measurements in Geomechanics*, Rio de Janeiro, Brazil.
- Knudsen, J., Sørensen, K.K., Steinfeld, T.J.S., and Trankjær, H. (2019). "Design of bored piles in Denmark—a historical perspective". *XVII European Conference on Soil Mechanics and Geotechnical Engineering*, Reykjavik, Iceland.
- Mascarucci, Y., Mandolini, A., and Miliziano, S. (2013). "Effects of residual stresses on shaft friction of bored cast in situ piles in sand". *Journal of Geo-Engineering Sciences*, 1(1), 37-51.
- Nguyen, M.H., and Fellenius, B.H. (2013). "Large diameter long bored piles in the Mekong delta". *International Journal of Case Histories*, www.casehistories.geoengineer.org, 2(3) 196-207.
- Platzek, P., and Gerressen, F.-W. (2010). "Overview of the state of the art of double rotary drilling methods". *DFI and EFFC 11th International Conference – Geotechnical Challenges in Urban Regeneration*, London, 8p.
- Touma, F.T., and Reese, L.C. (1972). "The Behavior of Axially Loaded Drilled Shafts in Sand". *Texas Highway Department, Research Report 176-1*, Austin, 275 p.

CHAPTER 4

LABORATORY INTERFACE SHEARING TESTS

4.1. Introduction

The purpose of the laboratory interface shearing tests was to investigate the soil-pile interaction under more controlled test conditions than the full-scale tests. Furthermore, the focus was on comparison of the results obtained from the laboratory and full-scale tests in order to support the findings from both tests. Finally, the effect of shearing rate on the development of the shear stress between the soil and the bitumen coated concrete block was investigated.

This chapter includes Conference Paper 4.

4.2. Assessment of the applied methodologies

The modified direct shear test apparatus was chosen for the laboratory interface shearing tests. The bottom half of the box was replaced with a steel, concrete or bitumen coated concrete block to simulate the soil-pile interfaces from the full-scale test setups. Different shearing rates were applied to obtain drained and undrained shearing conditions similar to short- (e.g. pile installation) and long-term (e.g. soil consolidation) soil-pile interaction.

Undisturbed soil samples from the full-scale test sites were used in the tests in order to directly compare the results. The tested soil was a soft clayey silt (regarded as gyttja). For an individual interface test (i.e. soil/soil, soil/steel or soil/gyttja/concrete) an individual soil sample was used i.e. it was not changed for a given normal stress, but it was changed for a given interface type. Different shearing rates, assumed as drained and undrained, were applied during an individual shearing phase.

4.3. Summary of the results

The ratio of the interface angle of friction to gyttja angle of friction for concrete and steel was 1.0 and 0.8 respectively. These values were comparable with the values found in the literature (Potyondy 1961) and also with the ratio obtained in the full-scale measurements

The shear stress on the bitumen coated concrete block was highly dependent on the shearing rate. The shear stress decreased with the decreasing shearing rate. Comparing to the undrained shear strength of the tested gyttja the reduction was about 95 % at the slowest strain rate of $2.8 \cdot 10^{-6}$ 1/s. Similar finding was observed in the full-scale tests (see Chapter 6).

4.4. Critical review

The horizontal displacement obtained in a direct shear box is limited. Therefore, the residual stresses of the tested soft gyttja were not defined. It would be interesting to conduct a similar series of tests using a ring shear apparatus, where the range of horizontal displacement is much larger. Another disadvantage was the inability to measure pore water pressure changes.

The tests were performed on undisturbed soil samples which is different from the full-scale test conditions (remoulded soil after pile driving).

In this study multiple shearing rates were applied during a single shearing phase. This could affect the magnitude of the shear stress for the individual shearing rate due to the distinct vertical displacement at slow and fast shearing rates.

4.5. PhD student's contribution

The PhD student contributed to Conference Paper 4 in the research (planning, conducting and analysing the results obtained from the tests) and the writing phase in the major way.

CONFERENCE PAPER 4

Kania, J.G., Sørensen, K.K., and Fellenius, B.H., 2020. Shear stress between a soft soil and various pile materials.

Status: manuscript planned for submission to the 73rd Canadian Geotechnical Conference, Calgary, Canada, September 13 - 16.

Shear stress between a soft soil and various pile materials

Jakub G. Kania
cp test a/s and Department of Engineering, Aarhus University

Kenny Kataoka Sørensen
Department of Engineering, Aarhus University

Bengt H. Fellenius
Consulting Engineer

Abstract:

The relative movement between a pile and a soil causes shear stress along the pile. The shear stress depends on various factors including interface type and shearing rate. This paper investigates the development of the shear stress between a soft soil and a steel, uncoated and bitumen coated concrete block for different shearing rates, ranging from 0.01 mm/h to 100 mm/h. The tests were performed using a modified direct shear-test box, where the lower half of the box was replaced with an appropriate pile material block. The ratio between the interface angle of friction and the internal friction angle of the soil was 1.0 and 0.8 for the concrete and the steel block respectively. The shear stress between the soft soil and the bitumen coated concrete block decreased with a decrease of shearing rate. The bitumen coating significantly reduced the shear stress at low shearing rates.

1 INTRODUCTION

Shear stress between a pile and a soil is an important component in the design of piled foundations. Previous studies have shown that the shear stress depends on various factors including interface type and shearing rate. Potyondy (1961) highlights the importance of determining the values of shear stress between different types of soils (sand, silt, and clay) and pile materials (steel, wood, and concrete) including various surface roughness (smooth and rough). Furthermore, he proposes using the ratio between interface angle of friction to soil angle of friction, since the unit shaft resistance of the pile cannot be greater than the shearing strength of the soil. Lehane and Jardine (1992) showed that an organic clayey silt sheared at different rates using a ring shear apparatus experienced a moderate positive rate effect (6 % / log cycle) up to a velocity of about 6000 mm/h.

In a subsiding soil, the development of shear forces along a pile builds up negative skin friction. This needs to be considered for the structural strength of the pile (Tan and Fellenius 2016). Bitumen coating may significantly reduce the negative skin friction. However, the degree of reduction depends on the applied rate of shearing and temperature (Baligh 1978).

This paper investigates the shear stress of a soft clayey silt (regarded as gyttja) when sheared between a steel plate, uncoated and bitumen-coated concrete blocks at rates, ranging from 0.01 mm/h to 100 mm/h. The tests were performed using a modified direct shear-test box, where the lower half of the box was replaced with an appropriate pile material block.

2 MATERIALS AND METHODS

2.1 Soft soil properties

The soil samples used in the tests were trimmed from undisturbed tube samples obtained from a test field in Randers, Denmark at depths between 4.1 and 6.3 m. The soil properties (average) are summarized in Table 1. The soil samples were slightly overconsolidated (OCR about 1.2).

Table 1. The soft soil properties (grain size distribution and organic content data from Savery 2019)

Water content, %	105
Liquid limit, %	106
Plastic limit, %	46
Grain size distribution, %	
clay particles	14
silt particles	78
sand particles	8
Undrained shear strength, kPa	21
Sensitivity	4
Organic content, %	8
Compression ratio, CR,	027
Recompression ratio, RR,	0.04

2.2 Interface shear tests

The interface shear tests were performed using a modified direct shear testing device (Figure 1), where the lower half of the box was replaced with an appropriate pile material block. The concrete blocks were made from run-of-the-mill concrete with smooth surface. One of the concrete blocks was coated with a 1 mm thick 80/100 penetration bitumen coating. Both, the uncoated and the bitumen coated block were about 4 years old and used in previous studies. Before the tests on the bitumen-coated concrete block, the coating was heated and brushed to obtain a smooth and even 1 mm (± 0.1 mm) thick layer. The tests were then carried out when the coating had cooled to room-temperature, which was 23 to 24 °C.

The first series of tests were conducted to investigate the shear stress between gyttja and different pile materials. A standard direct shear test on a gyttja sample was also conducted for comparison. The tests were performed at 20, 40, and 60 kPa normal stress. The same soil sample was used for each normal stress. However, a new soil sample was used for

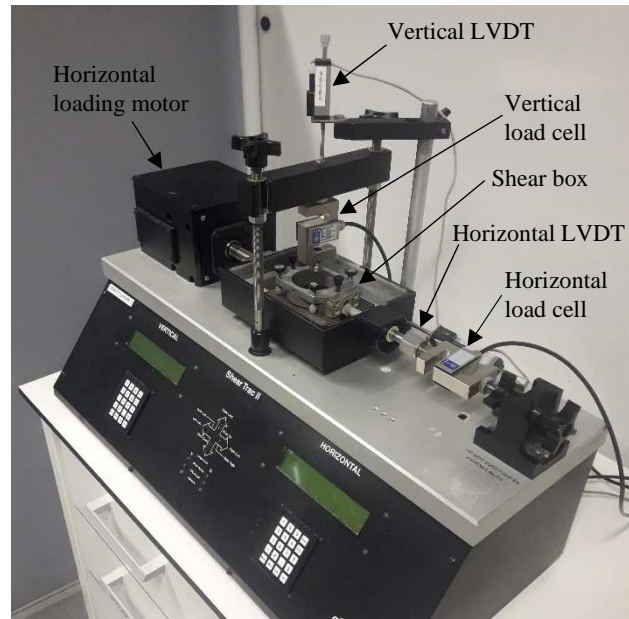


Figure 1. Interface shear test device.

each interface type. The shearing rates were defined as the value of the time to 100 % consolidation (based on the consolidation phase) multiplied by a factor of 12.7 and divided by the horizontal displacement required to reach constant volume (Head and Epps 2011). The distance before constant volume conditions was assumed as the maximum horizontal displacement planned in the test i.e. 10 % of the soil sample diameter (6.35 mm).

Table 2. Testing programme to investigate the effect of shearing rate on gytja.

Normal stress kPa	Shearing rate mm/h	Horizontal displacement mm
20	0.05	1.3-2.3; 3.3-4.3; 5.3-6.3
	0.25	0.0-0.8; 2.3-2.8; 4.3-4.8
	5	0.8-1.3; 2.8-3.3; 4.8-5.3
40	0.05	1.1-2.1; 3.1-4.1; 5.1-6.1
	0.25	0.0-0.6; 2.1-2.6; 4.1-4.6
	5	0.6-1.1; 2.6-3.1; 4.6-5.1
60	0.01	1.0-1.5; 3.0-3.5; 5.0-5.5
	0.05	1.5-2.0; 3.5-4.0; 5.5-6.0
	0.1	0.0-1.0; 2.0-3.0; 4.0-5.0

The second series of tests were performed to investigate the effect of the shearing rate on gytja and gytja/bitumen coated concrete block. The direct shear tests on the gytja sample was performed under three normal stresses applying five different shearing rates ranging from 0.01 to 5 mm/h as presented in Table 2. The interface shear test on gytja/bitumen coated concrete block was also performed under three normal stresses. Under each normal stress, the test specimen was sheared in two cycles: applying slow (drained conditions) or fast (undrained conditions) shearing rates as presented in Table 3.

Unfortunately, due to some unexpected events the testing programme was disturbed and some of the shearing cycles did not reach the planned maximum horizontal displacement (6.35 mm).

Table 3. Testing programme to investigate the effect of shearing rate on gyttja/bitumen coated concrete block.

Normal stress kPa	Cycle	Shearing rate mm/h	Horizontal displacement mm
40	Slow	0.01	1.8-2.3; 3.8-4.3; 5.8-6.3
		0.1	0.0-1.8; 2.3-3.8; 4.3-5.8
	Fast	1	1.0-1.5; 3.0-3.5;
		10	1.5-2.0; 3.5-4.0;
60	Slow	100	0.0-1.0; 2.0-3.0; 4.0-5.0
		0.01	1.8-2.3; 3.8-4.3; 5.8-6.3
	Fast	0.1	0.0-1.8; 2.3-3.8; 4.3-5.8
		1	1.8-2.3; 3.8-4.3;
80	Slow	10	0.0-0.8; 2.3-2.8; 4.3-4.8
		100	0.8-1.8; 2.8-3.8; 4.8-5.8
	Fast	0.01	1.8-2.3; 3.8-4.3;
		0.1	0.0-1.8; 2.3-3.8; 4.3-5.8
	Fast	1	0.0-0.2; 1.7-2.2; 3.7-4.2
		10	0.2-0.7; 2.2-2.7; 4.2-4.7
		100	0.7-1.7; 2.7-3.7; 4.7-5.7

3 RESULTS AND DISCUSSION

3.1 Effect of interface type

The results of the tests against different pile materials are presented in Figure 2. The shear stress on gyttja sample was increasing with the associated compression of the sample. Within the range of the horizontal displacement, none of the tests performed on gyttja samples mobilized a peak shear stress (the shear stress and the contractive vertical displacement was still increasing). The maximum mobilised shear stress at the maximum displacement of 6.35 mm on gyttja sample at 20, 40, and 60 kPa was 25.2, 37.3, and 61.8 kPa, respectively. In contrast, all tests on gyttja/pile material except one (gyttja/concrete at 20 kPa normal stress, Figure 2a), mobilized a peak shear stress followed by a plastic, strain softening or hardening response. The peak shear stress for the gyttja/steel sample at 20, 40, and 60 kPa was 10.1, 31.6, and 43.7 kPa, respectively. The peak shear stress for the gyttja/concrete sample at 20, 40, and 60 kPa was 15.4, 42.9, and 60.7 kPa, respectively. The peak shear stress occurred at about 2.3 and 4 mm for the gyttja/steel and gyttja/concrete interface respectively. The peak shear stress for the gyttja/bitumen/concrete sample at 20, 40, and 60 kPa was 3.2, 13.3, and 16.3 kPa, respectively. The peak shear stress occurred between 1 and 3 mm of horizontal displacement. The compression of the sample continued (gyttja/concrete interface) or stabilized after reaching the peak shear stress. The tests at given normal stress were carried out at shearing rates of the same order of magnitude.

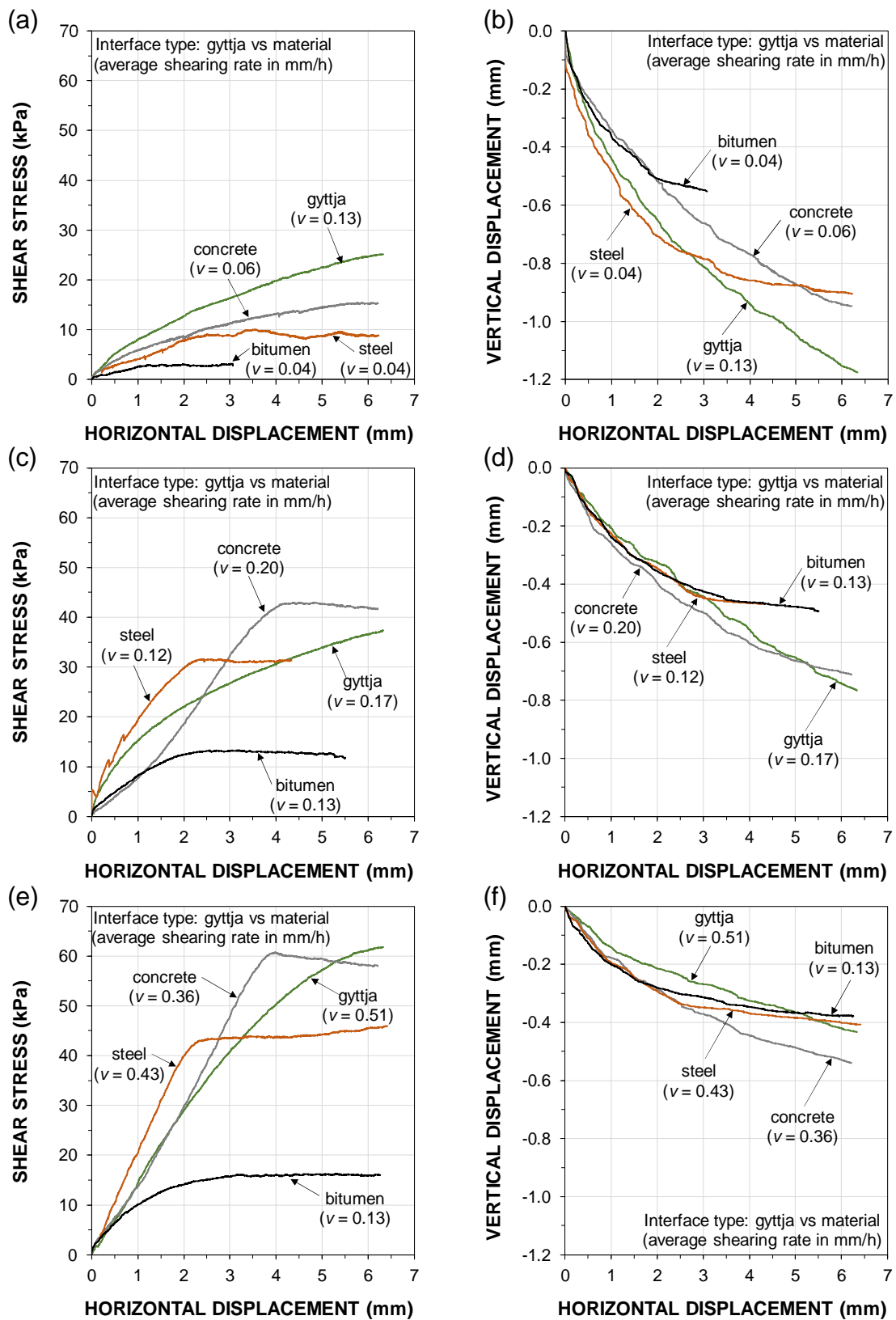


Figure 2. Shear stress and vertical displacement versus horizontal displacement from tests performed at: (a) and (b) 20 kPa, (c) and (d) 40 kPa, and (e) and (f) 60 kPa normal stress, respectively.

Figure 3 presents the failure envelopes for different interface types. The gyttja/concrete interface angle of friction, δ_c , was similar to the soil angle of friction, ϕ' ($\delta_c \approx 1.0\phi'$). The ratio of interface angle of friction to soil angle of friction for gyttja/steel shear test was 0.82. These results are in general agreement with results reported by Potyondy (1961) for silt-structure tests conducted using a shear box under normal stress ranging from 48 to 383 kPa.

As presented in Figure 3 the lowest interface friction angle was obtained for the gyttja/bitumen interface. However, according to the literature (Baligh 1978, Fellenius 1979, Khare and Gandhi 2009) the shear stress is highly dependent on the shearing rate, as also presented later in this study.

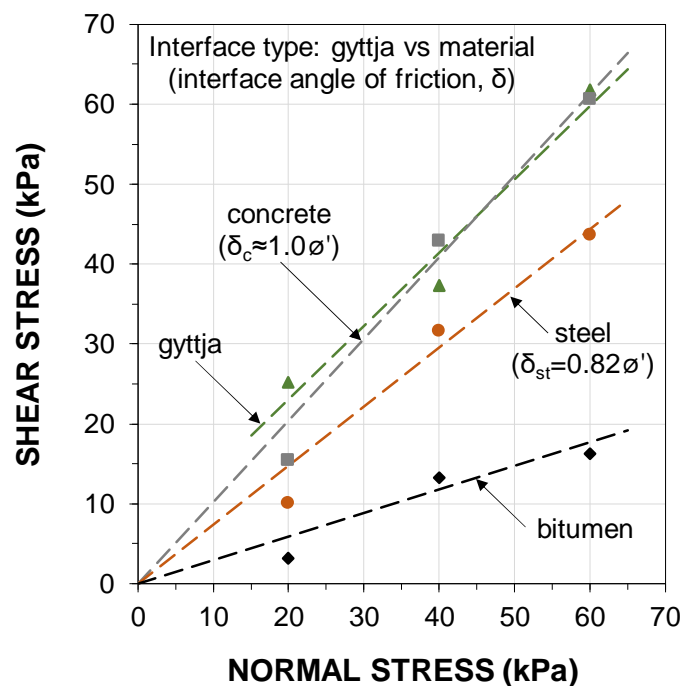


Figure 3. The maximum mobilised shear stress versus normal stress obtained from interface shear tests.

3.2 Effect of shearing rate

Figure 4 shows the results from direct shear tests on gyttja sample applying different shearing rates under three normal stress. The shear stress was increasing with increasing shearing rate. The contractive vertical displacement (Figure 4b) was increasing at low velocities (0.01 to 0.25 mm/h). However, the volume was constant at the largest velocity applied in this study (5 mm/h). This may indicate a shift from drained to undrained conditions. Tika et al. (1996) and Fearon et al. (2004) observed an increase or little volume change during fast shearing of cohesive soils using a ring shear apparatus. This finding was confirmed by Martinez and Stutz (2019) who studied the effects of shearing rates on kaolin clay samples sheared against steel plates with different roughness using a shear box device enhanced with an imaging system to analyse the soil deformation.

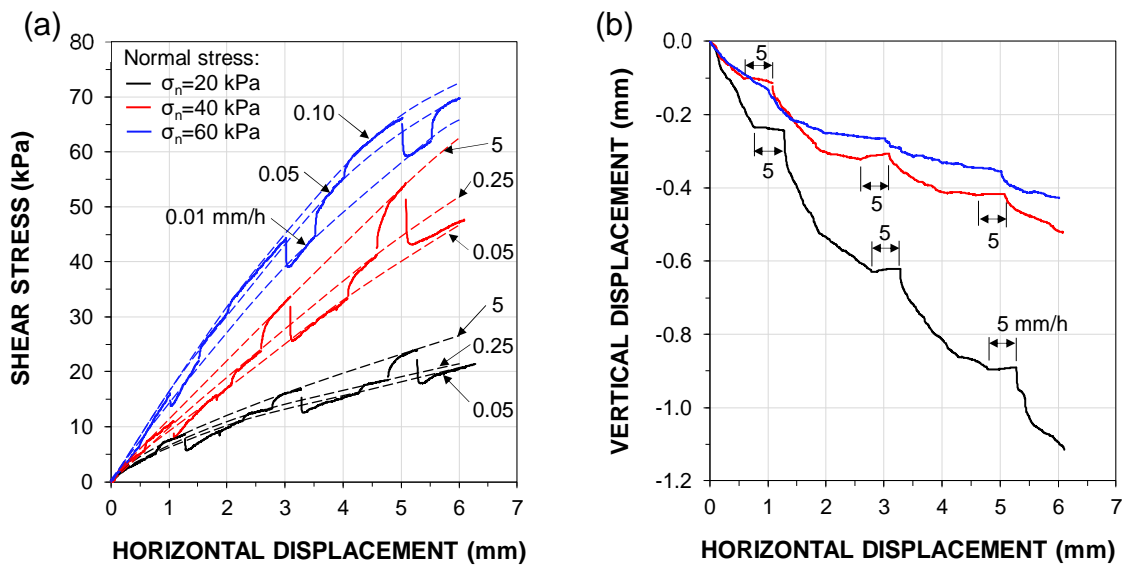


Figure 4. (a) Shear stress and (b) vertical displacement versus horizontal displacement at different normal stresses and shearing rates performed on a soil against soil sample.

Figure 5 presents the shear stress on gyttja samples normalized by the normal stress at different shearing rates. The increase in shear stress was about 16 % per log cycle. This finding is consistent with data reported by McCabe (2002) who found a positive rate effect from undrained triaxial tests performed on soft, organic, clayey silt. The tests were conducted under the confining stress of 100 kPa and subjected to triaxial compression at slow and fast axial strain rates ranging from 0.001 to 1 %/min. The author reported the increase of the undrained shear strength of 15 % per log cycle increase in strain rate.

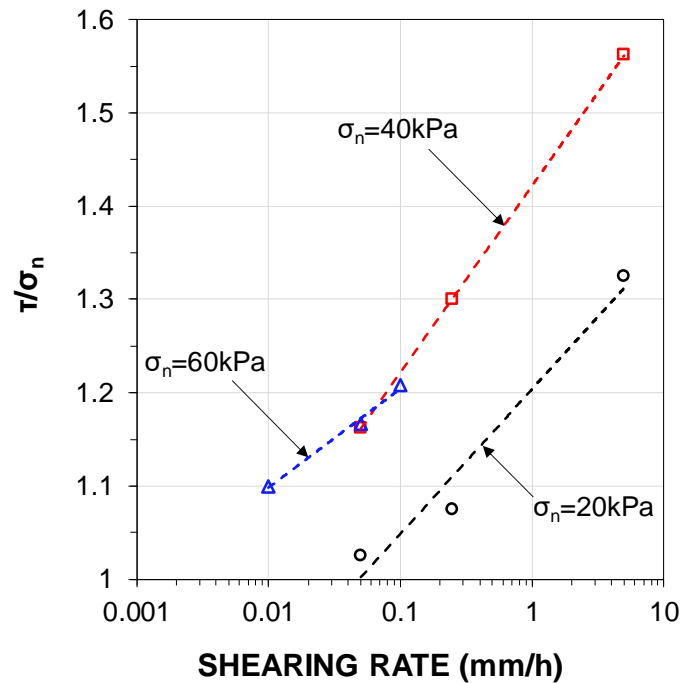


Figure 5. Normalized shear stress versus shearing rate (a gyttja sample).

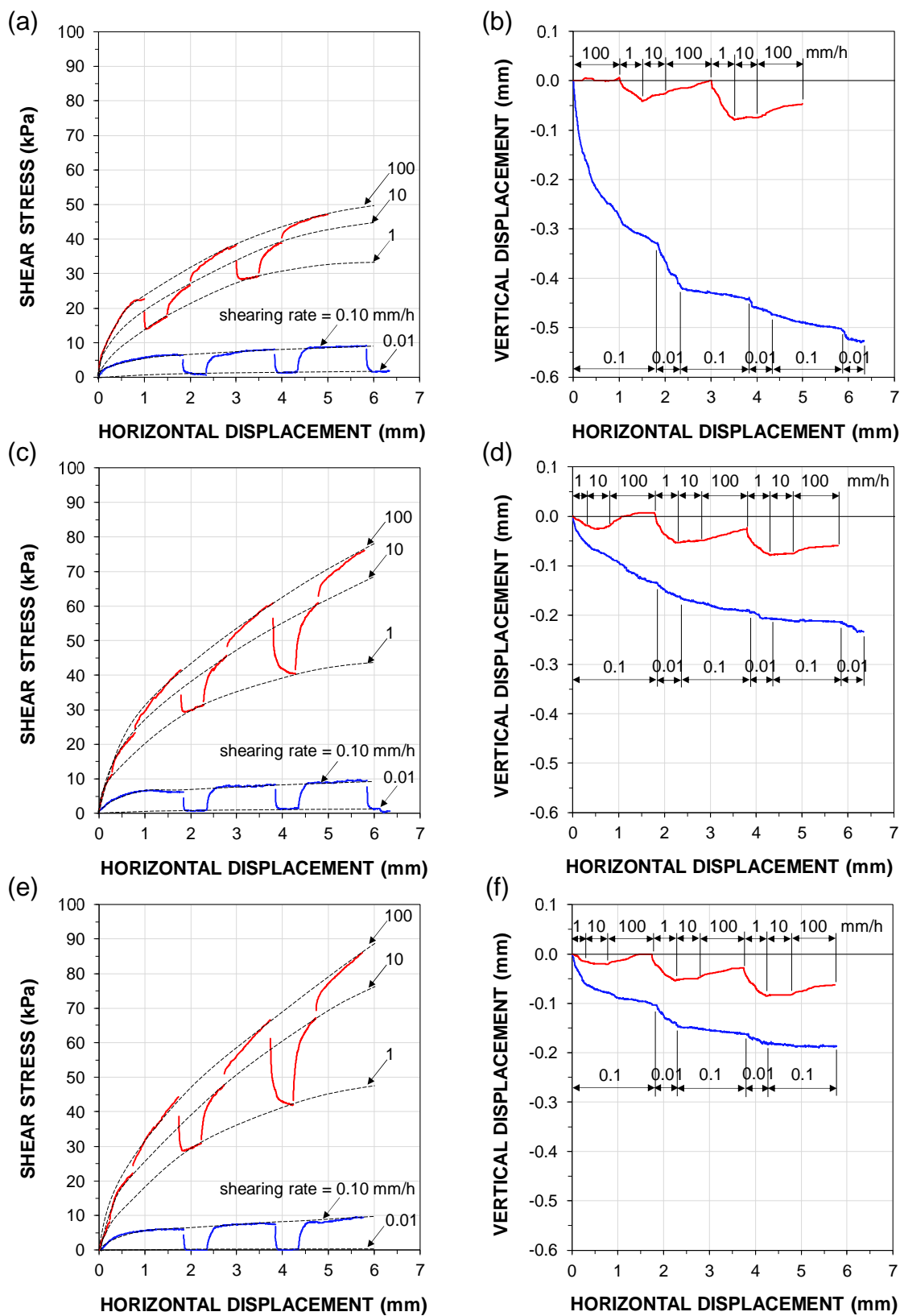


Figure 6. Shear stress and vertical displacement versus horizontal displacement from tests performed at: (a) and (b) 40 kPa, (c) and (d) 60 kPa, and (e) and (f) 80 kPa normal stress, respectively, and different shearing rates.

Figure 6 presents the results from the interface shear tests on the bitumen coated concrete block against the gyttja applying various shearing rates and normal stresses. The blue curves present the results from slow shearing tests and the red curves show the results from the fast shearing tests. There was a significant difference between the mobilized shear stress at slow (0.01 and 0.1 mm/h) and fast (1, 10, and 100 mm/h) shearing rates. The increase in shearing rate increased the shear stress. The contractive vertical displacement increased only at velocities equal to or slower than 1 mm/h.

Figure 7 presents the induced shear stress as a function of shearing strain rate. As can be seen from the graph, the shear stress was influenced by the strain rate. Below the strain rate of about $3 \cdot 10^{-5}$ the shear stress was equal for all three normal stresses. The lowest shear stress was obtained for the lowest strain rate and was about 1 kPa, which means 95% reduction to the undrained shear strength of the tested gyttja. At higher strain rates the shear stress increased with the increase of normal stress. The shear stress obtained at the highest strain rates was similar to the shear stress on gyttja samples. This finding was unexpected and may be explained by the penetration of soil particles into the coating. Khare and Gandhi (2009) investigated the shear stress of bitumen coated piles in sand using modified direct shear-test box and model piles. The authors showed that by increasing the normal stress from 50 to 75 kPa the shear stress increased by about 20 % for a 2- and 3-mm-thick bitumen coated sample using the shearing rate of 0.25 mm/min.

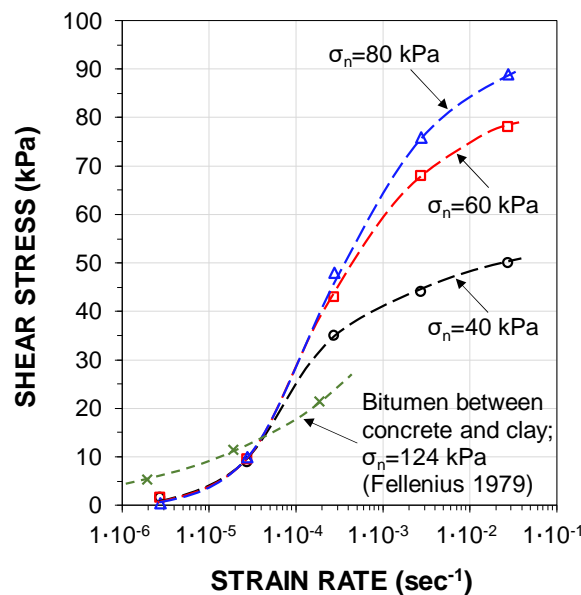


Figure 7. Shear stress versus shearing strain rate.

The findings are in general agreement with those of Fellenius (1979) who carried out laboratory shearing tests on soft clay/bitumen/concrete specimens to investigate the strain rate effect. In both studies the shear stress increased with increasing shearing rate. The higher shear stress at low strain rates obtained by the author could be explained by the lower temperature (4°C) at which the tests were conducted. The lower shear stress at higher strain rates may be explained by the soil type used in the author's study, which was soft and sensitive highly plastic clay (72 % clay size particles).

4 CONCLUSIONS

This paper has investigated the development of shear stress between gyttja and different pile materials and the effect of the shearing rate. The results of this investigation show that the ratio of interface angle of friction to gyttja angle of friction for concrete and steel was 1.0 and 0.8, respectively. The movement needed to reach the peak shear stress was 2.3 and 4 mm for the gyttja/steel and gyttja/concrete sample, respectively. The gyttja/bitumen/concrete sample needed 1 to 3 mm movement to reach the peak shear stress. After reaching the peak shear stress the response was plastic, strain softening or hardening. A peak shear stress was not reached at any normal stress on gyttja samples.

The magnitude of the shear stress between gyttja and the bitumen concrete block was strongly dependent on the applied shearing rate. The shear stress increased with increasing shearing rate. The bitumen coating significantly reduced the shear stress at low shearing strain rates and was independent of the applied normal stress. The reduction was 95 % compared to the undrained shear strength of gyttja at the shear strain rate of $2.8 \cdot 10^{-6} \text{ s}^{-1}$. At fast shear strain rates (above $3 \cdot 10^{-5}$), the shear stress increased with increasing normal stress.

The shear tests with variable shearing rates on gyttja showed a positive rate effect with a 16 % increase in shear stress per log cycle. The vertical displacements at the shearing rates higher than 5 mm/h were constant or reduce contraction of the sample.

5 ACKNOWLEDGMENTS

The authors would like to thank cp test a/s, Per Aarsleff A/S, Centrum Pæle A/S, DMT Gründungstechnik GmbH and Innovation Fund Denmark for providing funding for this study.

6 REFERENCES

- Baligh, M.M., Figi, H., and Vivatrat, V., 1978. Downdrag on bitumen-coated piles. *Journal of the Geotechnical Engineering Division*, 104(GT11) 1355-1370.
- Fearon, R.E, Chandler, R.J., and Bommer, J.J., 2004. An investigation of the mechanisms which control soil behaviour at fast rates of displacement. *Advances in geotechnical engineering: The Skempton conference*, Institution of Civil Engineers, London, UK, pp. 441-452.
- Fellenius, B.H., 1979. Downdrag on bitumen coated piles. *American Society of Civil Engineers, ASCE Journal of Geotechnical Engineering*, 105(GT10) 1262-1265.
- Head, K.H. and Epps, R.J., 2011. *Manual of Soil Laboratory Testing, Volume 2: Permeability, Shear Strength, and Compressibility Tests*. Dunbeath, UK: Whittles Publishing.
- Khare, M.G. and Gandhi, S.R., 2009. Share resistance of bitumen-coated piles in sand. *Proceedings of the Institution of Civil Engineers-Geotechnical Engineering*, 162(6), pp. 303-310.

- Lehane, B.M. and Jardine, R.J., 1992. Residual strength characteristics of Bothkennar clay. *Geotechnique*, 42(2), pp. 363-367.
- Martinez, A. and Stutz, H.H., 2019. Rate effect on the interface shear behaviour of normally and overconsolidated clay. *Geotechnique* 69(9), pp. 801-815.
- McCabe, B.A., 2002. Experimental investigations of driven pile group behaviour in Belfast soft clay. PhD thesis. Trinity College Dublin.
- Potyondy, J.G., 1961. Skin friction between various soils and construction materials. *Geotechnique* 11(4) 339-353.
- Savery, A.L., 2019. Gyttja deposits from Randers and Esbjerg – an investigation of composition and geotechnical properties. Department of Geoscience, Aarhus University, 46p.
- Tan, S.A. and Fellenius, B.H., 2016. Negative skin friction pile concepts with soil-structure interaction. *ICE Geotechnical Research Journal*, UK. Paper 16.00006. pp 1-11.
- Tika, T.E., Vaughan, P.R., and Lemos, L.J.L.J., 1996. Fast shearing of pre-existing shear zones in soil. *Geotechnique* 46(2), pp. 197-233.

CHAPTER 5

DISTRIBUTION OF STRAIN DUE TO INSTALLATION OF PILES AND SOIL MOVEMENT

5.1. Introduction

In December 2017 an opportunity occurred to establish a full-scale test site on a construction site in Esbjerg, where Per Aarsleff was building a new harbour. The purpose of this test setup was to investigate the development of negative skin friction along driven piles. The test setup consisted of four instrumented driven piles: two steel and two precast concrete. One of each type was bitumen coated. The effect of the pile installation process and the surcharge loading adjacent to the test piles, which happened before the fill around the piles was placed is described in Conference Paper 2. The results obtained after a 3 m high fill was placed are presented in Conference Paper 3. Unfortunately, both papers describe only the behaviour of the steel test piles. Due to the concrete cracks issue (see Chapter 2) and the malfunctioning of one of the strain DFOS cables the results obtained from the precast concrete piles are not discussed in the papers.

In general, the Esbjerg test site served as a trial test site before establishing the main one (with no construction activities) located at Randers Harbour (see Chapter 6).

5.2. Assessment of the applied methodologies

All the test piles (both steel and precast concrete) were instrumented with one pair of opposite mounted strain DFOS cables. Additionally, the steel test piles (both uncoated and bitumen coated) were instrumented with one line of VW gauges installed at four different depths. Unfortunately, due to bending and shearing of the piles, the strain data obtained from the VW gauges were not useful.

In order to limit the influence of concrete shrinkage on the strain measurements, the pile instrumentation was mounted on the piles casted 12 months before driving. The sensors were installed on the side surfaces of the pile and were exposed to concrete cracks due to driving. This made the interpretation of strain distribution along precast concrete piles difficult.

Only one temperature DFOS cable was mounted in total (on the bitumen coated precast concrete pile). This DFOS cable was damaged before driving the pile. As a backup for

temperature compensation of the strain DFOS data, the temperature records obtained from the VW gauges were therefore used.

The ground monitoring system consisted of settlement and pore water pressure sensors installed at different depths. Additionally, a standpipe piezometer was installed in the bottom sand layer to monitor the groundwater level. As a backup system for settlement measurements, two settlement plates at the working platform level were installed. During the monitoring period, the ground monitoring system performed well. Unfortunately, the ground monitoring system was installed after driving the piles. Therefore, the influence of pile driving on the soil movement and the changes in pore water pressure could not be monitored. Additionally, as it was revealed later, the test setup missed an inclinometer to monitor the lateral soil movement.

5.3. Summary of the results

Piles instrumented with at least one pair of opposite strain DFOS cables can provide the engineering quantities of lateral and vertical pile behaviour.

The results obtained in this study confirmed that driven piles are subjected to residual forces. Recognizing the existence of residual forces is especially important for an interpretation of the shaft and toe resistance of the pile.

It was shown that the bitumen coating reduces the magnitude of negative skin friction in the long-term measurements.

5.4. Critical review

The ground monitoring system should be installed before pile installation to help analyse the strain distribution induced due to pile installation. An inclinometer, which was not considered in the test setup, will support the analysis of lateral displacement of the test piles.

The instrumentation of the piles should include two pairs of opposite mounted DFOS cables in order to find the extreme quantities of lateral component. Each test pile should include at least one temperature DFOS cable (preferably two).

Conference Paper 2 focuses on the soil-pile interaction along uncoated and bitumen coated steel driven piles due to driving and one-sided surcharge loading. The authors concluded that bitumen coating reduces the magnitude of residual force. Based on the full-scale field measurements obtained from the test site in Randers (see Chapter 6), supported with the results of the laboratory interface shearing tests (see Chapter 4), the behaviour of bitumen coated piles depends significantly on the shearing rate (the shear force increases with increasing shearing rate). This implies that the bitumen coating reduces the long-term negative skin friction, however, it has little or no effect during fast shearing e.g. pile installation.

5.5. PhD student's contribution

The PhD student's contribution to Conference Paper 2 includes preparation of the DFOS sensors, instrumentation of the test piles, collecting data from the VW, the DFOS sensors and the ground monitoring system, analysing the data and writing the paper (major contribution).

The PhD student contributed to Conference Paper 3 in the research and writing phase in the major way.

CONFERENCE PAPER 2

Kania, J.G. and Sørensen, K.K., 2019. A case study of soil-pile interaction in soft soils. XVII European Conference on Soil Mechanics and Geotechnical Engineering, Reykjavik, Iceland, September 1-6, 8 p.

Status: published

A case study of soil-pile interaction in soft soils

Etude de cas de l'interaction sol-pieu en terrain meuble

J. Kania Corresponding / primary author
cp test a/s / Aarhus University, Vejle / Aarhus, Denmark

K. K. Sørensen
Aarhus University, Aarhus, Denmark

ABSTRACT: The results of soil-structure interaction of driven steel piles installed through soft soils are presented. Two instrumented, 12 m embedment, 406 mm diameter steel piles were installed at a construction site in Esbjerg, Denmark. One of the test piles was bitumen coated. The test piles were driven through 3.5 m of reclaimed sand and 3.6 m of soft soil into underlying sand layer. To investigate the soil-pile interaction due to pile installation and surcharge loading adjacent to the piles after installation, the test piles were instrumented with distributed fibre optic strain sensors along the full length of the piles. It was found that the test piles experienced compression loads after installation and lateral deflections due to surcharge loading in the soft soils. This case study documents the existence and magnitude of residual loads in driven steel piles after installation, the influence of bitumen coating and the effect of lateral thrust on the piles in an upper soft soil layer.

RÉSUMÉ: Les résultats de l'interaction sol-structure de pieux en acier installés au travers des terrains meubles sont présentés. Deux pieux de 406 mm de diamètre, enfouis 12m sous la surface, furent installés sur un chantier à Esbjerg au Danemark. L'un des pieux tests était enduit de bitume. Les pieux tests furent battus à travers 3,5 m de sable de récupération et 3,6 m de terre meuble avant d'atteindre une couche de sable sous-jacente. Afin d'examiner l'interaction entre le sol et le pieu après son installation et l'effet de surcharge adjacente aux pieux après cette même installation, les pieux tests furent équipés de senseurs en fibre optique distribués sur toute leur longueur. Il a ainsi été découvert que les pieux tests subissaient des forces de compression après installation, entraînant des déviations causées par l'effet de surcharge en terrain meuble. Cette étude de cas rend compte : de l'existence et de l'ampleur de charges résiduelles sur des pieux en acier battus après leur installation : de l'influence du revêtement bitumineux, et également de l'effet de poussée latérale sur les pieux au sein d'une couche supérieure de terrain meuble.

Keywords: residual load, lateral soil movement, bitumen coating, distributed fibre-optic sensors

1 INTRODUCTION

The function of piles is generally to transfer load from a structure through soft compressible soil layers to stiffer or less compressible soils. Soil-pile interaction involves a combination of vertical and horizontal loads. An example of vertical load is residual load. Residual load in a driven pile is

the axial load present in a pile after its installation. For each hammer blow a negative skin friction develops in the upper part of a driven pile and a positive shaft resistance in the lower part, due to the pile's upward movement during a rebound. The point of equilibrium exists where the shaft resistance reverse from negative direction to positive direction (Briaud and Tucker 1984,

Fellenius 2015). Horizontal loads occur when piles are installed in a soft soil layer which deforms increasing horizontal pressures. As a consequence bending moments develop in the piles and the piles experience deflections (Poulos 1973, Springman and Bolton 1990).

The test setup was designed to investigate negative skin friction under uniform loading. Unfortunately, due to construction activities an unplanned one-sided loading occurred, which affected the test site. This paper will focus on the residual load apparent after driving a steel pile with and without bitumen coating and deflections of the test piles due to surcharge loading adjacent to the piles.

This paper first gives details of the site conditions and the instrumentation of the test setup. The presentation and discussion of results will focus on the examination of the residual load on an uncoated and coated driven steel pile and the deflections due to one sided surcharge loading.

2 MATERIALS AND METHODS

2.1 Site conditions

The test site is located in Esbjerg, Denmark. At the site land was reclaimed from the sea by placing fill up to +4.5 m above sea level (ASL) to construct a new harbour. The ground profile consists of 3.5 m thick reclaimed uniform, fine to coarse sand fill layer on top of 3.6 m soft soil layer overlying a postglacial marine, dense, uniform, medium sand layer. Based on the previous site investigation carried out by GEO (GEO 2016) and Jysk Geoteknik (JyskGeoteknik 2017) and testing carried out on samples collected in connection to the installation of in-situ monitoring equipment for the test setup, the soft soil layer is found to be of postglacial marine origin, highly organic and consisting of gyttja (at roughly 3.5-4.3 m depth) and peat (at roughly 4.3-7.1 m

depth). The gyttja layer is characterized by an average water content of 61 %, an average plastic limit of 55 % and an average liquid limit of 136 %. The peat layer is characterized by an average water content of 285 %, an average plastic limit 256 % and an average liquid limit of 373 %. Based on the oedometer tests, the soft soil layer is normally consolidated. According to CPT sounding and the empirical approaches available for interpretation of undrained shear strength from CPT (Lunne, Robertson et al. 1997), the average undrained shear strength of soft soil layer is equal to 16 kPa (assuming the empirical cone factor N_k equal to 15).

2.2 Test setup and instrumentation

The test setup is illustrated in Figure 1. The setup consisted of four instrumented test piles and in-ground monitoring of water pressure and settlement.

Two instrumented Ø 406 diameter (8 mm wall thickness) steel test piles (with and without bitumen coating) and the two instrumented 350 mm x 350 mm square precast concrete piles (with and without bitumen coating) were driven to the approximate depth of 12 m by a Hitachi 180-3 piling rig with a 90 kN Junttan HHK9A hammer.

The instrumentation and the obtained results from concrete test piles will not be described in this paper due to malfunctioning of one of the installed strain distributed fibre optic sensors (DFOS).

All of the instrumentation and the test piles were installed from a working platform (0.0 m depth) at 1.5 m ASL. The test piles were installed in December 2017 and the field instrumentation was installed in January 2018.

To measure pore water pressure low air entry vibrating wire piezometers were installed at 5.0, 6.5, 7.7, and 12.2 m depth using the fully grouted installation method. The grout consisted of water, cement and bentonite with the 8:1:1 ratio by

weight (water:cement:bentonite). A stand pipe was installed with an intake zone at 12.5 m depth.

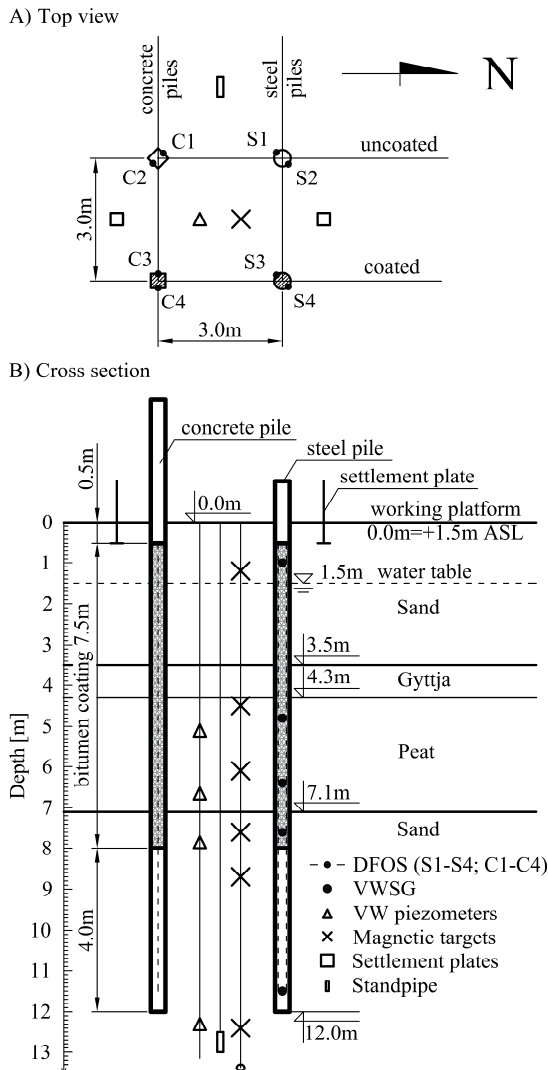


Figure 1. Soil profile and the test setup.

The settlement of the surface was measured by two settlement plates installed at 0.5 m depth, while the settlements at different depths were monitored by magnetic extensometers. The six magnetic targets (6 leaf spider magnets) and the datum magnet were installed at 1.2, 4.4, 6.1, 7.6, 8.7, 12.4, and 13.4 m depth respectively.

The steel test piles were instrumented with two opposite mounted strain distributed fibre optic sensors (DFOS). As presented in Figure 2, Brusens V9 cables were used as strain DFOS. All DFOS were placed along a welded (one side chain intermittent) Ø12mm steel rebar, pre-stressed to about 1000µε and glued using Araldite 2012 epoxy. Additionally, both steel test piles were equipped with one set of vibrating wire strain gauges (VWSG) installed at five different depths: 1.0, 4.8, 6.4, 7.6 and 11.5 m respectively on each steel pile. The VWSG were protected by welded on angle iron. One of the steel test piles was coated along 7.5 m (0.5-8.0 m depth) with a 1 mm thick, 80/100 penetration bitumen coating. Both steel piles were supplied with point-end pile shoe.



Figure 2. Installation of strain DFOS on the steel piles.

2.3 Temperature compensation of strain measurements

An optical distributed sensor interrogator based on Rayleigh scattering was used in this case study. The principle of Rayleigh-based distributed fibre-optical sensing techniques was presented in previous studies (Palmieri and Schenato 2013). Similar to strain gauges, fibre optic strain sensors mounted on a test object are sensitive to mechanically and thermally induced strain (Luna 2014).

Unfortunately, it was revealed before installation of the test piles that temperature DFOS was

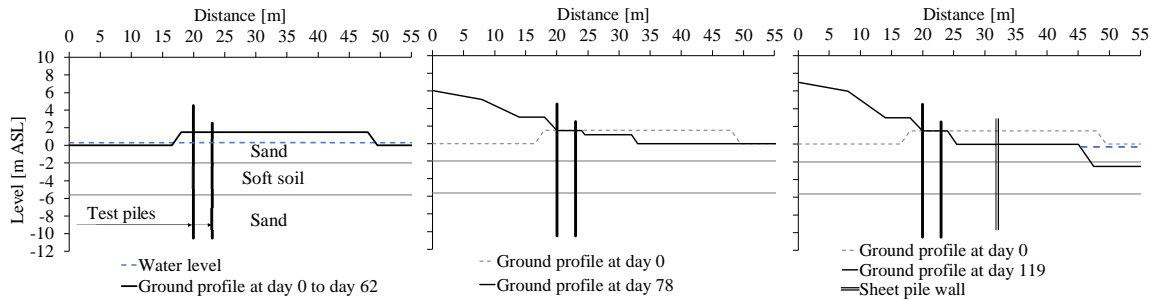


Figure 3. Construction activities around the test setup at selected days after installation of piles.

malfunctioning. To obtain temperature distribution with depth the temperature readings (at the depths of installation) were collected from the VWSGs and the interpolation between measuring points was made. Then the mechanical strains were obtained using the equation as given below:

$$\varepsilon_m^z = \varepsilon_t^z + \left(0,95 \cdot \frac{\Delta T^z}{k_T} \cdot k_\varepsilon + \Delta T^z \cdot \alpha_L \right) \quad (1)$$

Where ε_m^z ($\mu\varepsilon$) is mechanical strain at depth z , ε_t^z ($\mu\varepsilon$) is total (measured) strain at depth z , ΔT^z ($^\circ\text{C}$) is change in temperature at depth z , k_T ($^\circ\text{C}/\text{GHz}$) is temperature conversion factor equal to -0.638 $^\circ\text{C}/\text{GHz}$, k_ε ($\mu\varepsilon/\text{GHz}$) is strain conversion factor equal to -6.67 $\mu\varepsilon/\text{GHz}$, α_L is thermal expansion coefficient of steel assumed in this study as 12.2 $\mu\varepsilon/^\circ\text{C}$.

2.4 Expected distribution of residual load

In order to evaluate the measured distribution of residual load on uncoated and coated driven steel test pile estimations were made using commercially available GRLWEAP software. The modelling parameters are presented in Table 1. The Alm and Hamre (Alm and Hamre, 2002) soil model and standard skin and toe quake and damping parameters were used. Based on driving logs a 20 cm hammer stroke and 25 and 19 blow counts for every 20 cm at the end of driving the uncoated and coated pile were used respectively.

Table 1. Modelling parameters of soil layers

Soil type	$\gamma/\gamma_{\text{sat}}$ kN/m ³	Surface friction °	C_u kPa
Sand	18/20	28 – uncoated	-
		28 - coated	
Gyttja	16	-	16
Peat	11	28 – uncoated	-
		15 - coated	

2.5 History of construction activities around the test setup

Main construction activities around the test setup consisted of filling the area with reclaimed sand up to 4.5 m ASL and the installation of an anchored sheet pile wall for the new harbour. It can be seen from the sketches in Figure 3 that the major change took place 78 days after installation of the test piles, when the area at only one side (South side) was filled up to around +6.0 m ASL. This area was continuously filled with reclaimed sand until 119 days after installation of piles. Based on the author's field observations, the sheet pile wall near the test setup was completed around 91 days after installation of piles.

3 RESULTS

As mentioned in 2.2, only results obtained from the steel test piles are presented in this paper. In all figures negative values denote compression loads and positive values denote tension loads.

To smoothen the strain profiles, a moving average of 100 consecutive reading was used to present data obtained from DFOS (giving a virtual gauge length of roughly 0,26 m located every 2.6 mm).

3.1 Residual loads and deflection of the test piles after driving

The measured strain distribution of opposite mounted strain DFOS on the uncoated and coated steel test piles after installation of the piles are presented in Figure 4 and Figure 5 respectively. From the data in Figure 4 it appears that the uncoated steel test pile experienced arc-shape deflection after driving, since the opposite sensors are located at the opposite sides of the average along the full length.

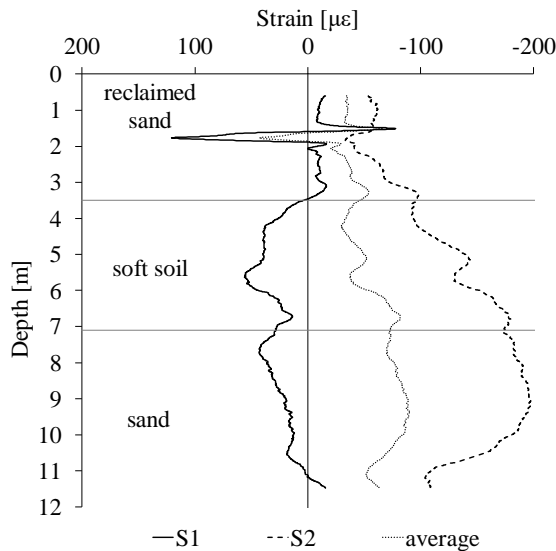


Figure 4. Measured strain distribution of opposite mounted DFOS on the uncoated steel test pile after pile installation

In contrast to the observed strain distribution of the uncoated pile, Figure 5 shows that the strain distribution of the coated steel test pile experienced S-shape deflection after driving with the intersection point located at approximately 4.7 m depth.

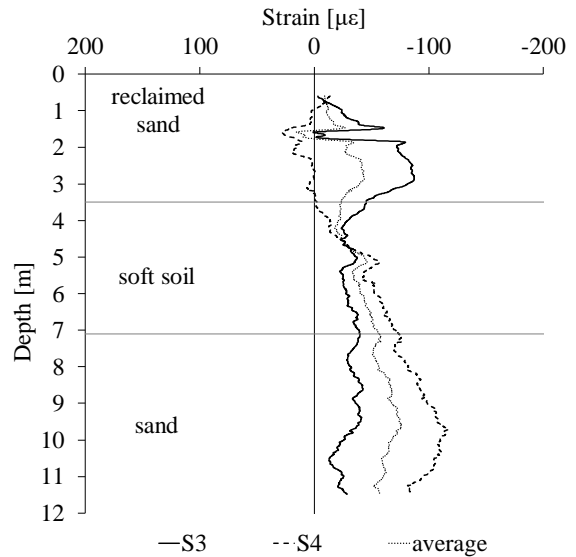


Figure 5. Measured strain distribution of opposite mounted distributed fibre optic sensor on the coated steel test pile after pile installation

The residual loads for the uncoated and coated steel test pile are presented in Figure 6 and Figure 7 respectively. The load distribution obtained from DFOS for each test pile was calculated based on averaging measured strain distributions of opposite mounted strain DFOS sensors and assuming the Young's modulus of steel equal to 210 GPa.

As shown in Figure 6 the residual load on the uncoated steel test pile obtained from DFOS and GRLWEAP reaches its maximum compression value of 190 kN (at 9.4 m depth) and 127 kN (at 8,0 m depth) respectively. The average unit shaft resistance within soft soil layer (3.5-7.1 m depth) is 30 kPa and 10 kPa obtained from DFOS and GRLWEAP respectively.

As shown in Figure 7 the residual load on the coated steel test pile obtained from DFOS and GRLWEAP reaches its maximum compression value of 160 kN (at 9.6 m depth) and 100 kN (at 8,0 m depth) respectively. The average unit shaft resistance within soft soil layer (3.5-7.1 m depth) is 19 kPa and 6 kPa obtained from DFOS and GRLWEAP respectively.

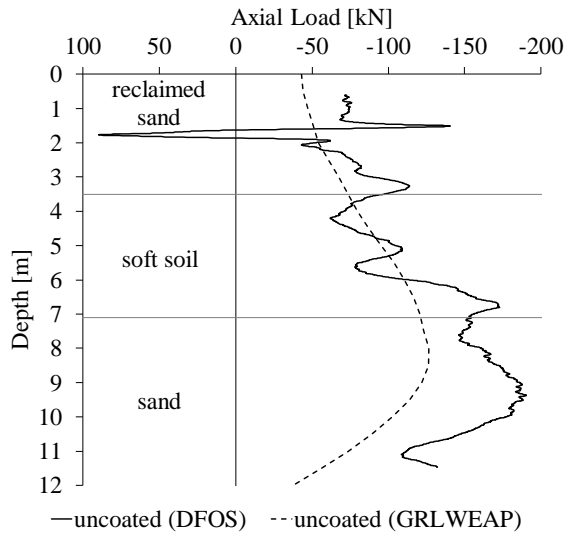


Figure 6. Residual load distribution on the uncoated steel test pile obtained from DFOS and GRLWEAP

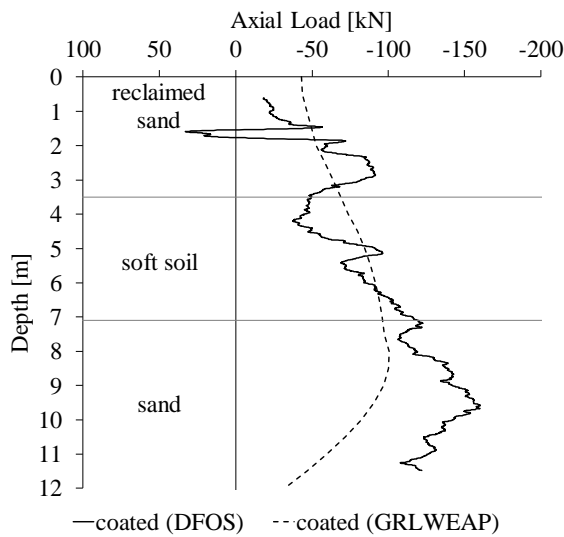


Figure 7. Residual load distribution on the coated steel test pile obtained from DFOS and GRLWEAP

3.2 The influence of surcharge loading adjacent to the test piles

To assess the influence of one sided surcharge loading adjacent to the test piles, the strain distributions were used. Figure 8 and Figure 9 present the measured strain distributions of opposite mounted distributed fibre optic strain sensors on

the uncoated and coated steel test piles respectively at selected days after pile installation.

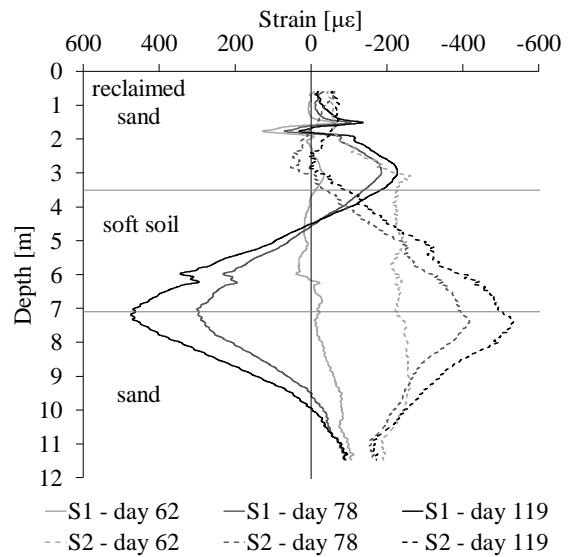


Figure 8. Measured strain distribution of opposite mounted DFOS on the uncoated steel test pile at selected days after pile installation

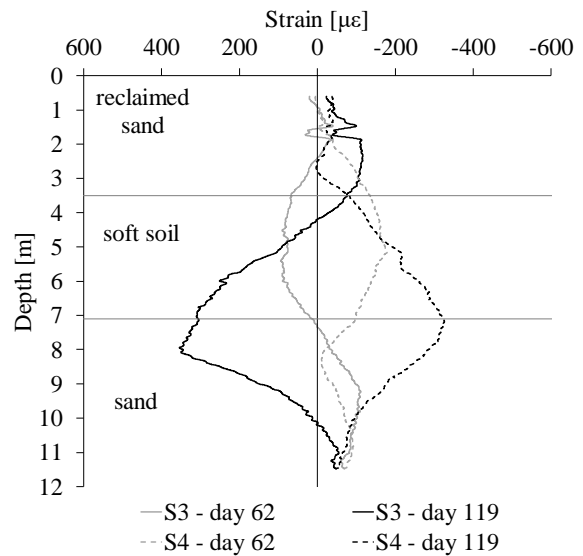


Figure 9. Measured strain distribution of opposite mounted DFOS on the coated steel test pile at selected days after pile installation

As shown in Figure 8, there was a significant difference between strain profiles obtained at day

62 and 78 after installation of the piles. The strain profiles obtained from the sensor S1 and S2 62 days after installation of piles indicate arc-shape deflection of the uncoated pile. At day 78 and later (day 119) the strain profiles indicate an S-shape deflection of the uncoated pile having an intersection point located around 4m depth and two local maximum tension and compression values located around 3.0 and 7.5 m depth. The strain profiles presented in Figure 9 indicate a deflection change of the coated pile. At day 62 the coated pile experienced an S-shape deflection with an intersection point at 8 m depth. At day 119 the deflection type was still S-shaped, however the intersection point had shifted to 3.5 m depth. The local maximum tension and compression values were located at the former intersection point around 8.0 m depth. Interestingly, above 3.5 m depth (intersection point at day 119) and below 8m depth (intersection point at day 62) the individual sensors S3 and S4 reversed its position e.g. S3 from tension to compression side at the top and from compression to tension side at the bottom.

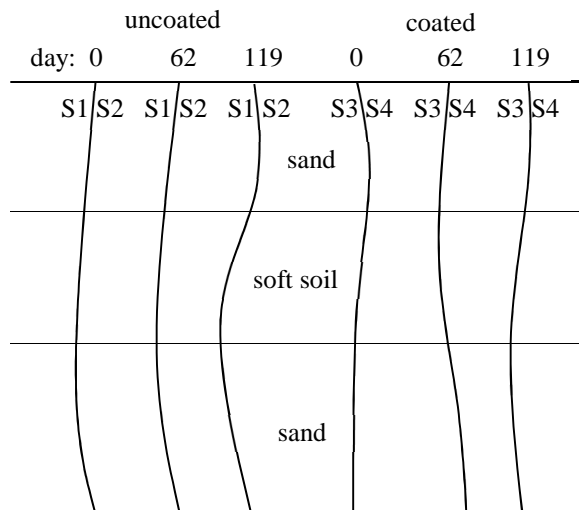


Figure 10. Sketch of deflection of the uncoated and coated pile at selected days after piles installation based on measured strain profiles

The deflection history of the test piles, based on the measured strain distribution is provided in Figure 10. It is important to note that the piles experienced additional compression loads due to residual loads and soil settlement.

4 DISCUSSION

Prior studies have noted the importance of residual load (Poulos 1987, Kim, Chung et al. 2011) and lateral thrust (Davisson 1970, Springman and Bolton 1990) to understand and properly assess soil-pile interaction. This study confirms the existence of residual load after driving steel piles and deflection of piles due to one sided surcharge loading.

In this case study the distributed fibre optic sensing interrogator based on Rayleigh scattering was used. Due to its spatial resolution (2.6 mm), very detailed strain profiles were obtained and characteristic points were precisely located. Unfortunately, the test setup did not involve inclinometers to monitor lateral soil movement, since the test setup was designed to investigate negative skin friction. Also, the test piles would have benefitted from having two pairs of diametrically opposite strain DFOS to locate the neutral axis and direction of bending. Additionally, at least one more temperature DFOS should be mounted as a backup.

The obtained residual load distributions are consistent with other studies which found that a negative skin friction is building up in the upper portion of a pile and a positive shaft resistance develops in the lower portion of a pile. The maximum residual loads obtained from DFOS were higher than obtained from GRLWEAP for the uncoated and coated steel test pile by 50 % and 60 % respectively. The maximum value of residual load obtained from DFOS and GRLWEAP on the coated steel test pile was smaller than on the uncoated pile. This finding suggests that bitumen coating reduces the residual load.

Interestingly, the point of equilibrium between negative skin friction and positive shaft resistance after driving for uncoated and coated steel test pile was located around the same depth. However, it was located deeper for DFOS (9.5 m depth) than GRLWEAP (8.0 m depth).

The consequence of not considering the presence of residual load will lead to overestimating the shaft resistance along the upper section and underestimating the shaft resistance along the lower section of the pile (Fellenius 2015).

The assumed deflection of piles, based on measured strain profiles, supports previous research regarding passive lateral thrust on piles. It can therefore be assumed that these factors (residual load and lateral thrust) can affect any further measurements of soil-pile interaction e.g. negative skin friction.

5 CONCLUSION

This case study has shown that:

- 1) Residual load is present after installation of a driven steel pile with and without bitumen coating.
- 2) Bitumen coating reduces the magnitude of residual load, but it does not change the point of equilibrium between negative skin friction and positive shaft resistance.
- 3) Surcharge loading adjacent to piles installed through soft soils causes deflection of piles.
- 4) DFOS can be successfully installed on driven steel piles.
- 5) The instrumentation of a test setup to monitor soil-pile interaction located on ongoing construction site should be carefully planned.

6 ACKNOWLEDGEMENTS

The authors would like to thank cp test a/s, Per Aarsleff A/S, Centrum Pæle A/S, DMT Gründungstechnik GmbH and Innovation Fund Denmark for providing funding for this study and Per Aarsleff A/S for providing data and for installing the instrumented test piles.

7 REFERENCES

- Alm, T., Hamre, L. 2002. Soil model for pile driveability predictions based on CPT interpretations. *Proceedings of The International Conference on Soil Mechanics and Geotechnical Engineering* **2**, 1297-1302, AA Balkema Publishers.
- Briaud, J.-L., Tucker, L. 1984. Piles in sand: a method including residual stresses. *Journal of Geotechnical Engineering* **110**, 1666-168.
- Davissou, M. 1970. Lateral load capacity of piles. *Proceedings: 49th Annual Meeting of the Highway Research Board*, 104-112, Washington District of Columbia, United States.
- Fellenius, B. H. 2015. Static tests on instrumented piles affected by residual load. *DFI Journal - The Journal of the Deep Foundations Institute* **9**, 11-20.
- GEO. 2016. *Esbjerg Strand, Laboratorieforsøg*. JyskGeoteknik. 2017. *Geoteknisk Datarapporter*.
- Kim, S. R., Chung, S. G., Fellenius, B. H. 2011. Distribution of residual load and true shaft resistance for a driven instrumented test pile. *Canadian Geotechnical Journal* **48**, 583-598.
- Luna. 2014. *Distributed Fiber Optic Sensing: Temperature Compensation of Strain Measurement* (EN-FY1402).
- Lunne, T., Robertson, P., Powell, J. 1997. *Cone penetration testing in geotechnical practice*. Spon Press, Abingdon.
- Palmieri, L., Schenato, L. 2013. Distributed optical fiber sensing based on Rayleigh scattering. *The Open Optics Journal* **7**, 104-127.
- Poulos, H. G. 1973. Analysis of piles in soil undergoing lateral movement. *Journal of Soil Mechanics & Foundations Div* **99**, 391-406.
- Poulos, H. G. 1987. Analysis of residual stress effects in piles. *Journal of Geotechnical Engineering* **113**, 216-229.
- Springman, S., Bolton, M. 1990. *The effect of surcharge loading adjacent to piles*, Transport and Road Research Laboratory (TRRL), Wokingham, Berkshire, United Kingdom.

CONFERENCE PAPER 3

Kania, J.G., Sørensen, K.K., and Fellenius, B.H., 2020. Driven piles installed in soft soils subjected to vertical and lateral soil movements.

Status: manuscript planned for submission to the 73rd Canadian Geotechnical Conference, Calgary, Canada, September 13 - 16.

Driven piles installed in soft soils subjected to vertical and lateral soil movement

Jakub G. Kania

cp test a/s and Department of Engineering, Aarhus University

Kenny Kataoka Sørensen

Department of Engineering, Aarhus University

Bengt H. Fellenius

Consulting Engineer

Abstract:

This paper presents the behaviour of 406 mm diameter, 12 m long, instrumented, driven steel piles at a construction site in Esbjerg, Denmark. One pile was uncoated, and one was bitumen coated. The piles were driven through a 1.5 m thick layer of reclaimed sand underlain by naturally deposited soils consisting of a 2.0 m thick layer of sand, a 3.6 m thick layer of soft soil above a thick sand layer. The instrumentation comprised distributed fibre optic cables. Due to its spatial resolution (2.6 mm), very detailed strain profiles were obtained. The distribution of strain in the piles was induced by, first, the pile installation, building up a residual force in the piles and, then, additional force, drag force, due to negative skin friction developing after placing a 3 m thick fill around the piles. Due to construction activities an unplanned one-sided loading occurred inducing considerable bending moment and shear force in the test piles.

1 INTRODUCTION

Understanding a soil-pile interaction is essential in a piled-foundation design. Piles can be subjected to vertical (Fellenius 1972, Indraratna et. al 1992) and lateral soil movement (Poulos 1973). Additionally, the installation process may build up a residual force in piles (Fellenius 2015). Conventionally, piles have been instrumented with telltales or strain gages in order to obtain strain distribution and monitor the short- and long-term pile axial behavior. More recently, piles were instrumented with distributed fibre optic sensing (DFOS) systems based on Brillouin scattering (Kechavarzi et al. 2019).

This paper presents the results of monitoring two instrumented steel piles driven at a construction site in Esbjerg, Denmark. One pile was bitumen coated and one was uncoated. Both were instrumented with DFOS cables using a Luna ODiSI-B interrogation unit based on Rayleigh backscattering with a 2.6 mm spatial resolution.

The paper presents the soil data with a description of the test setup and pile instrumentation followed by the results and analysis with discussion.

2 MATERIALS AND METHODS

2.1 Soil profile

The test site was located in Esbjerg, Denmark. The natural deposits at the site consisted of 2.0 m thick layer of uniform, fine to coarse sand underlain by a 3.6 m thick layer of soft, organic soil above a thick sand layer. A 1.5 m layer of reclaimed uniform fine to coarse sand was placed on top of the original sand layer. The soft soil layer is found to be of postglacial marine, organic and consisting of gyttja and peat. The bottom layer is a postglacial marine, dense, uniform, medium sand.

The soil profile, distribution of water content in the soft soil layer, and Atterberg limits are presented in Figure 1. The water content of the soft soil layer ranged from about 77 % to about 273 % with an average of 158 %. The plastic limit, w_p , ranged from 63 % to 383 % and the liquid limit, w_l , ranged from 145 % to 499 %. An average measured unit density of the soft soil layer was about 1,200 kg/m³.

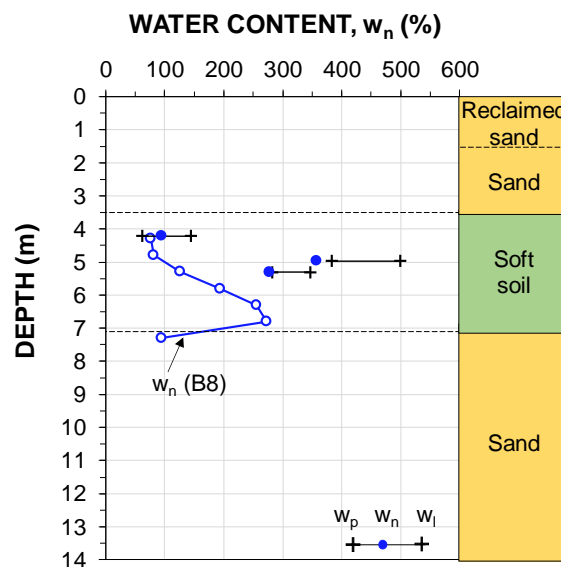


Figure 1. Soil profile, atterberg limits (soil samples collected in connection to the installation of in-situ monitoring equipment for the test setup on January 16-18, 2018) and distribution of water content (soil boring B8 performed on October 15, 2008)

The grain size distribution, presented in Figure 2, shows the dominant particle size, on average, to be 69 % silt size, 11 % clay size, and 20 % sand size. The organic content in the soft soil layer ranged from 12.9 to 91.4 % with an average of 56 %.

The results of two CPTU soundings pushed on February 17-20, 2017 are presented in Figure 3. The CPTU 1 and CPTU 2 sounding was pushed about 55 and 70 m from the test piles, respectively. As indicated in the enlarged portion of the q_c -diagram, both results showed the existence of the soft soil layer between about 3.0 to 4.5 m depth. An undrained shear strength of the soft soil layer $c_u = 16$ kPa was determined based on the CPTU soundings applying a cone factor, N_k , of 15.

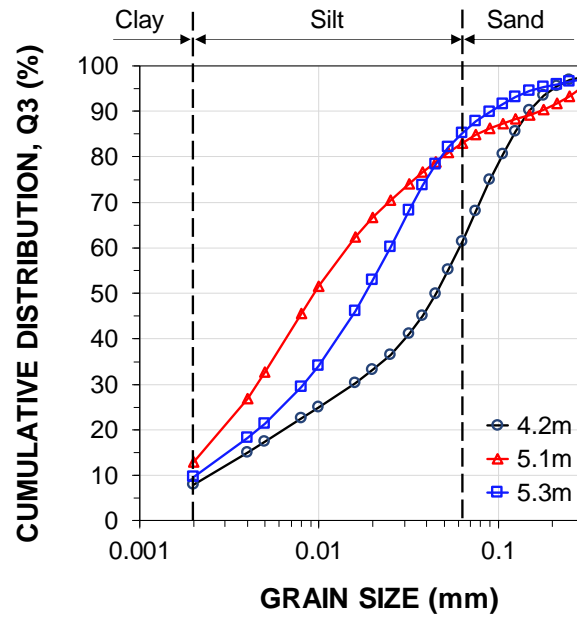


Figure 2. Grain size distribution by laser diffraction performed on soil samples collected in connection to the installation of in-situ monitoring equipment (data from Savery 2019).

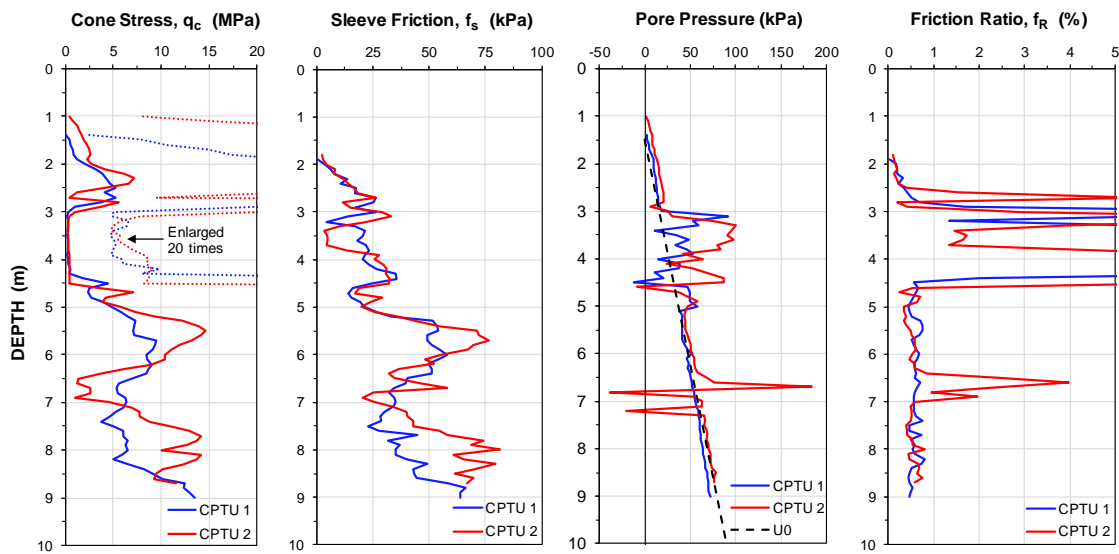


Figure 3. CPTU diagrams (CPTU 1 and CPTU 2 from soundings pushed about 55 m and 70 m from the test piles on February 17-20, 2017).

Four oedometer tests from 4.1, 4.3, 5.1, and 5.33 m depth have been carried out to determine the compressibility characteristics of the soft soil layer. From the tests Janbu modulus number, m , was found to be about 6, corresponding to a compression ratio, CR , of 0.44. The recompression modulus number, m_r , was about 48, corresponding to a recompression ratio, RR , of 0.056. The coefficient of consolidation, c_v , was about $2.9 \text{ m}^2/\text{year}$. The soft soil layer was normally consolidated.

2.2 Test setup and instrumentation

The test setup consisted of four instrumented test piles and a ground monitoring system (Figure 4). The test piles were two instrumented 406 mm diameter (8 mm wall thickness) steel piles (STP1 and STP2) and two instrumented 350 mm square precast concrete piles (CTP1 and CTP2). The piles were driven with a 90 kN Junttan HHK9A hammer from a working platform (elevation +1.5 m above mean sea level) to the approximate depth of 12 m. Piles STP1 and CTP1 were without bitumen coating and piles STP2 and CTP2 were coated with a 1 mm thick layer of 80/100 penetration bitumen to 8 m depth. The ground monitoring system consisted of several vibrating wire piezometers, settlement stations, and one standpipe piezometer, which all were installed from the working platform. The fill was placed up to +4.5 m ASL over approximately 125 x 150 m area around the test piles.

The pore water pressures were measured using low air-entry vibrating wire piezometers installed at 5.0, 6.5, 7.7, and 12.2 m depth using the fully grouted installation method. The grout consisted of water, cement, and bentonite with the 8:1:1 ratio by weight (water:cement:bentonite). In addition, one open standpipe piezometer was installed with the intake zone at 12.5 m depth.

The settlement at different depths was measured by magnetic extensometers (6 leaf spider magnets) installed at 1.2, 4.4, 6.1, 7.6, 8.7, and 13.4 m (datum magnet). The settlement of the surface was monitored by two settlement plates installed at 0.5 m depth.

Figure 5 shows the instrumentation of the steel piles. A pair of opposite mounted strain DFOS cables (BRUsens V9) was used. Two Ø 12 mm steel rebars were welded (one side intermittent fillet weld with weld length of 50 mm and pitch of 150 mm) along the test piles as a guide and protection for the DFOS cables. After placing the cables along the additional rebars, the DFOS cables were pre-strained to about 1,000 µε. The cables were glued using Araldite 2012 epoxy afterwards. Additionally, one line of vibrating wire strain gages (VW) was installed at five different depths: 1.0, 4.8, 6.4, 7.6, and 11.5 m respectively. The VWs were protected by an angle iron. Both steel test piles were supplied with pointed pile shoe.

Due to malfunctioning of one of the strain DFOS cables installed on the precast concrete pile, the instrumentation and the results obtained from the other strain DFOS cables will not be presented in this paper.

2.3 Test schedule

The planned test schedule consisted of two phases: Phase 1 to investigate the effect of the pile installation and Phase 2 to monitor the build up of drag force due to negative skin friction. The piles (steel and precast concrete) were driven on December 21, 2017 (Day 0)

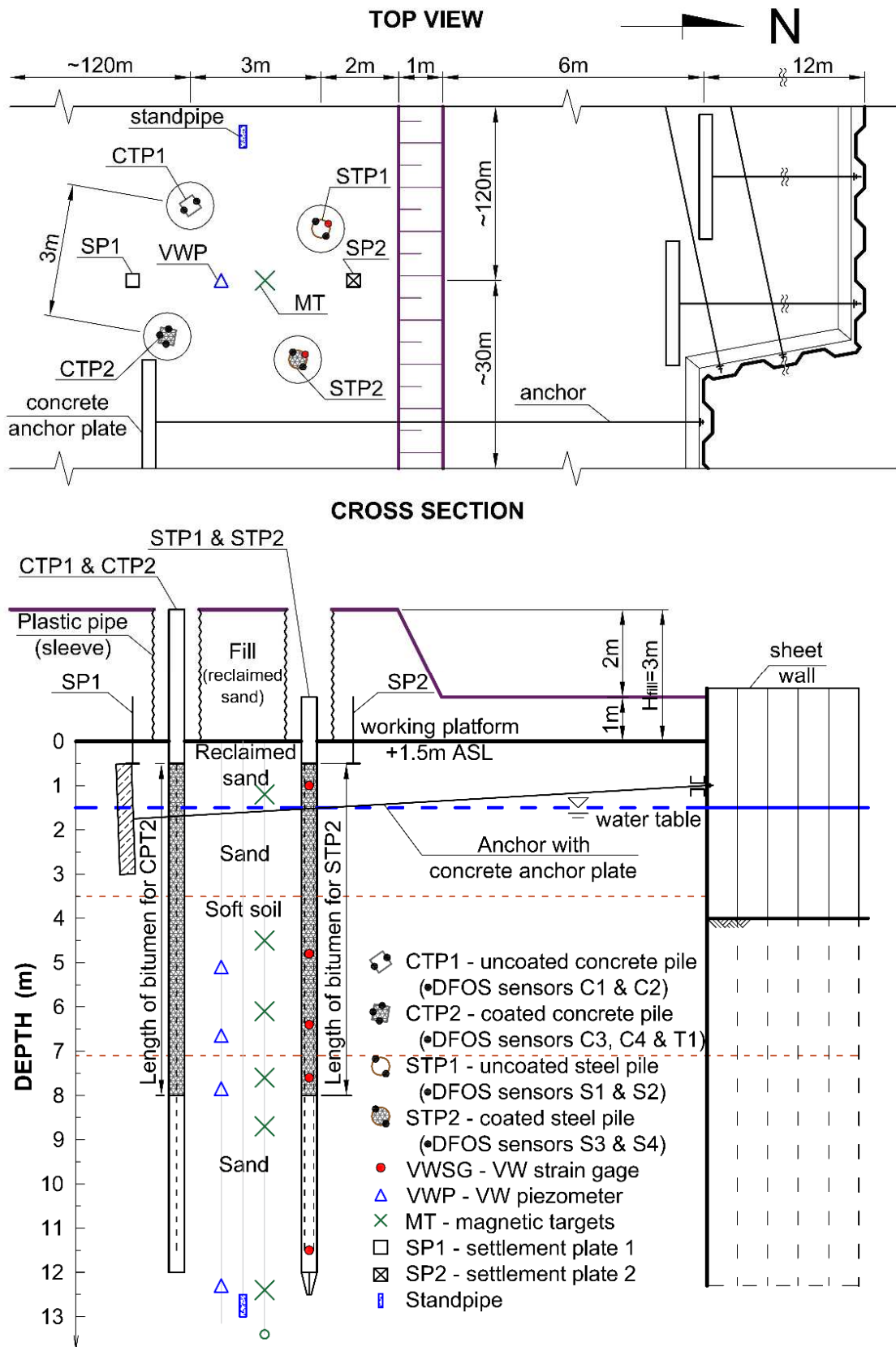


Figure 4. Soil profile and the test setup.

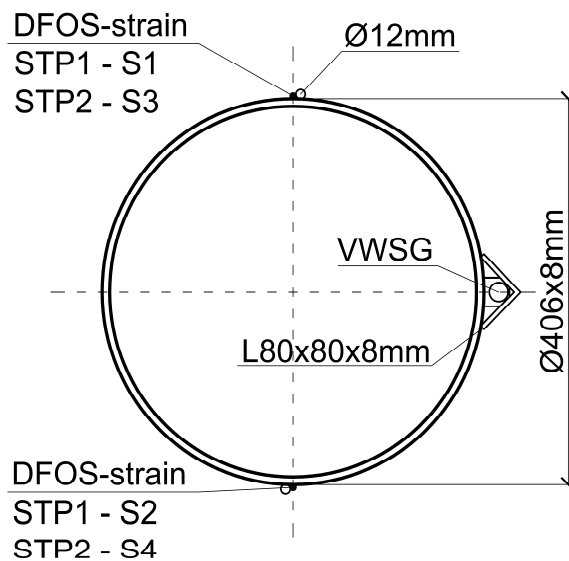


Figure 5. Cross-section of the instrumented steel test pile.

and the installation process took about 4 hours. The piles were installed with a 1 m stick-up above the ground surface (Depth 0). Then, on between May 1 and 3, 2018 (Days 131 through 133) placing of a 3 m thick fill around the test piles took place. Placing of the fill was completed in two 1.5 m stages. Monitoring of Phase 2 continued from May 3, 2018 through December 13, 2019 (Days 133 through 722).

The ground monitoring system was installed between January 16-18, 2018 (Days 26 through 28). The settlement and the pore water pressure data are referenced to the “zero” reading at Day 28. The strain measurements are referenced to the before-driving state, unless stated differently.

The first set of measurements was taken immediately after all four test piles had been driven, thereafter, seven sets of Phase 1 measurements were taken on Days 25, 48, 62, 78, 91, 119, and 126 until starting Phase 2 on May 3, 2018 (Day 133).

Construction activities, including installation of a sheet pile wall, anchor plates and filling the area in-between the sheet pile wall up to the final level of +4.5 m ASL, in the close proximity to the test piles continued during Phase 1 and 2 until about Day 200. As shown in Figure 6 (a), an unplanned one-sided loading occurred during Phase 1. The sheet pile wall was installed at Day 91. Further details on the construction activities around the test piles during Phase 1 are provided in Kania and Sørensen (2019). The concrete anchor plates were installed in the proximity to the test piles (about 3 m away from the bitumen coated steel pile) between Days 123-125 as presented in Figure 6 (b).



Figure 6. Test site at (a) Day 78 and (b) Day 126 (before placing the 3.0 m fill). The concrete slabs in (b) are anchor plates for the sheet pile wall seen in the background.

2.4 Data analysis

2.4.1 Temperature compensation

The strain data recorded from the DFOS cables must be thermally compensated in order to obtain mechanically induced strains. Unfortunately, the temperature DFOS cable installed on the bitumen coated precast concrete pile (see Figure 4, sensor T1 on CTP2) was damaged before the pile installation. Therefore, the temperature data with depth and time for temperature correction of the strain DFOS records were obtained using the thermistor readings from the VW gages. The point-to-point temperature correction proposed in (Luna 2014) was accordingly modified into the following:

$$\varepsilon_m^z = \varepsilon_t^z - \left(0,95 \cdot \frac{\Delta T^z}{k_T} \cdot k_\varepsilon + \Delta T^z \cdot \alpha_L \right) \quad (1)$$

where ε_m^z = mechanical strain at depth z
 ε_t^z = total (measured) strain at depth z
 ΔT^z = change in temperature at depth z
 k_ε = strain conversion factor (strain/frequency) = -6.67 $\mu\varepsilon/\text{GHz}$
 k_T = temperature conversion factor ($^\circ\text{C}/\text{frequency}$) = -0.638 $\text{C}^\circ/\text{GHz}$
 α_L = thermal expansion coefficient of steel = 12.2 $\mu\varepsilon/\text{C}^\circ$

2.4.2 Data interpretation

The following information was calculated from the two diametrically opposite placed DFOS cables:

$$\varepsilon_{m,a}^z = \frac{1}{2} (\varepsilon_{m,1}^z + \varepsilon_{m,2}^z) \quad (2)$$

$$\kappa^z = \frac{1}{d} (\varepsilon_{m,1}^z - \varepsilon_{m,2}^z) \quad (3)$$

$$M^z = EI\kappa^z \quad (4)$$

$$Q^z = \frac{d}{dz} EI\kappa^z \quad (5)$$

where $\varepsilon_{m,a}^z$	=	averaged axial mechanical strain at depth z
$\varepsilon_{m,1}^z$	=	mechanical strain of cable 1
$\varepsilon_{m,2}^z$	=	mechanical strain of cable 2
κ^z	=	curvature at depth z
d	=	distance between two opposite strain DFOS cables
M^z	=	bending moment at depth z
E	=	Young's modulus of steel = 210 GPa
I	=	moment of inertia of the steel test piles = $1.98 \cdot 10^{-4} \text{ m}^4$
Q^z	=	shear force at depth z

Then, assuming the boundary conditions, the gradient and the lateral displacement are derived using the following equations:

$$\vartheta^z = \int_0^z \kappa \, dz + A \quad (6)$$

$$u^z = \int_0^z \vartheta \, dz + B \quad (7)$$

where ϑ^z	=	gradient at depth z
u^z	=	lateral displacement at depth z
A and B	=	integration coefficients as determined by the boundary conditions

3 RESULTS

3.1 Soil settlements

Figure 7 shows the soil settlement at selected days after pile driving. It can be seen from the graph, that the settlement occurred mainly due to the compression of the soft soil layer. The maximum settlement of 33 mm before placing the fill (Day 126) was recorded from the settlement gage located at 1.2 m depth. The settlement during Phase 1 is thought due to consolidation of the soft soil layer due to the placing a 1.5 m thick layer of reclaimed sand to form a working platform. Placing the additional 3 m high fill layer significantly increased the compression of the soft soil layer. The maximum settlement at Day 722 was recorded to be 381 mm as recorded at 1.2 m depth.

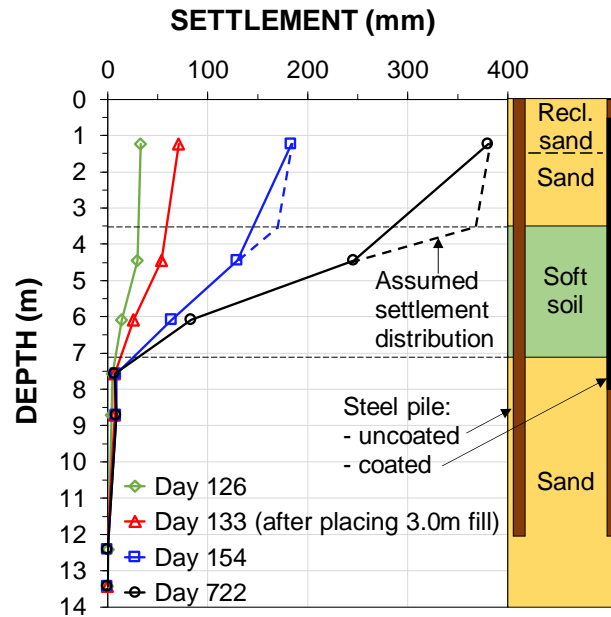


Figure 7. Soil settlement profiles at selected days after pile driving.

As shown in Figure 8, the individual settlement gages installed above 6.1 m depth are still settling albeit at a decreasing rate. The settlement of the gage located at 1.2 m depth is mainly due to compression of the soft soil layer. Placing of the fill is seen to cause only small settlement of the gages located in the sand below 7.6 m depth.

Small settlements of the pile head (1-4 mm) were recorded during Phase 1 and Phase 2.

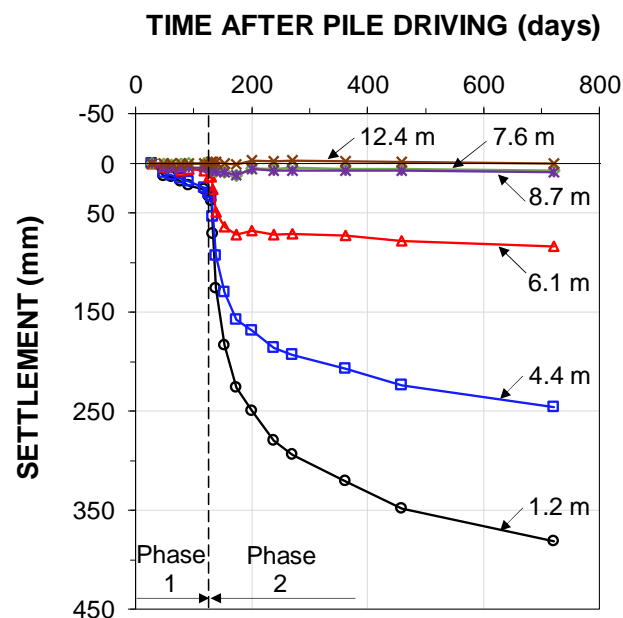


Figure 8. Settlement of individual gages with time after pile driving.

3.2 Pore water pressures

Figure 9 presents the measured pore water pressures with time. Immediately after placing the fill the piezometer located at 5.0, 6.5, and 7.7 m depth recorded an increase of 12.4, 11.5 and 8.9 kPa, respectively. The piezometer installed at 12.2 m depth (sand layer) did not record any increase of pore water pressure immediately after placing the fill. Between Day 133 and Day 141 the pore water pressure decreased by 4.9, 5.2, and 4.2 kPa from the piezometer installed at 5.0, 6.5, and 7.7 m depth, respectively. After Day 141, all the piezometers recorded an increase of pore water pressure. As can be seen from the graph the ground water table level in the bottom sand layer was increasing after placing the fill. It is therefore likely that the reduction in the pore water pressure due to consolidation is cancelled out by the increase due to rise in the water table. The piezometer installed at 12.2 m depth was following the increase of ground water table level.

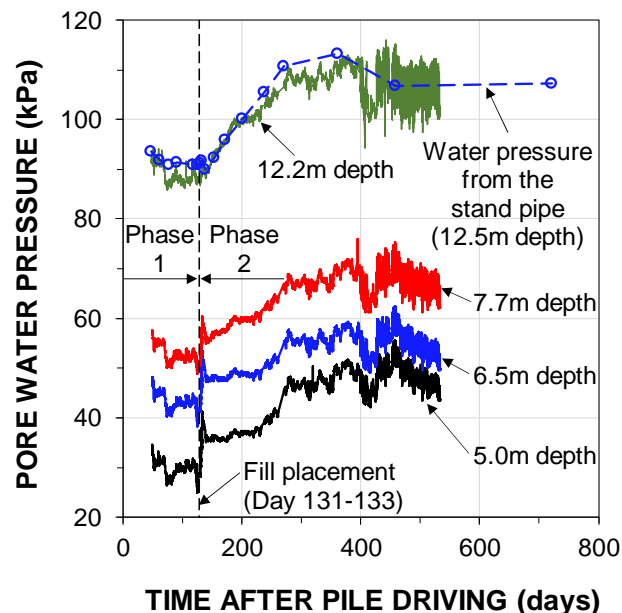


Figure 9. Pore water pressure recorded from individual piezometers located at different depths and the water pressure calculated from the standpipe water level records.

Figure 10 shows the hydrostatic and measured pore water pressure profiles at selected days after pile installation. At Day 48, the piezometer in the sand layer (12.2 m depth) showed a hydrostatic pore pressure corresponding to a ground water level at 3 m depth (1.5 m below mean sea level), while the water level measured from the ground surface corresponded to 1 m depth (0.5 m above mean sea level). The other piezometers confirmed the non-hydrostatic pore water pressure distribution. At Day 533, the piezometer installed at 5.0 m depth showed about 10 kPa excess pore water pressure, while the piezometers located at 6.5, 7.7, and 12.2 m depth showed hydrostatic distribution.

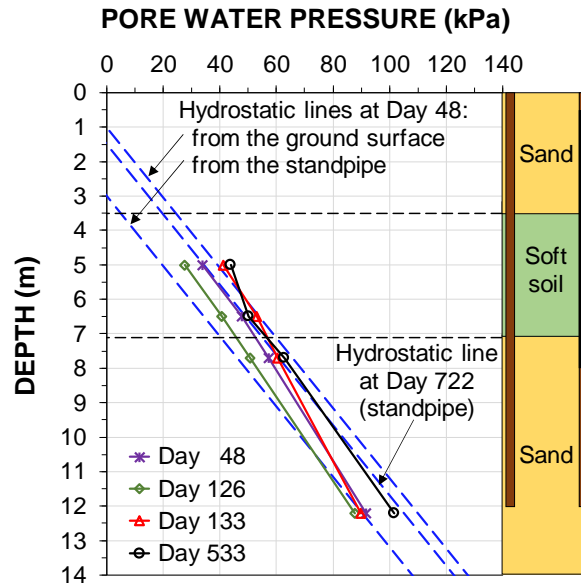


Figure 10. Pore water pressure profiles at selected days after pile driving.

3.3 Strain distributions

Figure 11 shows the strain distribution obtained from the individual strain DFOS cables along (a) the uncoated and (b) bitumen coated steel pile at selected days after pile driving. Negative values denote compression. To smoothen the strain DFOS data, a moving average over 100 readings was calculated giving a virtual gage length of 0.26 m. The strain records obtained immediately after driving (Day 0) from the uncoated (STP1) and bitumen coated (STP2) steel pile indicate bending of the piles. The observed increase in strain between Day 0 and Day 126 (before placing the fill around the test piles) i.e., S1 and S3—increase in tension and S2 and S4—increase in compression, could be attributed to the aforementioned unplanned one-sided loading occurring before Day 126 and causing bending of the piles. The maximum compression and tension values were recorded around the boundary between the soft soil and the bottom sand layer. The changes in strain distribution occurring between Day 126 and Day 722 is primarily a result of placing the fill. It can be seen that placing of the fill increased the extreme compression and tension values along the uncoated steel pile, while they remain unchanged for the coated pile. For the uncoated pile, placing of the fill is seen to increase the compressive strain values and unchange the tensile strain values in the soft soil and bottom sand layer. This result may be explained by the fact that negative skin friction (causing an increase of the compressive strain in both sensors) is masking the effect of bending the pile (causing an increase of the compressive and tensile strain along two opposite sensors). For the bitumen coated pile, placing of the fill is seen to increase both compressive and tensile strain values in the soft soil layer, which indicate an increase in bending of the pile. As expected, the bitumen coating reduced the increase in compressive strain along both sensors. In both piles, bending was less pronounced at the pile toe level.

Due to the bending, the readings obtained from the single line of VW gages were not analysed and are not presented in this paper.

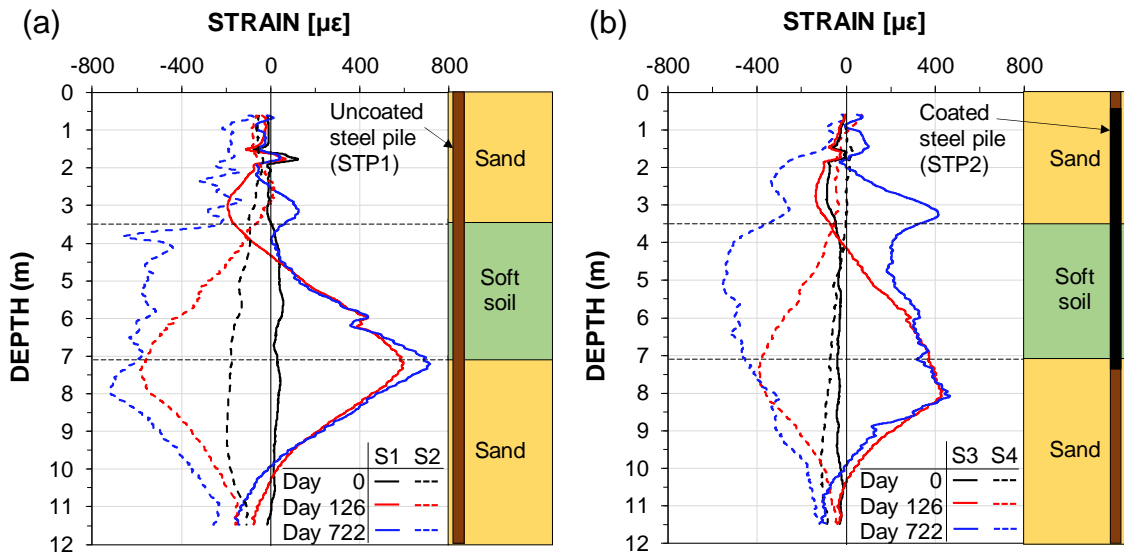


Figure 11. Strain profiles in (a) the uncoated steel pile (sensor S1 and S2) and (b) coated steel pile (sensor S3 and S4). The plots show measured data immediately after driving (Day 0), before placing the fill (Day 126), and 589 days after placing the fill (Day 722).

4 ANALYSIS

4.1 Deformation of the test piles

In order to investigate the deformation of the test piles, it was assumed that the piles worked as cantilever beam fixed at the pile toe after driving. The reference readings were the ones recorded immediately after driving. This allowed to determine the integration coefficients (cf. Eqs. 6 and 7). Figure 12 shows the curvature (a) and (b), gradient (c) and (d), and the lateral displacement (e) and (f) of the uncoated and bitumen coated steel pile, respectively. It can be seen from the graphs that both piles experienced similar deformation before placing the fill (Day 126). Afterwards (Day 722), the curvature, gradient, and lateral displacement of the uncoated steel pile (STP1) increased above 10.5 m depth. In contrast, the lateral deformation of the bitumen coated steel pile (STP2) was unchanged below 7.5 m depth.

4.2 Influence of the pile deformation on the distribution of internal forces.

Figure 13 shows the distribution of axial force (a) and (b), the bending moment (c) and (d), and the shear force (e) and (f) along the uncoated (STP1) and bitumen coated (STP2) steel pile respectively. These features were determined directly from the strain data with reference readings before pile driving. Positive values of axial force denote compression. In order to obtain an appropriate shear force distribution, the bending moment was smoothed (using a moving average) before differentiation. Even though, the shear force diagram above 4.5 m depth along the STP1 was scattered (Figure 13 (e)). Smoothing the data should be used with caution, since it can easily alter or disguise the meaningful data points.

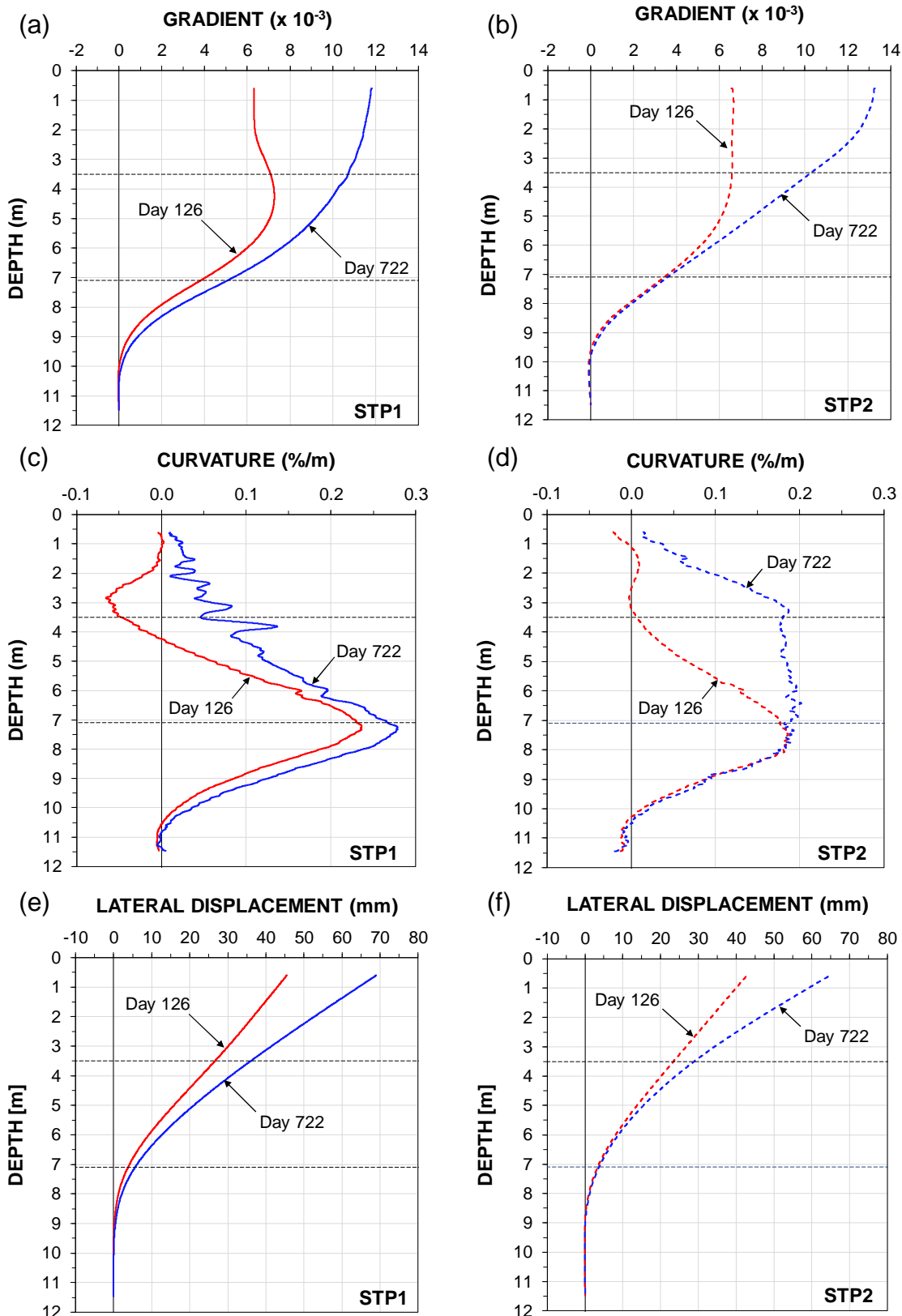


Figure 12. Curvature ((a) and (b)), gradient ((c) and (d)) and lateral displacement ((e) and (f)) of the uncoated (STP1) and bitumen coated (STP2) steel test pile recorded at Day 126 (before placing the fill) and Day 722 (589 days after the end of placing the fill). Data for STP1 at Day 126 from Kania et al. 2020.

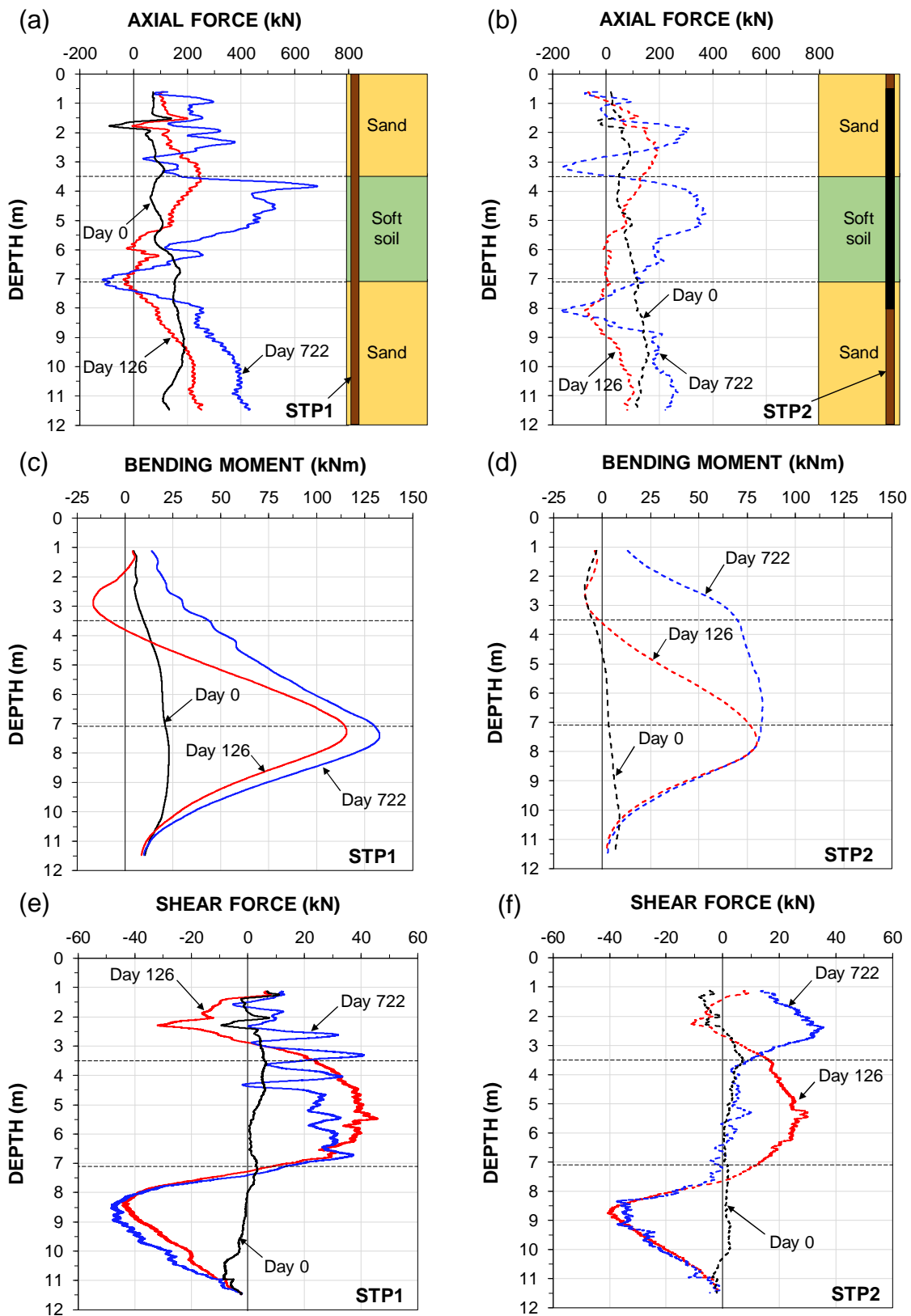


Figure 13. Axial force ((a) and (b)), bending moment ((c) and (d)) and shear force ((e) and (f)) along the uncoated (STP1) and bitumen coated (STP2) steel test pile recorded at Day 0 (immediately after driving), Day 126 (before placing the fill) and Day 722 (589 days after the end of placing the fill).

It can be seen from the graphs in Figure 13 that the development of internal forces immediately after driving (Day 0) and during the Phase 1 (Day 126) was similar in both test piles. Placing of the fill (Day 722) changed the bending moment and the shear force distribution, which significantly affected the axial force profiles. The bending moment increased along the uncoated and bitumen coated steel test pile. However, interestingly, it reached a constant value in the soft soil layer along the bitumen coated steel pile (Figure 13 (d)). The constant bending moment resulted in a neutralization of the shearing force in the soft soil layer. The presence of shear forces, especially at the boundaries between sand and the soft soil layer (at 3.5 and 7-8 m depth), generated tensile strain within the shear plane and affected the interpretation of axial force distribution.

5 CONCLUSIONS

Driven piles instrumented with DFOS cables can provide detailed information about the strain distribution. At least a pair of opposite mounted cables should be installed to determine the influence of lateral and vertical soil movement.

To obtain mechanically induced strains, recorded strain data from DFOS cables must be thermally corrected.

Axial strain, curvature and bending moment are directly obtained from the strain measurements. Therefore, they are more reliable than the gradient and lateral displacement distribution, which requires assumptions regarding boundary conditions.

Although shear force distribution can be calculated by differentiation of a bending moment, the bending moment distribution should be smoothed to obtain an appropriate shear force profile. However, smoothing must be applied with caution because it can disguise sudden data changes.

The distribution of axial force was induced by the pile installation, building up a residual force in the piles, and placing of the fill. However, it was disturbed by the shear force in the test piles caused by lateral soil movement. The presence of shear forces generated tensile strain at the location of shear planes and influenced the interpretation of axial force distribution.

6 ACKNOWLEDGMENTS

The authors would like to thank cp test a/s, Per Aarsleff A/S, Centrum Pæle A/S, DMT Gründungstechnik GmbH and Innovation Fund Denmark for providing funding for this study and Per Aarsleff A/S for providing data and for installing the instrumented piles.

7 REFERENCES

- Fellenius, B.H., 1972. Downdrag on piles in clay due to negative skin friction. *Canadian Geotechnical Journal*, 9(4), 323-337.
- Fellenius, B.H., 2015. Static tests on instrumented piles affected by residual load. *Journal of the Deep Foundation Institute*, 9(1), 11-20.

- Indraratna, B., Balusubramanimam, A.S., Phamvan P., and Wong, Y. K., 1992. Development of negative skin friction on driven piles in soft Bangkok clay. *Canadian Geotechnical Journal*, 29(3), 393-404.
- Kania, J.G., and Sørensen, K.K., 2019. A case study of soil-pile interaction in soft soils. XVII European Conference on Soil Mechanics and Geotechnical Engineering, Reykjavik, Iceland.
- Kania, J.G., Sørensen, K.K., and Fellenius, B.H., 2020. Application of distributed fibre optic cables in piles. *Geotechnical Engineering Journal of the SEAGS and AGSSEA* (accepted).
- Kechavarzi, C., Soga, K.B., Battista, N.D., Pelecanos, L., Elshafie, M.Z.E.B., and Mair, R.J., 2016. Distributed fibre optic strain sensing for monitoring civil infrastructure - a practical guide, ICE Publishing, London, UK, 264 p.
- Luna Inc., 2014. Distributed Fiber Optic Sensing: Temperature Compensation of Strain Measurement. Engineering note EN-FY1402, Roanoke, Virginia, United States, 7 p.
- Poulos, H.G., 1973. Analysis of piles in soil undergoing lateral movement. *ASCE Journal of Soil Mechanics & Foundations Division*, 99(5), 391-406.

CHAPTER 6

SOIL-PILE INTERACTION IN A SUBSIDING SOIL

6.1. Introduction

The main test site was established at Randers Harbour. Similarly to the Esbjerg test site (see Chapter 5), the purpose of this test setup was to investigate the soil-pile interaction in a soft, subsiding soil. The test setup consisted of two instrumented steel piles and two instrumented precast concrete driven piles. One pile of each type was bitumen coated. The piles were driven through gyttja on top of a sand layer. A 2 m high fill was placed to initiate the soil movement. Some of the lessons learnt from the Esbjerg test setup were implemented, e.g. instrumentation of the test piles. Others were assumed to be negligible in that case, e.g. lateral soil movement.

This chapter includes Journal Paper 3.

6.2. Assessment of the applied methodologies

The ground monitoring system consisted of settlement and pore water pressure sensors installed at different depths. Additionally, the groundwater level in the gyttja and sand layer was continuously monitored using TD-DiverTM system (Van Essen Instruments 2018). As a backup system for settlement measurements, two settlement plates at the working platform level were installed. The ground monitoring system was installed before driving the test piles (except the two settlement plates which were installed after the pile driving) which allowed to monitor the soil disturbance due to driving. It was assumed that inclinometers were not needed, because no construction activities were planned at the site during the monitoring period that could induce lateral soil movement.

The steel test piles were instrumented with two pairs of opposite mounted strain DFOS cables and one pair of opposite mounted temperature DFOS cables. As a backup system, a pair of opposite mounted VW gauges at four different depths was installed. Both systems were able to withstand the installation process and provided long-term measurements.

The precast concrete piles were instrumented with two pairs of opposite mounted strain DFOS cables and a single temperature DFOS cable. As a backup system, a pair of opposite mounted VW gauges at four different depths was installed. The surface mounted VW gauges were installed in pre-cut spots on the side surfaces of the piles and filled with a high-strength repair mortar. Unfortunately, it was revealed before driving that most of

the VW gauges were fluctuating and/or showing out of the range records, meaning that the reference reading could not be established. After driving, all but four VW gauges recorded out of the range strain data and were fluctuating. However, it was still possible to obtain the temperature data, which were used for temperature compensation of the measured strain DFOS data.

The vibrating wire piezometers and strain gauges were connected to a data logger which allowed to capture the influence of pile driving on the pore water pressure and also the decrease in the drag force along bitumen coated steel pile after placing the fill.

Installation of two opposite temperature DFOS cables allowed to recognize the issue related to the performance of these cables while installed in driven piles (see Chapter 2).

In order to limit the influence of concrete shrinkage on the strain measurements, the pile instrumentation was mounted on the piles casted 12 months before driving. The sensors were installed on the side surfaces of the pile and were exposed to concrete cracks due to driving. This made the interpretation of strain along the precast concrete piles difficult.

Placing of the 2 m high fill was sufficient to mobilise a relative movement between the test piles and the soil. The resolution of the DFOS system used in this study, allowed to distinguish very small strain changes along the test piles induced by placing of the fill.

The obtained unit shaft resistance was normalized by the vertical effective stress showing the development of the beta-coefficient with time. According to the literature (Johannesen and Bjerrum 1965, Burland 1973), the effective stress method is appropriate to calculate the unit shaft resistance for piles in cohesive soils. However, in this study the development of the beta-coefficient was determined only after placing the fill.

6.3. Summary of the results

The mobilised long-term beta-coefficient along the uncoated steel and precast concrete pile was 0.13 and 0.19, respectively.

The obtained pile material factor for steel was 0.7 (assuming the pile material factor for concrete equal to 1.0) and was comparable to the one obtained in the laboratory interface shearing tests (see Chapter 4).

The bitumen coating significantly reduced the magnitude of shearing forces along the piles. Its efficiency was dependent on the rate of relative movement between the pile and the soil as also reported in the laboratory interface shearing tests.

6.4. Critical review

The study presents the development of the unit shaft resistance after placing the fill only based on the strain DFOS sensors.

The DFOS system provided very detailed strain distributions, especially within the transition zone, where negative skin friction changes into positive shaft resistance. This was almost impossible to achieve with conventional strain monitoring systems (i.e. telltales or strain gauges). However, the current study did not propose any analytical method to predict the distribution of shaft resistance, with focus on the transition zone, and the magnitude of toe resistance due to the drag force.

6.5. PhD student's contribution

The PhD student's contribution to Journal Paper 3 includes preparation of the DFOS sensors, instrumentation of the test piles, collecting data from the VW, the DFOS sensors and the ground monitoring system, analysing the data and writing the paper (major contribution). The oedometer tests were performed together with a bachelor student. The grain size analysis and the organic content analysis were performed by the bachelor student.

JOURNAL PAPER 3

Kania, J.G., Sørensen, K.K., and Fellenius, B.H. The development of unit shaft resistance along driven piles in a subsiding soil. Planned for a journal submission.

Status: manuscript planned for a journal submission

The development of unit shaft resistance along driven piles in a subsiding soil

Jakub G. Kania

cp test a/s and Department of Engineering, Aarhus University

Kenny Kataoka Sørensen

Department of Engineering, Aarhus University

Bengt H. Fellenius

Consulting Engineer

Abstract:

This paper describes and analyses the results of a test programme focused on the development of unit shaft resistance along driven piles installed in a subsiding soil. Two instrumented $\text{\O} 406$ mm diameter, steel test piles (with and without bitumen coating) and two instrumented 400 mm x 400 mm, square precast concrete piles (with and without bitumen coating) were driven at a test site in Randers, Denmark to depths of 13.8 and 12.8 m, respectively. The test piles were driven through roughly 1 m of fill layer on top of 9 m soft soil layer overlying a postglacial, marine, medium dense sand layer. The unit shaft resistance was developed due to the soil set-up from the installation of the test piles (the first phase) and the placement of the fill (the second phase). The development of unit shaft resistance along uncoated driven piles is related to an increase in effective stress, a soil settlement after dissipation of excess pore water pressure and a rate of relative movement between the pile and the soil. The development of the unit shaft resistance along bitumen coated piles is related to a rate of relative movement between the pile and the soil. The bitumen coating reduced the drag force along the steel pile by 73 %.

Keywords

Soil-pile interaction, soft soil, bitumen coating, instrumented piles, distributed fibre optic sensors

1 INTRODUCTION

Placing the fill or lowering the groundwater table at a site induces soil settlement. For a piled foundation, settlement will develop negative skin friction along the upper length of the piles and positive shaft resistance along the lower length. An equilibrium force will develop at a depth called "neutral plane" (N.P.) between the sum of the sustained load on the pile plus the drag force (due to accumulated negative skin friction) above the N.P. and the sum of the positive shaft resistance and the mobilized toe resistance below the N.P.. Because the transition at the N.P. from negative to positive direction of shaft resistance involves a gradual movement change, a transition zone will develop above and below the N.P..

One of the first full-scale tests investigating the development of negative skin friction involved telltales to obtain a distribution of load in the test piles (Johannessen and Bjerrum 1965, Bjerrum et al. 1969). However, the limitation with telltales is that measurements were usually only obtained after driving. Therefore, the load distribution in the piles caused by driving were not defined. This disadvantage was eliminated by using load cells, strain gages, or vibrating wire strain gages directly attached or embedded in a test pile. Fellenius (1969; 1971; 2006) reported full-scale test results concerning the effects of the pile installation, the reconsolidation of the soil after the pile driving, the load distribution in the test piles due to placing the load on the pile head, and as finally caused by placing fill around the test piles. However, the above-mentioned sensors can provide strain data only at discrete points. Therefore, it was difficult to define the transition zone around the N.P.

Previous full-scale tests have been mainly performed to study the development of drag force and downdrag along steel and precast concrete driven piles installed in soft marine clay (Bozozuk and Labrecque 1969, Indraratna et al. 1992). Little information is available on the subject for driven piles installed in gyttja, a typical soft soil of Denmark.

In order to reduce the drag force (Baligh et al. 1978) proposed, electroosmosis, placing a casing outside the pile, or coating the pile with bitumen. Among the aforementioned methods, bitumen coating is considered the most efficient method. The efficiency of the bitumen coating is controlled by the shearing rate, thickness of the bitumen coating, and temperature (Fellenius 1979, Hutchinson and Jensen 1968). The most common type of the bitumen coating used in the previous studies was 60/70 or 80/100 with a thickness of about 1-1.5 mm. However, Briaud and Tucker (1997) recommended a 10-mm thickness.

The results from the cited full-scale tests showed that only small relative movement between the pile and the soil is required to develop unit shaft resistance (Fellenius 1984). Its magnitude can be analysed using either total or effective stress principles. Total stress method applies an empirical coefficient, α , to the stress-independent shear strength, c_u , (Tomlinson 1957) and the effective stress method applies an empirical coefficient, β , to the effective overburden stress (Burland 1973). The coefficients depend on soil composition, strength, and reconsolidation as well as pile type and construction method.

It was therefore decided to start an experimental programme to investigate force distribution in uncoated and bitumen coated, steel and precast concrete, instrumented driven piles installed in gyttja. In July 2018, a field test comprising four driven piles was started. The piles were instrumented with distributed fibre optic sensors (DFOS) and vibrating wire (VW) gages. The details of the DFOS cable arrangements and results were presented by Kania et al. (2020).

This paper describes and analyses the results of the experimental full-scale test setup focused on the development of shaft resistance for uncoated and bitumen-coated driven piles in the subsiding soft soil. The subsidence was induced by placing a 2 m thick fill around the test piles.

2 MATERIALS AND METHODS

2.1 Soil profile

The test site was located at Randers Harbour, Denmark. The initial step in the overall development of the Randers Harbour area was a site improvement scheme employing vertical drains for acceleration consolidation settlement, but for an about 30 m wide strip reserved for the pile test. The planned surcharge over the general area has not yet been placed.

The soil profile consisted of a 1 m thick old fill above an 8 to 10 m thick soft soil layer (the thickness varies 8-10 m) overlying a postglacial, marine, medium dense sand. The soft soil layer is postglacial marine origin organic clayey silt trace sand, locally regarded as gyttja. The soil properties are shown in Figure 1 showing in Figure 1a the distribution of water content and soil density, in Figure 1b the undrained shear strength, and in Figure 1c the grain size distribution. The depth refers to depth below the original ground surface. The grain size distribution was determined by laser diffraction performed on four soil samples from different depths.

The soil samples were collected in connection to the installation of the ground monitoring system (i.e. between the location of the test piles).

The water content of the soft soil layer ranged from about 70 % to about 150 % and was close to the liquid limit. The lower about 1 m thick layer of the soft soil had larger water content and the CPTU showed an increase of U2 pore pressure. The plastic limit ranged from 42 to 52 %. The measured unit densities of the soft soil layer ranged from 1,390 to 1,510 kg/m³ with an average value of 1,430 kg/m³.

The grain size distribution shows, on average, that the dominant particle size in the soft soil was silt (75 to 81 %), the clay size was 16 %, and the sand size was 7 %. The organic content ranged from 7.5 to 9.1 % with an average of about 8 %.

The undrained shear strength of the soft soil was determined from field vane shear tests that were adjusted by a factor $k = 0.77$ based on the plasticity index (Bjerrum 1972, Holtz and Broms 1972, Ovesen et al. 2012) and ranged from 13 to 35 kPa with an average of 21 kPa. The groundwater table in the old fill was close to the ground surface.

Two oedometer tests from 2.6 and 4.5 m depths showed the compressibility of the soft soil layer, expressed in terms of the Janbu modulus number, m , to be about 8 (c.f., Janbu 1963; 1998 and Fellenius 2018), corresponding to a compression ratio, CR, of 0.29. The recompression modulus number, m_r , determined in both oedometer tests was about 55, corresponding to a recompression ratio, RR, of 0.04. The coefficient of consolidation, c_v , was about 0.7 m²/year. The preconsolidation margin determined in both oedometer tests was about 20 kPa, which corresponds to an OCR at 2.6 m and 4.5 m depths of about 3 and 1.6, respectively.

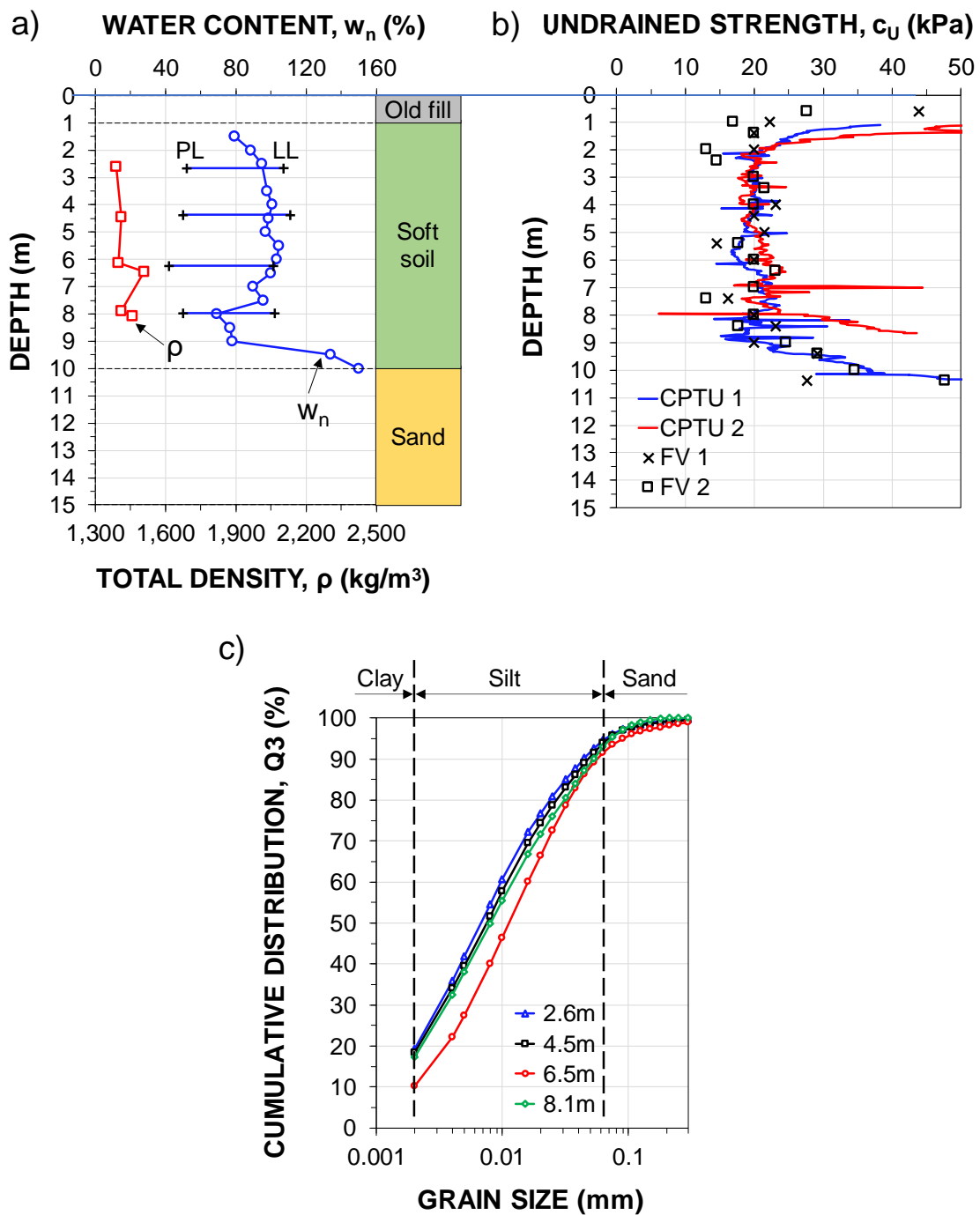


Figure 1. Soil properties: a) Atterberg limits and water content, b) undrained shear strength, c) grain size distribution by laser diffraction (data from Savery 2019).

The results of two CPTU soundings pushed on June 19-20, 2018 are presented in Figure 2. The CPTU 1 and CPTU 2 were pushed 1 m from the uncoated steel pile and the bitumen coated precast concrete pile, respectively. A cone factor, N_k , of 9 correlated the cone stress, q_t , to the vane shear strength. The sensitivity of the soft soil (the ratio of peak to remolded shear strength) ranged from 3 to 7 with an average of 4. The U2 pore pressure measurements of the CPTU soundings on June 19-20, 2018 showed the pore pressures in the sand to be hydrostatically distributed with a slight artesian head to about 0.6 m above the ground surface

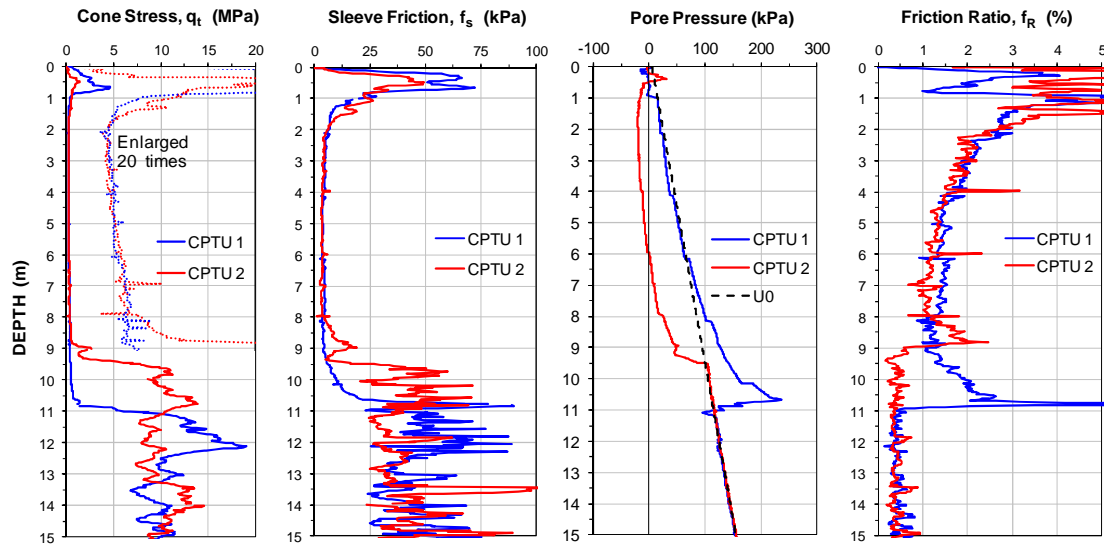


Figure 2. CPTU diagrams.

2.2 Test setup and Instrumentation

The test site is located about 10 m outside of the area treated with vertical drains. The test piles were two instrumented 406 mm diameter (8 mm wall thickness) steel piles (STP1 and STP2) and two instrumented 400 mm square precast concrete piles (CTP1 and CTP2). All piles were driven on July 3, 2018, with a 70 kN Junttan hammer through the soft soil to about 3 m into the sand. Piles STP1 and STP2 were driven to 13.8 m and 12.8 m depth and Piles CTP1 and CTP2 were driven to 12.8 m depth. The penetration through the soft soil was by the weight of the hammer and pile. Piles STP1 and CTP1 were without bitumen coating. The upper lengths of Piles STP2 and CTP2 were coated with a 1 mm thick layer of 80/100 penetration bitumen between the ground surface and the depths of 10.8 and 9.8 m, respectively. Figure 3 shows a photo taken on July 3, 2018, just when all four piles had been installed and the pile driver removed.



Figure 3. Photo of test piles after completed installation.

The settlement at different depths was monitored by magnetic extensometers (6 leaf spider magnets) installed at 1.2, 3.6, 6.0, 8.4, 9.7, and 14.6 m (datum magnet) depth and two settlement plates installed at about 0.4 m depth. The datum magnet located at 14.6 m depth, 1.8 m below the precast concrete pile toe level served as "zero " reference to all settlement gages.

The pile installation of all 4 piles took about 8 hours. Dynamic monitoring with the Pile Driving Analyzer was performed during the driving of the last 1 m of the steel test piles and during the entire driving of the precast concrete piles. The results of the monitoring are not reported here.

2.2.1 Steel test pile

Figure 5 shows the instrumentation of the steel piles. One pair of diametrically opposite surface-mounted vibrating wire strain gages (VW) were placed at four different depths: 1.0, 5.9, 10.8, and 13.3 m, respectively. Additionally, the steel test piles were instrumented with two pairs of opposite mounted DFOS cables and a pair of opposite mounted temperature DFOS cables. A BRUsens V9 cable was used as strain DFOS cable and a BRUsens Temperature 85°C cable was used as temperature DFOS cable. Six $\text{Ø} 10 \text{ mm}$ steel rebars were welded (one side intermittent fillet weld with the weld length of 50 mm and the pitch of 100 mm) along the test piles as a guide and protection for all the DFOS cables. The strain DFOS cables were pre-strained to about $1,100 \mu\epsilon$. All the DFOS cables were glued using Araldite 2012 epoxy. The VW gages were protected by an angle iron welded to the steel piles. Both steel test piles were supplied with a flat pile shoe.

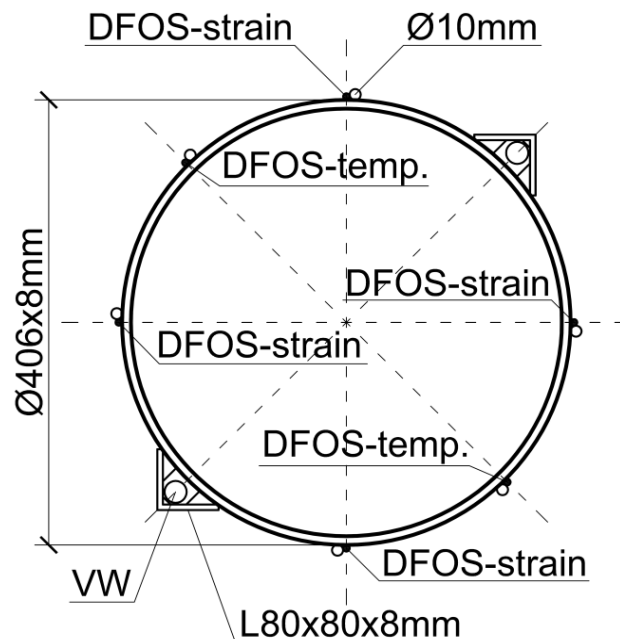


Figure 5. Cross-section of the instrumented steel test pile.

2.2.2 Precast concrete test piles

Figure 6 shows the instrumentation of the precast concrete piles. The piles were cast 14 months before driving. They were instrumented with pairs of diametrically opposite position of surface-mounted VW gages at four depths: 1.2, 5.5, 9.7, and 12.3 m, respectively. (As mentioned below, the VW gage records turned out to be unusable and had to be discarded). They were also equipped with two pairs of diametrically opposite surface-mounted strain DFOS cables and one temperature DFOS cable. A BRUsens V9 cable and a BRUsens Temperature 85°C cable were used to measure strain and temperature, respectively. The strain DFOS cables were pre-stressed to about $1,100 \mu\epsilon$.

As shown in Figure 7, the DFOS cables were placed along pre-prepared grooves on the side surfaces of the precast concrete piles and covered with Araldite 2012 epoxy. The figure also shows that the resin anchor end blocks were installed in pre-cut spots on the surface of the precast concrete piles. The VW (and cables) were then protected by filling the cuts with a high-strength repair mortar.

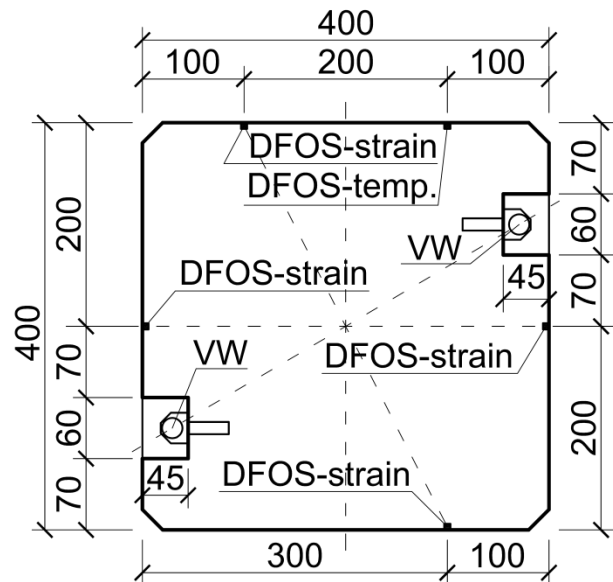


Figure 6. Cross-section of the instrumented precast concrete test pile



Figure 7. Installation of a DFOS cable and a VW on a precast concrete pile

2.3 Test programme

The test programme consisted of two phases. Phase 1 addressed the effects due to pile installation and Phase 2 those due to placing of the fill.

All ground monitoring systems were installed in June 2018 (except two settlement plates which were installed after the pile driving). The test piles were driven on July 3, 2018 (Day 0) 12 days after completing the installation of the ground instrumentation.

The uncoated steel test pile (STP1) was installed first followed by the bitumen-coated steel test pile (STP2), the uncoated precast concrete pile (CTP1), and the bitumen-coated precast concrete pile (CTP2).

The piles were installed with a 2.2 m stick-up above the ground surface. Before placing the fill, all four test piles were sleeved along the stick-up length with a plastic pipe (\varnothing 600 mm) to protect them from the fill.

The first set of measurements was taken on were installed in June 2018 immediately after driving the piles. Afterwards, seven sets of measurements were recorded, (Days 1, 3, 6, 9, 41, 50, and 65) between driving the piles and starting the second phase at Day 72, September 13, 2018.

Between September 13 and 14, 2018 (Days 72 through 73), a 2 m high embankment was placed over a 10 x 19 m footprint area around the test piles with an edge slope of 1:1 (c.f., Figure 4.). The fill was completed in two 1 m stages.

2.4 Obtaining Strain in DFOS Cables

To obtain mechanically induced strain from DFOS cables it is necessary to thermally correct the DFOS measurements (Kechavarzi et al., 2016). Unfortunately, due to malfunctioning of the temperature DFOS cables, the equation proposed in (Luna 2014) to obtain mechanically induced strain had to be modified into the following form of Eq. 1.

$$\varepsilon_m^z = \varepsilon_t^z - \left(0.95 \cdot \frac{\Delta T^z}{k_T} \cdot k_\varepsilon + \Delta T^z \cdot \alpha_L \right) \quad (1)$$

where ε_m^z = mechanical strain at depth z
 ε_t^z = is total (measured) strain at depth z
 ΔT^z = change in temperature at depth z ($^{\circ}\text{C}$)
 k_T = temperature conversion factor from temperature to frequency
(in this study equal to $-0.638 \text{ }^{\circ}\text{C}/\text{GHz}$)
 k_ε = strain conversion factor from temperature to strain
(in this study equal to $-6.67 \text{ } \mu\varepsilon/\text{GHz}$)
 α_L = thermal expansion coefficient of the pile material
set as 12.2 and $10.4 \text{ } \mu\varepsilon/^{\circ}\text{C}$ for the steel and concrete piles, respectively

The cross-section area was calculated as 0.01 and 0.16 m² for steel and precast concrete test piles, respectively. The elastic modulus, E , was assumed to be 210 for the steel piles. The elastic modulus of concrete, E_c , for the precast concrete piles was assumed to be 37 GPa as based on the type of concrete (C50/60) and laboratory tension tests conducted on different piles from the same factory (Sørensen 2015). The temperature data with depth and time were obtained from the VW gages.

3 RESULTS AND DISCUSSION

The results are divided into Phases 1 and 2. Phase 1 was for period before and Phase 2 was for the period after placing the fill. The records of ground monitoring systems (settlement and pore water pressure) during Phases 1 and 2 are referenced to Day 0.

The temperature before driving was about 40 °C (as heated by the sun) and reduced after driving to about 10 °C in the soil. Unfortunately, due to malfunctioning of the temperature DFOS cables and the non-uniform temperature along the test piles before and immediately after driving, the temperature correction of measured strain DFOS data was not possible. A possible explanation for the malfunctioning of the temperature DFOS cables is that they were sensitive to mechanical strain (Kania et al. 2020).

Also the VW gages installed on the precast concrete test piles malfunctioned before the driving and all VW strain records in the concrete piles were had to be discarded. Some of the sensors showed out of range records and some were fluctuating.

For the steel piles, STP1 and STP2, only the VW records are reliable for Phase 1. For Phase 2, both the VW and DFOS systems provided reliable records.

For the concrete piles, CTP1 and CTP2, only the DFOS gages provided reliable strain records and only for Phase 2. The DFOS strain data were referenced to change of readings on Day 65 before placing the fill.

3.1 Soil and Pile Movements

3.1.1 Movements due to Pile Installation, Phase 1

Figure 8 presents soil settlements immediately after driving the test piles and at Days 9 and 65. The maximum settlement, 17 mm, was obtained from the settlement gage located at 9.7 m depth. The measurements above 7 m depth indicated that the soil heaved due to the pile installation and then settled back a small amount (about 8 mm) during the 65-day observation period. The maximum heave was 22 mm, as measured at the depth of the first settlement gage located at 1.2 m depth. The heave decreased with depth. Below 7 m depth, the soil was pushed downward by the pile installation. The maximum downward movement was 18 mm and occurred at between 8 and 9 m depth. The downward movement did not change significantly during the Phase 1 observation period (0 through Day 65).

The settlement of the pile heads was small (zero to 1 mm) during Phase 1.

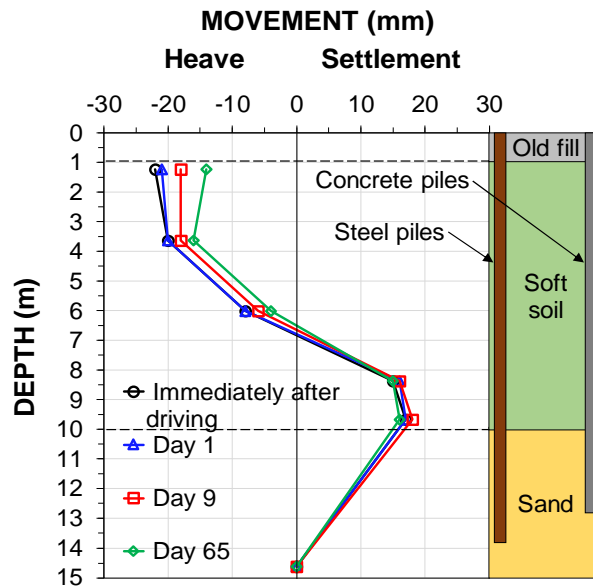


Figure 8. Soil movement profiles immediately after and at selected days after driving.

3.1.2 Movements due to Fill, Phase 2

Figure 9 presents the distribution soil settlements at selected days due to the placing of the fill (start of placing it was Day 72) and the final soil settlement calculated at the center of the test site using the compressibility and consolidation parameters (c.f., Section 3.1). The stress distribution due to the fill placement (embankment) was calculated using equation by Osterberg (1957) based on integrating the Boussinesq solution and later verified by calculations employing UniSettle4 software (Goudreault and Fellenius 2015). As expected, the settlement occurred mainly in the soft soil layer due to the consolidation process. The settlements of the bottom sand layer were small; the recorded settlement of the gage located at 9.7 m depth (the closest gage to the bottom sand layer) was 3 mm 277 days after placing the fill (Day 350).

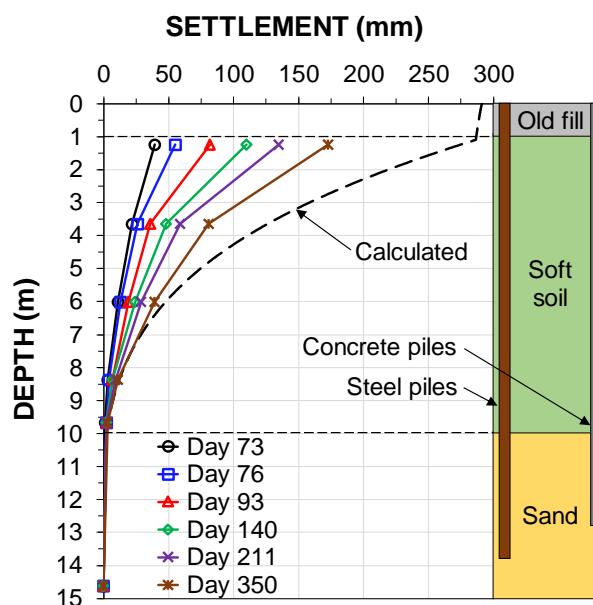


Figure 9. Soil settlement profiles due to placing of the fill at selected days after driving

The observed settlements of the individual gages due to the fill are shown in Figure 10. It can be seen from the graph, that the soil is still settling albeit with a decreasing rate. The placing of the fill caused only small settlement (3 mm) in the sand (gage located at 9.7 m depth). The settlement gages located at 1.2, 3.6, 6.0, and 8.4 m depth recorded 173, 81, 39, and 11 mm settlement, respectively.

Small settlements of the pile heads (1-3 mm) occurred during the Phase 2.

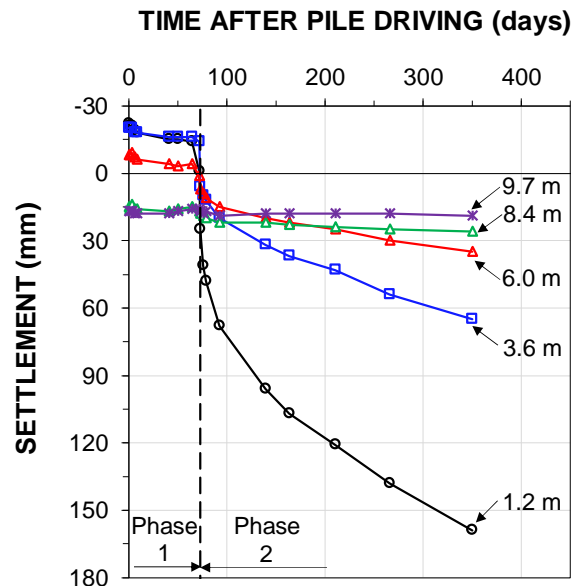


Figure 10. The settlement of individual gages with time after pile driving.

3.2 Pore Water Pressure

3.2.1 Phase 1

Figure 11 shows the excess pore water pressures as measured in the VW piezometer string installed at the center of the test area. The pore pressures were corrected for measured atmospheric variations (amounting to about 1 kPa on average) and variation of free water table in the sand layer (about 2 kPa on average), but have not been adjusted for heave or settlement of the respective piezometer gage. The excess pore pressures were referenced to the average pore pressures measured over four days before the start of the pile installation. The zero reading of time was taken at 07:45h the day the piles were installed.

Small excess pore pressure resulted from the soil displacement during the pushing down of Pile STP1 4.5 m away from the piezometer string. The installation of Piles STP2 and CPT1, both 1.5 m away from the piezometer string resulted in the maximum increase of pore water pressure: the piezometers located at 2.6, 5.8, and 9.0 m depth indicated the pore water pressure increase of 19.0, 32.3, and 42.2 kPa, respectively. The measured pore water pressure exceeded locally the total vertical stress by 31 to 44 % with an average of 37 %, which indicates a corresponding increase in horizontal stress. The measured pore pressure dissipated rapidly to an excess pore pressure of about 5 kPa at 5.8 and 9.0 m depth and about 1.5 kPa at 2.6 m depth 65 days after the pile driving. Also the piezometer installed in the sand at 12.8 m depth registered increase of pore pressure due to the driving. This increase dissipated within hours after the pile driving.

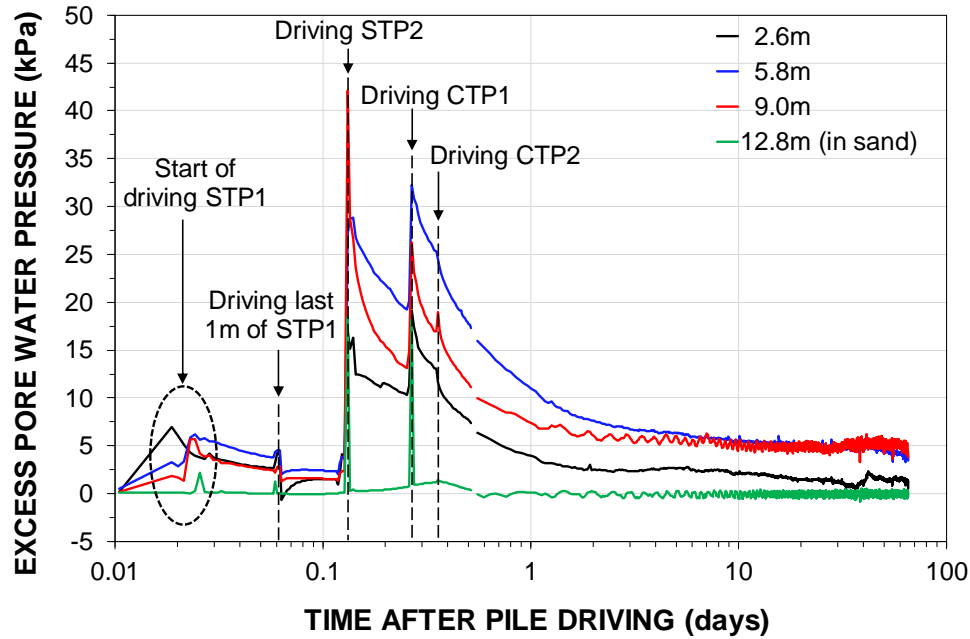


Figure 11. Excess pore water pressure due to pile installation and its dissipation with time until Day 65 (Phase 1).

3.2.2 Phase 2

Figure 12 shows the excess pore water pressure and its dissipation with time after placing the fill. It can be seen from the data, that the excess pore water pressure decreased with time reaching stable readings about 80 days after placing the fill. The maximum values at the end of placing the fill are rather low when considering 2-m-high fill (expected $\Delta\sigma_v = 36$ kPa). Based on the coefficient of consolidation, c_v , determined from the laboratory oedometer tests, the time to achieve 90 % of consolidation is more than 27 years. A possible explanation for this fast dissipation of pore water pressure may be due to the mentioned presence of vertical drains installed about 10 m from the test site. The piezometer located at 5.8 m depth recorded some unexpected increase of pore water pressure between Days 157-161 and Days 171-232. The cause is not known, but it is probably unrelated to the test piles and fill.

Figure 13 shows the hydrostatic and measured pore water pressure profiles with depth. The hydrostatic line was defined according to the readings obtained from the standpipe in the sand layer and a 0.5 m deep excavation performed at Day 0 from the ground surface in the old fill layer. During the monitoring period (Day 0 - Day 350) the water table level in the soft soil layer ranged from 0.1 to 0.7 m with an average of 0.4 m above the ground surface. The water table level in the sand layer ranged from 0.3 to 1.2 m with an average of 0.7 m above the ground surface. The pore water pressure profile before driving was between hydrostatic pore water pressure profiles. The greatest pore water pressure profile was obtained immediately after driving the piles.

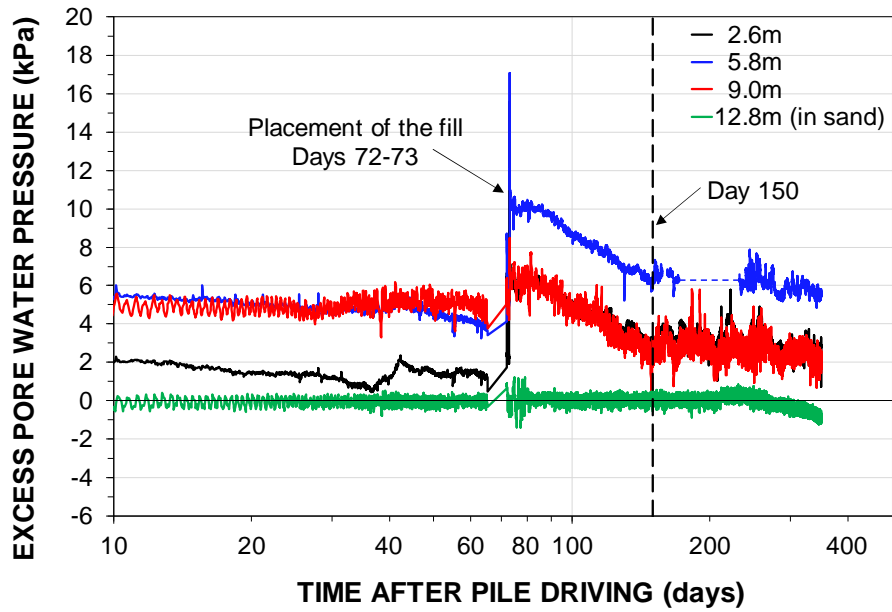


Figure 12. Excess pore water dissipation with time after placing the fill.

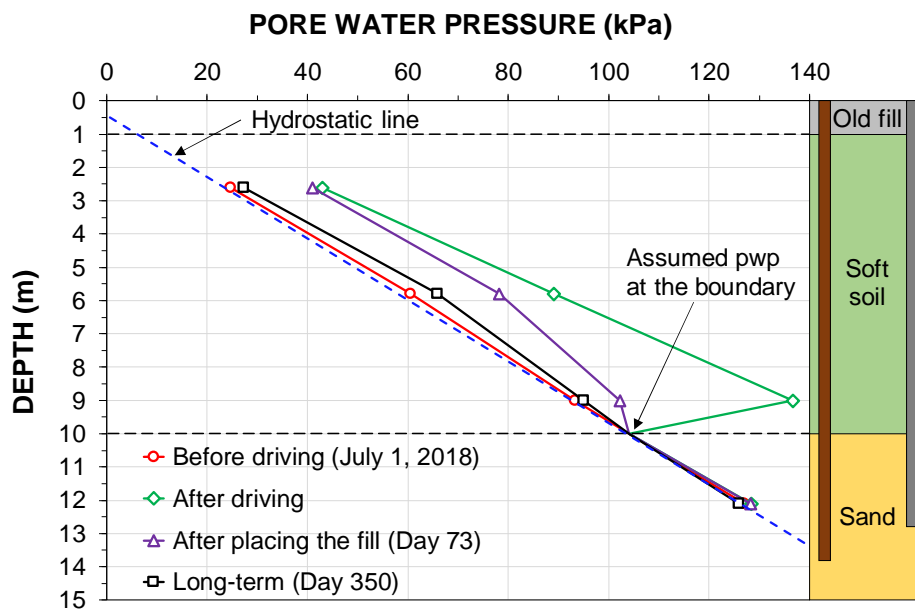


Figure 13. Pore water pressure, pwp, profiles with depth: hydrostatic, before driving, maximum measured after driving (July 3, 2018), maximum measured after placing the fill (Day 73) and final long-term (Day 350).

3.3 Axial Pile Forces

3.3.1 Phase 1

Figure 14a presents the drag force distribution obtained from the VW gages along the uncoated steel test pile (STP1) immediately and at selected days after driving. The reference reading was taken before the pile driving (the pile was lying on the ground surface) and all later records of force indicate the change in respect to the reference reading. Positive values denote compression.

Immediately after driving, the drag force distribution showed the highest values of 47 and 44 kN at the uppermost and lowermost gage and bottom of the STP1, respectively. The minimum value of 14 kN was obtained at 5.9 m depth. The drag force distribution immediately after driving could be explained by rapid compression of the old fill layer and heave of the upper soft soil layer (above 7 m depth). The drag force distribution increased with time in the middle and at the bottom of the pile. The unit shaft resistance can be calculated as the difference in force between the VW gages acting over the pile shaft area between the gages. Figure 15a shows the calculated unit shaft resistance along the SPT1 immediately and at selected days after driving. The unit shaft resistance of the fill layer and of the soft soil layer are comparable with the undrained shear strength (see Figure 1) and remoulded shear strength obtained from the field vane test, respectively.

The drag force distributions immediately and at selected days after driving the SPT2 (coated steel pile) are presented in Figure 14b. Similarly to the STP1, the reference reading was taken before driving the test pile. As can be seen from the data, the drag force distribution changed with time. The compressive axial force at the lowermost gage (13.3 m depth) increased by 30 kN at Day 1 and remained until Day 65. This result can be explained by the influence of driving the neighbouring pile (i.e. CTP1) located 3 m from the STP2. The gage located within the soft soil layer (at 5.9 m depth) recorded decrease in compression (10-15 kN) during Phase 1. The uppermost VW gage (at 1.0 m depth) generally recorded increase in compression. What is surprising is that the VW gages located at 10.8 m depth indicated tension of the STP2. Two opposite mounted VW gages located at that depth recorded compression and tension at opposite sides with similar magnitude. This result suggests deformation of the pile at that depth, which could be an explanation to the issue. The unit shaft resistance along the STP2 immediately and at selected days after driving is presented in Figure 15b. As expected, the unit shaft resistance within the soft soil layer at Day 65 is low about 5 kPa. Due to aforementioned issues with the VW gages located at 10.8 m depth, the calculated unit shaft resistance of the lower part of the pile need to be interpreted with caution.

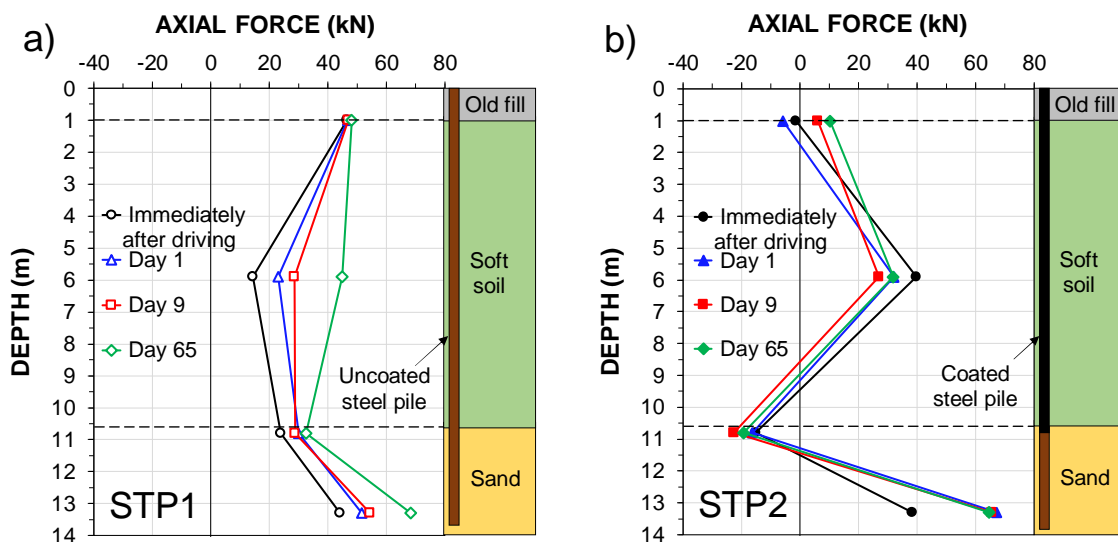


Figure 14. Axial force distribution along the a) STP1 (uncoated steel pile) and b) STP2 (coated steel pile)

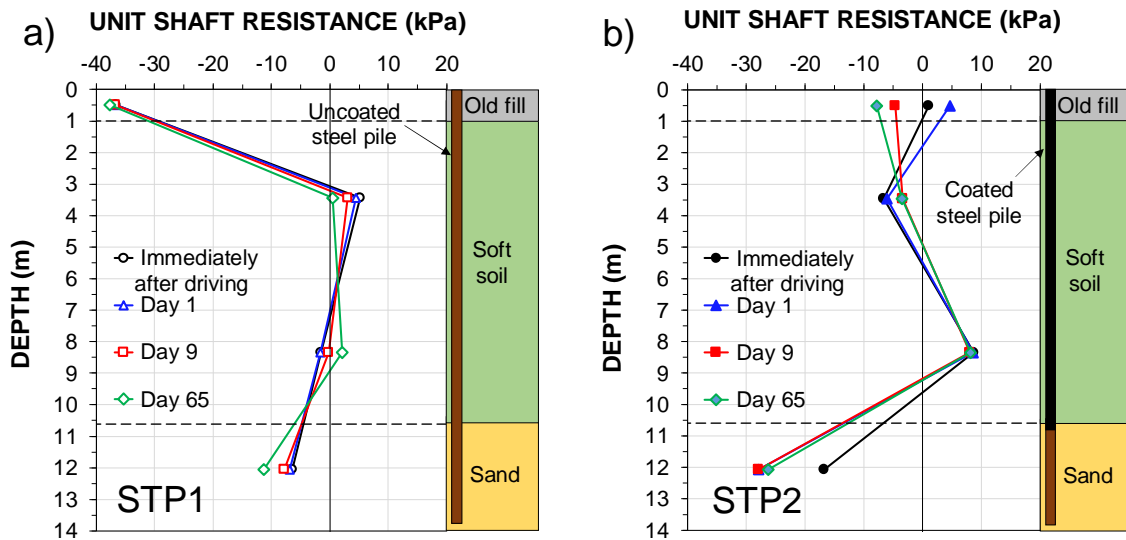


Figure 15. Unit shaft resistance along the a) STP1 and b) STP2 immediately and at selected days after driving.

3.3.2 Due to placing of the fill, Phase 2

Figure 16 presents the drag-force distribution along the uncoated (STP1) and bitumen coated (STP2) steel test pile immediately (Day 73) and 277 days after placing the fill (Day 350). As shown in Figure 16, the drag force distributions obtained from the DFOS immediately after placing the fill were the same along the uncoated and bitumen coated pile. With time, the drag force distribution along the uncoated and bitumen coated pile has increased and decreased, respectively. The obtained long-term maximum drag force on the uncoated and bitumen coated pile was 87 and 24 kN, respectively. Hence, the bitumen coating has resulted in an approx. 73 % reduction in the maximum drag force. This result was confirmed by the VW gages mounted on the uncoated and bitumen coated pile.

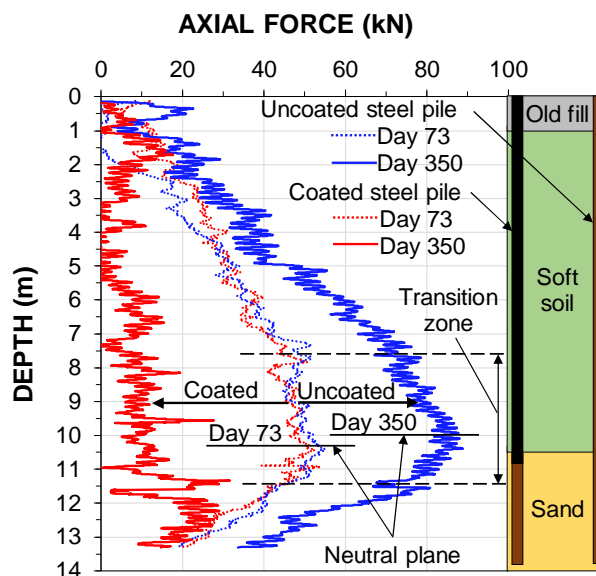


Figure 16. Drag force distribution along the STP1 (uncoated) and STP2 (bitumen coated) immediately (Day 73) and 277 days after placing the fill (Day 350).

Figure 17 shows the development of drag force distribution at 5.9 m depth (average value) obtained from two opposite mounted VW gages along the uncoated and bitumen coated steel pile. It can be seen, that the magnitude of the drag force on both piles is similar during the fill placement. During the first 8 days after placing the fill, the drag force on the uncoated pile was constant (about 30 kN) and increased afterwards with a decrease of excess pore water pressure (see Figure 12). Interestingly, the drag force on the uncoated pile was still increasing even after dissipation of excess pore water pressure. In contrast, the drag force on the bitumen coated pile was significantly reduced during the first 8 days after placing the fill (reaching a value of 4 kN) and does not show significant change afterwards. This result support other research which found that the drag force can be significantly reduced by the use of bitumen coating (Walker and Darvall 1973, Fellenius 1975, Fukuya et al. 1982).

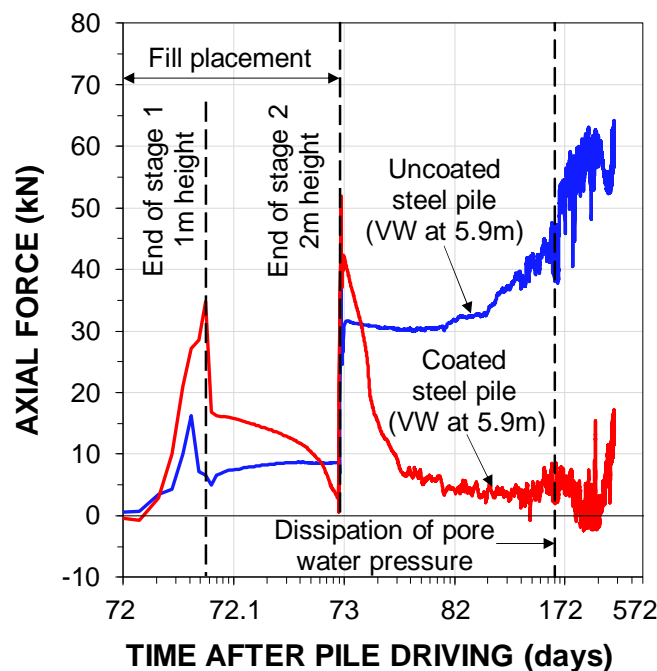


Figure 17. Axial force at 5.9 m depth along the STP1 (uncoated) and STP2 (bitumen coated) with days after fill placement.

Owing to the spatial resolution of the DFOS it was possible to determine the location of the neutral plane, at which the maximum drag force occurs, and distinguish the transition zone, where negative direction of shear changes into positive (Figure 16). The neutral plane along the uncoated steel pile was located in the soft soil layer and moved up slightly with time (by about 0.3 m between Day 73 and Day 350). This finding is in agreement with Endo et al. (Endo et al. 1969) who observed that the neutral plane moved up and stayed at certain depth with time. As can be seen from Figure 16, the transition zone (277 days after placing the fill) on the uncoated steel pile extends from about 2.3 m above the neutral plane (7.8 m depth) to about 1.4 m below the neutral plane (11.5 m depth). Disregarding the occurrence of the transition zone will result in overestimating the maximum drag force. In contrast, it is difficult to determine the transition zone (277 days after placing the fill) along the bitumen coated pile.

Figure 18 shows the drag force distribution along the uncoated precast concrete pile (CTP1) only at an early stage of the second phase (up to 20 days after placing the fill). The strain profiles recorded from the strain DFOS after this stage were scattered and their interpretation was difficult. A possible explanation for this is the existence and evolution of cracks on the sides of the precast concrete test piles (Kania et al. 2020). As shown in Figure 18, the neutral plane was located at about 7.8 m depth and the transition between negative and positive direction of shear was sharp at that stage. The maximum recorded drag force of 86 kN occurred 20 days after placement of the fill (Day 93).

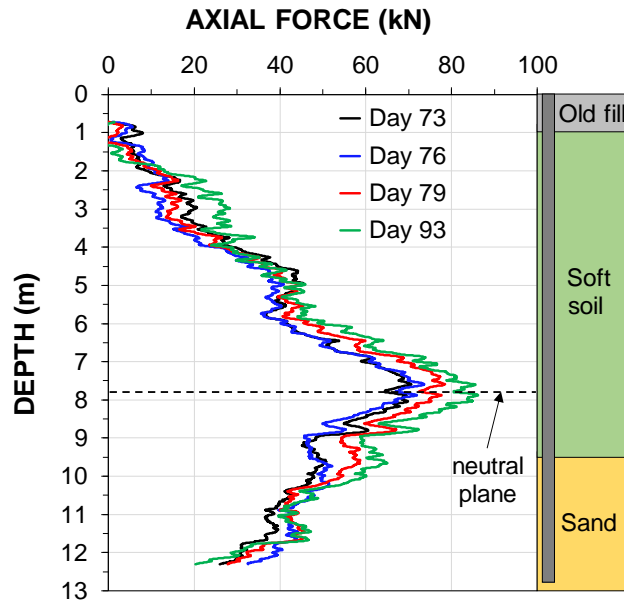


Figure 18. Axial force distribution (determined from the DFOS data) along the uncoated precast concrete pile (CTP1) at selected days after placing the fill.

The evolution of cracks and its magnitude was even greater along the bitumen coated precast concrete pile (CTP2). Thus, the interpretation of the strain DFOS data was difficult. The DFOS results obtained from the CTP2 will not be presented in this paper.

4 ANALYSIS OF RESULTS, PHASE 2

4.1 Unit shaft resistance distribution

Figure 19 shows the unit shaft resistance distributions with depth along the uncoated and bitumen coated steel test pile and the uncoated precast concrete pile at selected days after placing the fill. The unit shaft resistance distribution along the uncoated and bitumen coated steel test pile immediately after placing the fill (Day 73) was similar. With time the unit shaft resistance (in both: negative and positive direction) was increasing along the uncoated steel test pile. In contrast, the unit shaft resistance (also in both directions) was decreasing along the bitumen coated steel test pile with time. The negative and positive unit shaft resistance along the uncoated precast concrete test pile was also increasing with time. The transition between negative and positive direction of shear was longer on the uncoated steel test pile than on the uncoated precast concrete test pile. The neutral plane (Figure 16 and Figure 18) is located at the depth where the unit shaft resistance is equal 0.

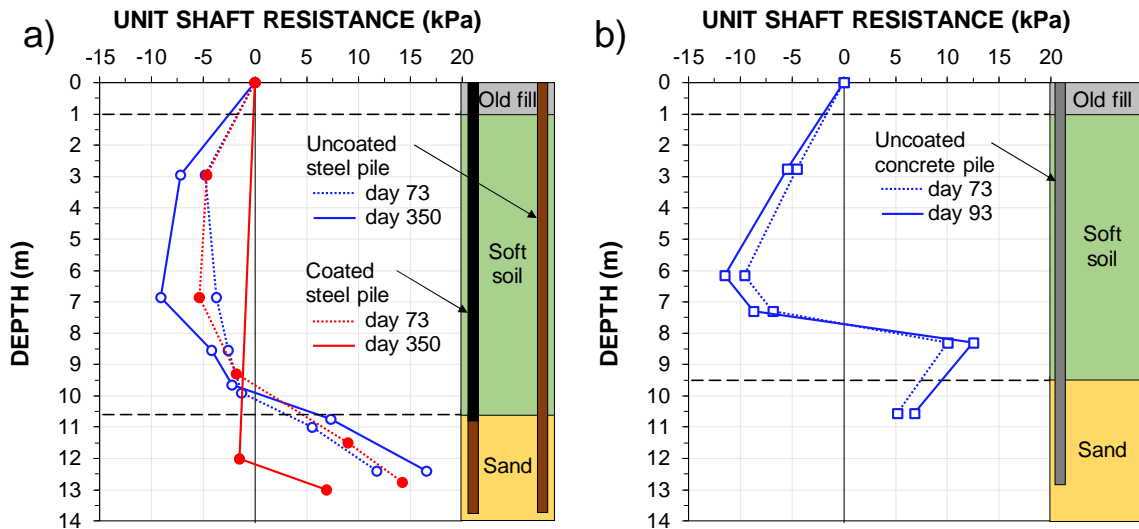


Figure 19. Unit shaft resistance distributions with depth along: a) the uncoated (STP1) and the bitumen coated (STP2) steel test pile immediately (Day 73) and 277 days after placing the fill (Day 350) and b) the uncoated precast concrete pile (CTP1) immediately (Day 73) and 20 days after placing the fill (Day 93).

4.2 Development of the unit shaft resistance along the steel test piles

Figure 20 presents the development of negative skin friction along the uncoated and bitumen coated steel pile. The data were obtained from the change in the drag force at certain depths (obtained from the DFOS) and divided by the shaft area. Similarly to the drag force development, the negative unit shaft resistance on uncoated and bitumen coated pile was increasing and decreasing, respectively. The negative unit shaft resistance on the uncoated and the bitumen coated pile immediately after placing the fill was about 4-5 kPa. These values correspond to the remoulded undrained shear strength determined from the field vane shear tests. The negative unit shaft resistance on the uncoated pile started to increase about 8 days after placing the fill along both determined layers (0-5.9 and 5.9-7.8 m depth) and was still increasing after dissipation of pore water pressure. In contrast, the negative unit shaft resistance was decreasing during the first 8 days on the bitumen coated pile reaching a stable value of almost 1 kPa and did not change with time.

Figure 21 presents the development of the beta-coefficient along the uncoated and bitumen coated steel piles after placing the fill. The beta-coefficient immediately after placing the fill was 0.07-0.12 (depending on the layer) and 0.10 (average along the bitumen coated section of the pile) for the uncoated and bitumen coated pile, respectively. Afterwards (Day 350), the beta-coefficient increased to about 0.15 and decreased to about 0.01 for the uncoated and bitumen coated pile, respectively.

A possible explanation for the long-term unit shaft resistance increase along the uncoated pile is an increase of effective stress due to dissipation of the excess pore water pressure and further settlement due to soil settlements under constant effective stress (Fellenius 2020). The gradual reduction of the negative unit shaft resistance increase could be caused by the gradual decrease of the increase in soft soil layer compression (Figure 10) cancelled out by the reducing effect of the decreasing shearing rate. Figure 22 shows the development of negative unit shaft resistance on the uncoated and bitumen coated pile

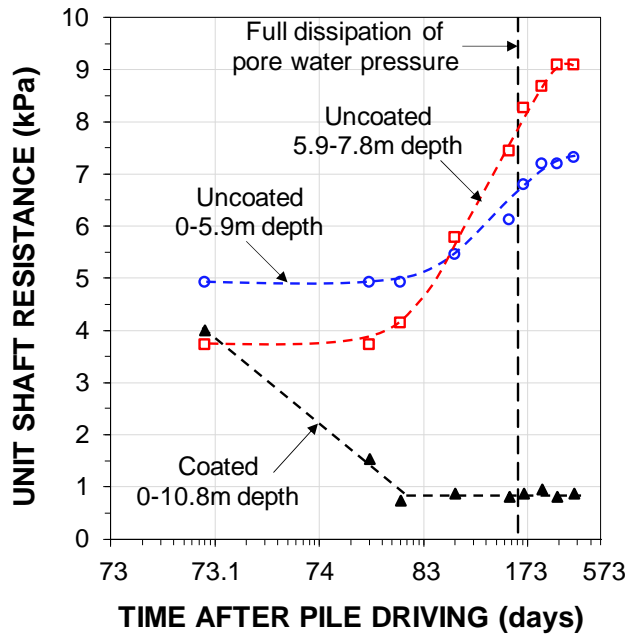


Figure 20. Development of negative skin friction along the uncoated STP1 (at two determined soil layers above transition zone) and the bitumen coated STP2 (entire bitumen coated section of the pile).

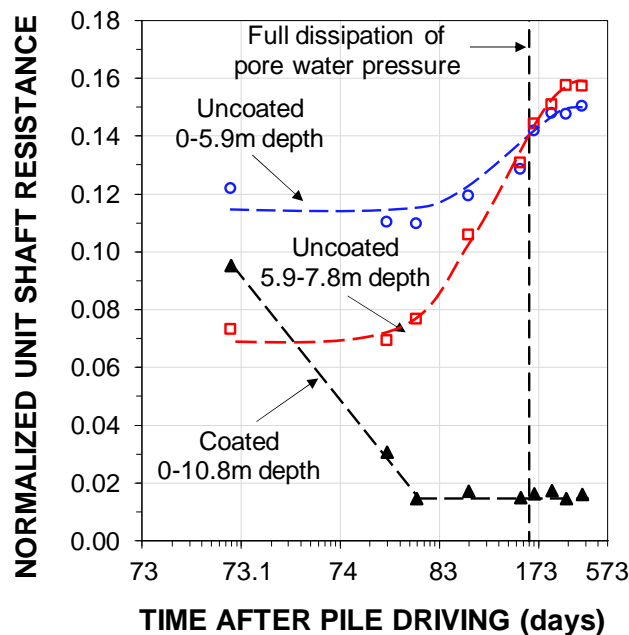


Figure 21. Development of the beta-coefficient (unit shaft resistance normalized by vertical effective stress) along the uncoated STP1 (at two determined soil layers above transition zone) and the bitumen coated STP2 (entire bitumen coated section of the pile).

against shearing rate. It can be seen that the decreasing shearing rate reduces the gradual increase of the unit shaft resistance. This finding supports other research which found the development of negative unit shaft resistance to be close related to the shearing rate (Walker and Darvall 1973).

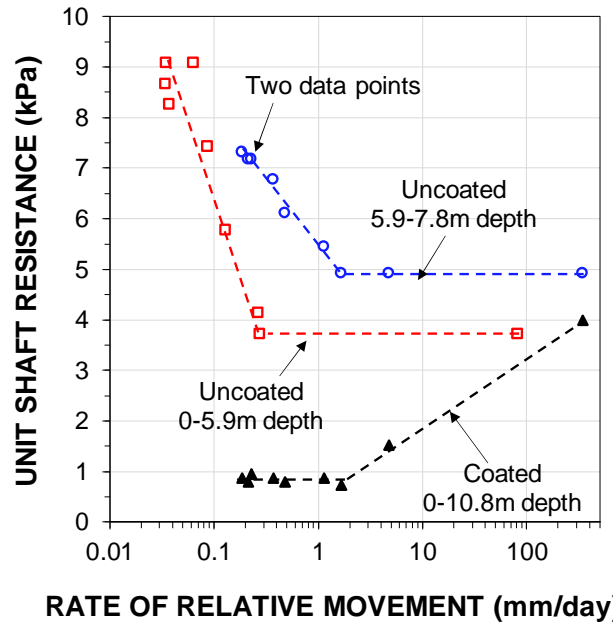


Figure 22. Development of negative skin friction along the uncoated (STP1) and bitumen coated (STP2) pile versus rate of relative movement.

Figure 23 presents the results from the laboratory direct shear tests on an undisturbed soft soil sample collected at the objective test site. The soft soil sample was sheared under three different normal stresses (20, 40 and 60 kPa) at different shearing rates during shearing. It can be seen from the data, that reduction of the shearing rate reduces the shear stress. It can thus be suggested that the aging effect (soil shear strength increase due to void ratio reduction) will be balanced with time by the positive shearing rate effect. The obtained positive shearing rate effect (i.e. soil shear strength decrease with decreasing rate) in soft silt is in agreement with (McCabe 2002, Lehane et al. 2003, Doherty and Gavin 2009).

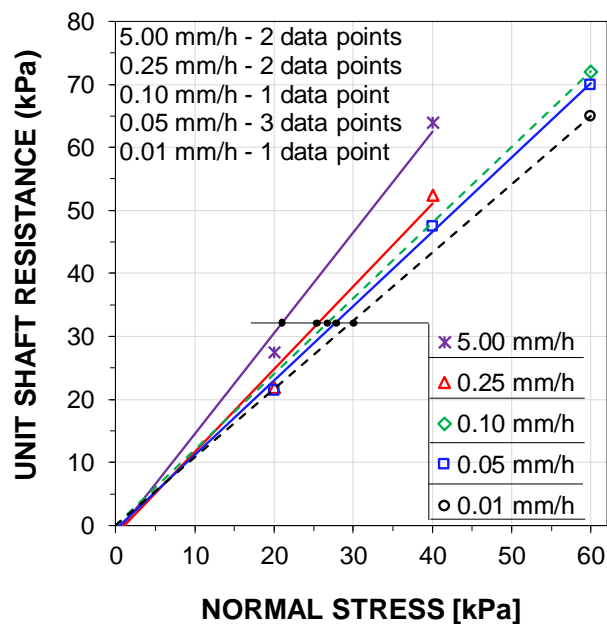


Figure 23. Direct shear test results on an undisturbed soft soil sample with different shearing rates.

The observed decrease in unit shaft resistance along the bitumen coated pile due to reduction of the shearing rate was also confirmed in the laboratory direct shear tests. Figure 24 presents the shear stress curves from the laboratory direct shear test on an undisturbed soft soil sample sheared against a bitumen coated concrete block. As shown in Figure 24, the shear stress was independent of the normal stress during slow shearing (drained conditions) reaching low shear stress values (1-10 kPa) and varied during fast shearing (undrained conditions) reaching much higher values (75-85 kPa). The pore water pressure was not measured during the test.

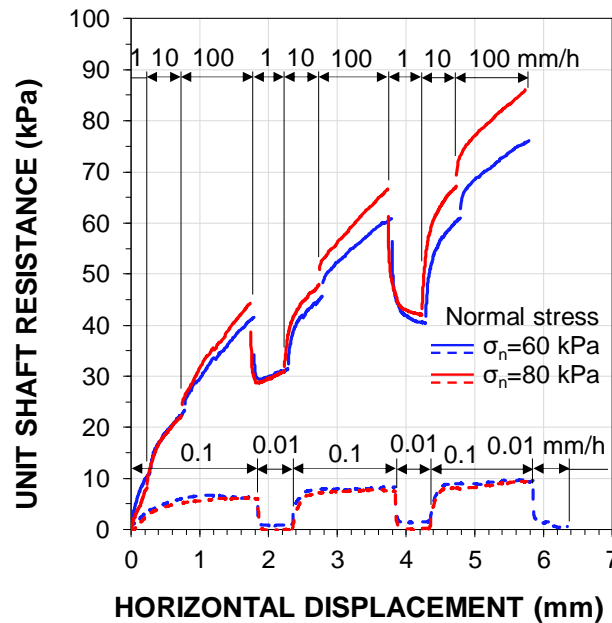


Figure 24. Unit shaft resistance curves from laboratory tests on soft soil samples at $\sigma_n = 60$ kPa and $\sigma_n = 80$ kPa against bitumen coated concrete block.

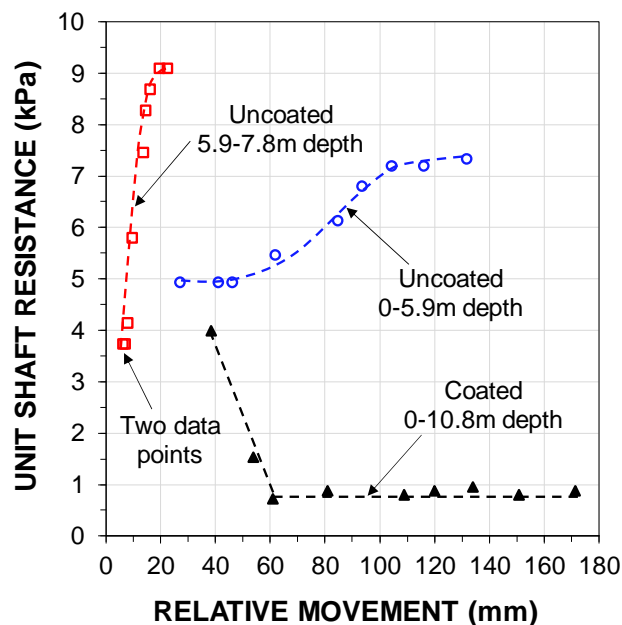


Figure 25. Development of negative skin friction along the uncoated (STP1) and bitumen coated (STP2) pile relative movement at determined soil layers.

Figure 25 shows the development of negative unit shaft resistance along determined layers on uncoated and bitumen coated pile versus relative movement. As can be seen from the data, that the maximum mobilized unit shaft resistances at different depths along the uncoated and bitumen coated pile occurred at different relative movement. It is therefore likely, that the development of unit shaft resistance is independent of the magnitude of the relative movement between the soil and pile. However, it is important to note, that the relative movement between soil and pile is required to initiate the development of unit shaft resistance.

4.3 Comparison between the uncoated steel and precast concrete pile

Figure 26 shows the development of the average beta-coefficient and the excess pore water pressure dissipation with time. It can be seen from the data, that the increase of the beta-coefficient along the uncoated precast concrete and steel pile is similar. Considering the beta-coefficient along the uncoated precast concrete pile as a reference (material surface factor of 1.0), the material surface factor for steel can be calculated as 0.7. The calculated material surface factor for steel is consistent with those proposed by Kulhawy (Kulhawy 1983). Based on this ratio, the long-term increase of the beta-coefficient was extrapolated and drawn in Figure 26 (red dashed line). The maximum obtained beta-coefficient for the uncoated steel and uncoated precast concrete pile was 0.13 and 0.19, respectively.

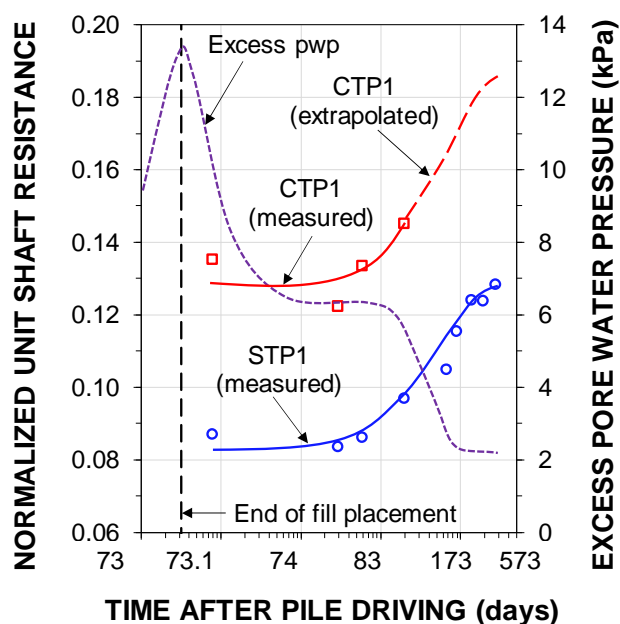


Figure 26. Comparison of the development of the negative skin friction normalized by the vertical effective stress along the uncoated precast concrete pile (CTP1) and the uncoated steel pile (STP1). The secondary scale is showing the excess pore water pressure dissipation with time.

5 CONCLUSIONS

The following conclusions can be drawn based on this case study:

- a) The relative movement between a pile and soil is needed to initiate the development of unit shaft resistances along driven piles in a subsiding soil.
- b) The unit shaft resistance increases due to an increase in effective stress and further reduction of void ratio after dissipation of excess pore water pressure (aging effect).
- c) The beta-coefficient along the uncoated steel and precast concrete pile was 0.13 and 0.19, respectively.
- d) With time, the decreasing rate of relative movement between the uncoated test piles and the soil reduce the increase of the unit shaft resistance.
- e) The magnitude of the unit shaft resistance along the bitumen coated driven piles is related to the rate of relative movement between the pile and the soil.
- f) The bitumen coating significantly reduced the maximum long-term drag force (about 73 % reduction on the steel piles). However, the bitumen coating has no effect on the drag force distribution during fast shearing (undrained conditions).
- g) Based on limited measurements prior to full mobilisation of the negative unit shaft resistances, the obtained material surface factor for steel was 0.7 (considering the negative unit shaft resistance along the precast concrete pile as a reference i.e. 1.0).

6 ACKNOWLEDGMENTS

The authors would like to thank cp test a/s, Per Aarsleff A/S, Centrum Pæle A/S, DMT Gründungstechnik, GmbH and Innovation Fund Denmark for providing funding for this study and Per Aarsleff A/S for installing the instrumented test piles and ground monitoring equipment.

7 REFERENCES

- Baligh, M.M., Figi, H., and Vivatrat, V., 1978. Downdrag on bitumen-coated piles. *Journal of the Geotechnical Engineering Division*, 104(GT11), 1355-1370.
- Bjerrum, L., Johannessen, I., and Eide, O., 1969. Reduction of negative skin friction on steel piles to rock. *Proc. 7th ICSMFE, Mexico, August 25-29, Vol. 2, pp. 27-33.*
- Bjerrum L., 1972. Embankments on soft ground. *Proc. of the ASCE Specialty Conference on Performance of Earth and Earth-supported Structures. Purdue University, Lafayette, June 11-14, 1972, Vol. II, pp. 1-54.*
- Bozozuk, M. and Labrecque, A., 1969. Downdrag measurements on 270-ft composite piles. *Proc. of Symposium of Deep Foundations, STP 444, Edited by R. Lundgren and E. D'Appolonia, ASTM 71st Annual Meeting, San Francisco June 23 28, pp. 15 - 40.*
- Briaud, J.-L. and Tucker, L., 1997. Design and construction guidelines for downdrag on uncoated and bitumen-coated piles. *NCHRP Report 393. Transportation Research Board. Washington, DC, 126p.*
- Burland, J.B., 1973. Shaft friction of piles in clay—A simple fundamental approach. *Ground Engineering, Foundation Publications Ltd. London 6(3) 30-42.*

- Doherty, P. and Gavin, K., 2009. Experimental investigation of the effect of shearing rate on the capacity of piles in soft silt. Proc. from the International Foundation Congress and Equipment Expo, Orland, Florida, United States, March 15-19, pp. 575-582.
- Endo, M., Minou, A., Kawasaki, I., and Shibata, T., 1969. Negative skin friction acting on steel pipe pile in clay. Proc. 7th ICSMFE, Mexico, August 25-29, Vol. 2, pp. 85 - 92.
- Fellenius, B.H. and Broms, B.B., 1969. Negative skin friction for long piles driven in clay. Proc. 7th ICSMFE, Mexico, August 25-29, Vol. 2, pp. 93-97
- Fellenius, B.H., 1971. Negative skin friction on long piles in clay. Results from a full scale investigation and General views and design recommendations. Swedish Geotechnical Institute, Proceedings No. 25, 38 p. (Also in Royal Swedish Academy of Engineering Sciences, Commission on Pile Research, Bulletin No. 18).
- Fellenius, B.H., 1975. Reduction of negative skin friction with bitumen slip layers. Discussion. ASCE Journal of Geotechnical Engineering Division, 101(GT4) 412 - 414.
- Fellenius, B.H., 1979. Downdrag on bitumen coated piles. American Society of Civil Engineers, ASCE Journal of Geotechnical Engineering, 105(GT10) 1262-1265.
- Fellenius, B.H., 1984. Negative skin friction and settlement of piles. Proceedings of the Second International Seminar, Pile Foundations, Nanyang Technological Institute, Singapore, November 28 - 30, 12p.
- Fellenius, B.H., 2006. Results from long-term measurement in piles of drag load and downdrag. Canadian Geotechnical Journal, 43(4) 409-430.
- Fellenius, B.H., 2020. Basics of foundation design—a textbook. Electronic Edition, www.Fellenius.net, 524p.
- Fukuya, T., Todoroki, T., and Kasuga, M., 1982. Reduction of negative skin friction with steel tube NF pile. Proc. of the Seventh Southeast Asian Geotechnical Conference, Hong Kong, November 22-26, pp. 333-347.
- Goudreault, P.A. and Fellenius, B.H., 2011. UniSettle Version 4 tutorial with background and analysis examples. UniSoft Geotechnical Solutions Ltd. [www.UniSoftGS.com], 85 p.
- Holtz, R.D. and Broms, B.B., 1972. Embankments on soft ground. Proc. of the ASCE Specialty Conference on Performance of Earth and Earth-supported Structures. Purdue University, Lafayette, June 11-14, Vol. I, pp. 435-464.
- Hutchinson, J.N. and Jensen, E., 1968. Loading tests on piles driven into estuarine clays at the Port of Khorramshahr, Iran, and observations on the effect of bitumen coatings on shaft bearing capacity. Norwegian Geotechnical Institute Publ. 78, 12p.
- Indraratna, B., Balasubramaniam, A., Phamvan, P., and Wong, Y., 1992. Development of negative skin friction on driven piles in soft Bangkok clay. Canadian Geotechnical Journal, 29(3), 393-404.
- Johannesen, I.J. and Bjerrum, L., 1965. Measurement of compression of a steel pile to Rock due to settlement of the surrounding clay. Proc. 6th ICSMFE, Montreal, September 8-15, Vol. 2, pp. 261-264.
- Kania, J.G., Sørensen, K.K., and Fellenius, B.H., 2020. Application of distributed fibre optic cables in piles. Geotechnical Engineering Journal of the SEAGS and AGSSEA, March 2020, 51(1), 9 p.
- Kechavarzi, C., Soga, K.B., Battista, N.D., Pelecanos, L., Elshafie, M.Z.E.B., Mair, R.J., 2016. Distributed fibre optic strain sensing for monitoring civil infrastructure - a practical guide, ICE Publishing, London, UK, 264p.

- Kulhawy, F.H., 1983. Transmission line structure foundation for uplift-compression loading. Report EL-2870, Electric Power Research Institute.
- Lehane, B.M., Jardine, R.J., and McCabe, B.A., 2003. Pile group tension cyclic loading: field test programme at Kinnegar, Northern Ireland. Health and Safety Research Report RR101.
- Luna, 2014. Distributed Fiber Optic Sensing: Temperature Compensation of Strain Measurement. Luna Inc.
- McCabe, B.A., 2002. Experimental investigations of driven pile group behaviour in Belfast soft clay. PhD thesis. Trinity College Dublin.
- Osterberg, J.O., 1957. Influence values for vertical stresses in semi-infinite mass due to embankment loading. Proc. 4th ICSMFE, London, August 12-24, Vol. 1, pp. 393-394.
- Ovesen, N.K., Fuglsang, L.D., Bagge, G., Krogsbøll, A., Sørensen, C.S., Hansen, J.B., Bødker, K., Thøgersen, L., Galsgaard, J., and Augustesen, A.H., 2012. Lærebog i Geoteknik, Polyteknisk Boghandel og Forlag (in Danish).
- Savery, A.L., 2019. Gyttja deposits from Randers and Esbjerg – an investigation of composition and geotechnical properties. Department of Geoscience, Aarhus University, 46p.
- Sørensen, K.K., 2015. Fuldskala pæleforsøg på Randers havn/Full-scale pile testing at Randers Harbour, presentation.
- Tomlinson, M., 1957. The adhesion of piles driven in clay soils. Proc. 4th ICSMFE, London, August 12-24, Vol. 2, pp. 66-71.
- Walker, L.K., and Darvall, P.L.P., 1973. Dragdown on coated and uncoated piles. Proc. 8th ICSMFE, Moscow, August 12-19 1973, USSR National Society for SMFE, Vol. 2, Paper 3/41, pp. 257-262.

CHAPTER 7

CONCLUSIONS

This dissertation summarises the industrial PhD project titled “Soil-pile interaction in soft soils” in collaboration between cp test a/s and Aarhus University. The overall objective of the project was to extend the current knowledge of the complex soil-pile interaction in soft, subsiding soils. To achieve this, a program consisting primarily of full-scale field tests and supplementary laboratory tests was conducted. A total number of thirteen driven piles (six steel and seven precast concrete) and one cased continuous flight auger pile were instrumented with distributed fibre optic strain and temperature sensors and vibrating wire strain gauges and installed at construction or test sites around Denmark. Additionally, ground monitoring systems consisting mainly of settlement gauges and vibrating wire piezometers were installed at most of the test sites to monitor the soil behaviour before and after the pile installation and after placement of the fill. The supplementary laboratory tests gave greater knowledge about the soil-pile interaction and the controlling factors.

The following conclusions can be drawn from the present study:

A relative movement between a pile and a soil is needed to initiate the soil-pile interaction and the development of the shaft resistance. Soil settlement develops negative skin friction in the upper part of a pile and positive shaft resistance in the lower part and mobilises a toe resistance. A smooth transition between negative and positive direction of shear occurs along a transition zone. Within the transition zone, at a depth called the neutral plane, a force equilibrium exists between the drag force and the sum of positive shaft resistance and the mobilised toe resistance and a settlement equilibrium between the pile and the soil.

A residual force was present in all driven test piles. The existence and magnitude of strain induced by the pile installation process must be recognized and implemented in the analysis of the shaft and toe resistance of the pile.

Lateral soil movements caused shear forces in piles. The presence of the shear forces generates tensile strain at the location of shear planes and affects the axial strain distribution.

The research has shown that the long-term (drained) beta-coefficient for a soft, organic, clayey silt (regarded as gyttja) for the uncoated steel and precast concrete driven pile was 0.13 and 0.19, respectively.

The results of the laboratory interface shearing tests indicated that the ratio of the interface angle of friction to gyttja angle of friction for concrete and steel was 1.0 and 0.8, respectively. These results were in agreement with the full-scale field measurements which provided the ratio for steel equal to 0.7 (assuming the ratio for concrete equal to 1.0).

The laboratory shearing tests on gyttja have also shown a positive rate effect with about 16 % increase in shear stress per log cycle.

The results of this study indicate that the bitumen coating can significantly reduce the drag force. Based on the full-scale test measurements, the drag force along the bitumen coated steel pile was reduced by 73 %.

Both laboratory interface shearing tests and full-scale field tests have shown that the development of shear forces along bitumen coated piles significantly depends on the shearing rate. The shear force increases with increasing shearing rate. The findings from these studies suggest that bitumen coating has limited effect on reducing the shear force during fast shearing (undrained conditions); e.g. driving of the piles or placing of the fill.

The evidence from this study suggests that both bored and driven piles (steel and precast concrete piles) can be successfully instrumented with distributed fibre optic sensing cables. The field strain measurement showed good agreement between the data obtained from VW gauges and DFOS sensors.

Due to the high spatial resolution of the Rayleigh-based analyser (a few millimetres) used in this study, it was possible to obtain a good shear force measurement along the test piles, which would be difficult using Brillouin-based analysers. Furthermore, it was also possible to detect cracks in concrete and local changes in pile stiffness. Unfortunately, the concrete cracks, present on the side surfaces of the piles, made the strain data interpretation difficult.

It is very important to thermally correct the strain data obtained from DFOS cables despite the pile material it is attached/embedded to. It can be assumed that the cable will undergo the thermal expansion of the pile material. However, a refractive index of a fibre (inside the DFOS cable) depends on temperature changes.

The loose-tube, gel-filled, temperature DFOS cables used in this study were not suitable for driven piles. The full-scale test results have shown that these cables were sensitive to mechanical strain.

CHAPTER 8

FURTHER WORK

This PhD thesis has provided a significant insight to the strain distribution along driven piles caused by installation process and soil movement (lateral and vertical). Yet, further work should be conducted.

A theoretical analysis should be carried out simulating the soil-pile interaction in soft, subsiding soils with the emphasis on the transition zone, where negative skin friction changes into positive shaft resistance.

Additional tests performed on the already installed piles are recommended. Static lateral loading tests conducted on the piles driven at the test site in Esbjerg (see Chapter 5) preceded by an installation of inclinometers can support the use of DFOS systems in e.g. retaining walls. Static loading tests conducted on the test piles installed at the test site in Randers (see Chapter 6) could support the theory that negative skin friction (or residual force) is only prestressing the pile, which means that a transient load equal to the drag force can be successfully supported by the pile without significant settlement (Bozozuk 1981, Tan and Fellenius 2016). Additionally, it could provide evidence that the results from a static loading test on an instrumented pile subjected to negative skin friction (or residual force) overestimate the shaft resistance and underestimate the toe resistance.

It would be interesting to assess the interaction between different soil types e.g. loose sand or soft clay and driven or bored piles. Such research could be conducted under more controlled conditions in the laboratory as model scale testing to bridge the gaps in results obtained from full-scale field tests.

The existence of residual force in driven piles was confirmed in this study. However, further work needs to be done to establish to what extent bored piles are affected by residual force. According to the literature (Fellenius 2020) a bidirectional static loading test is independent of residual force.

As presented in Chapter 3, the Danish National Annex to Eurocode significantly limits the shaft and toe resistance of bored piles. Therefore, more instrumented pile loading tests are needed to provide documentation to allow modifying the now overly conservative rules in regard to bored piles.

Further investigation and experimentation into performance of temperature DFOS cables installed along driven piles is strongly recommended.

Moreover, studies on application of DFOS systems as pile monitoring instrumentation should be conducted. The temperature DFOS cables embedded in bored piles (and not affected by mechanical strain) could serve as an alternative to the Thermal Integrity Profiler (Becker et al. 2015). The benefit of using the DFOS system as the thermal integrity profiler is higher spatial resolution. Another application of DFOS systems could be to monitor the integrity of a precast concrete driven pile after driving (Camp and Hussein 1991, Profound 2018). As stated in Chapter 1, fibre optic cables are sensitive to micro- and macrobends. An attenuation along the fibre optic cable embedded in a precast concrete pile could be measured using a standard optical time domain reflectometer and indicate the location of a damage. The same fibre optic cable can be used later to provide strain data. Finally, a production of DFOS instrumented driven concrete piles could be of potential interest to the industry knowing that one system can supplement the benefits of several existing pile monitoring systems.

COMPLETE LIST OF REFERENCES

- Aamann-Svale, R., and Møller, O., 2017. Midtbyens Gymnasium, Viborg. Statisk prøvebelastning. Aarsleff, Viby J, 23 p.
- Alberdi-Pagola, M., 2018. Design and performance of energy pile foundations. PhD thesis. Aalborg University, 354 p.
- Alm, T., and Hamre, L., 2002. Soil model for pile driveability predictions based on CPT interpretations. Proceedings of The International Conference on Soil Mechanics and Geotechnical Engineering 2, 1297-1302, AA Balkema Publishers.
- Baligh, M.M., Figi, H., and Vivatrat, V., 1978. Downdrag on bitumen-coated piles. Journal of the Geotechnical Engineering Division, 104(GT11), 1355-1370.
- Becker, M.L., Coleman, T.L., and Belardo, D.S., 2015. Thermal integrity profiling of ACIP piles. Proc. of the International Foundation Congress and Equipment Expo, San Antonio, Texas, March 17-21, pp. 723-737.
- Bersan, S., Bergamo, O., Palmieri, L., Schenato, L., and Simonini, P., 2018. Distributed strain measurements in a CFA pile using high spatial resolution fibre optic sensors. Engineering Structures, 160, pp. 554-565.
- Bjerrum, L., Johannessen, I., and Eide, O., 1969. Reduction of negative skin friction on steel piles to rock. Proc. 7th ICSMFE, Mexico, August 25-29, Vol. 2, pp. 27-33.
- Bjerrum L., 1972. Embankments on soft ground. Proc. of the ASCE Specialty Conference on Performance of Earth and Earth-supported Structures. Purdue University, Lafayette, June 11-14, 1972, Vol. II, pp. 1-54.
- Bozozuk, M. and Labrecque, A., 1969. Downdrag measurements on 270-ft composite piles. Proc. of Symposium of Deep Foundations, STP 444, Edited by R. Lundgren and E. D'Appolonia, ASTM 71st Annual Meeting, San Francisco June 23 28, pp. 15 - 40.
- Bozozuk, M., 1972. Downdrag measurements on a 160-ft floating pipe test pile in marine clay. Canadian Geotechnical Journal 9(2) 127-136
- Bozozuk, M., 1981. Bearing capacity of pile preloaded by downdrag. Proc. of 10th International Conference on Soil Mechanics and Foundation Engineering, Stockholm, June 15-19, pp. 631 – 636.
-

-
- Briaud, J.-L. and Tucker, L. 1984. Piles in sand: a method including residual stresses. *Journal of Geotechnical Engineering* 110, 1666-168.
- Briaud, J.-L. and Tucker, L., 1997. Design and construction guidelines for downdrag on uncoated and bitumen-coated piles. NCHRP Report 393. Transportation Research Board. Washington, DC, 126p.
- Burland, J.B., 1973. Shaft friction of piles in clay—A simple fundamental approach. *Ground Engineering*, Foundation Publications Ltd. London 6(3) 30-42.
- Camp, W. and Hussein, M., 1991. Pile integrity testing to determine storm-induced damage. *Transportation Research Record* 1331, pp. 45-49.
- Clemente, F.M., 1981. Downdrag on bitumen coated piles in a warm climate. Proc. of 10th International Conference on Soil Mechanics and Foundation Engineering, Stockholm, June 15-19, pp. 673 – 676.
- Culshaw, B. and Kersey, A., 2008. Fiber-optic sensing: A historical perspective. *Journal of lightwave technology*, 26(9), pp. 1064-1078.
- Davisson, M. 1970. Lateral load capacity of piles. Proceedings: 49th Annual Meeting of the Highway Research Board, 104-112, Washington District of Columbia, United States.
- Doherty, P. and Gavin, K., 2009. Experimental investigation of the effect of shearing rate on the capacity of piles in soft silt. Proc. from the International Foundation Congress and Equipment Expo, Orland, Florida, United States, March 15-19, pp. 575-582.
- DS/EN 1997-1 DK NA, 2015. National Annex to Eurocode 7: Geotechnical design - Part 1: General rules. 36 p.
- Dunnicliff, J., 1993. Geotechnical instrumentation for monitoring field performance. John Wiley & Sons, 578 p.
- Endo, M., Minou, A., Kawasaki, I., and Shibata, T., 1969. Negative skin friction acting on steel pipe pile in clay. Proc. 7th ICSMFE, Mexico, August 25-29, Vol. 2, pp. 85 - 92.
- Eslami, A., 1996. Bearing capacity of piles from cone penetrometer test data. Ph. D. Thesis, University of Ottawa, Department of Civil Engineering, 516 p.
- Fearon, R.E, Chandler, R.J., and Bommer, J.J., 2004. An investigation of the mechanisms which control soil behaviour at fast rates of displacement. *Advances in geotechnical engineering: The Skempton conference*, Institution of Civil Engineers, London, UK, pp. 441-452.
-

-
- Fellenius, B.H. and Broms, B.B., 1969. Negative skin friction for long piles driven in clay. Proc. 7th ICSMFE, Mexico, August 25-29, Vol. 2, pp. 93-97.
- Fellenius, B.H. and Haagen, T., 1969. A new pile-force gage for accurate measurements of pile behavior. Canadian Geotechnical Journal 6(3) 356-362.
- Fellenius, B.H., 1970. Undersökning av skjuvkrafter i lera under långsam deformation. National Swedish Council for Building Research, Report on Research Grant C230, 19 p. (In Swedish).
- Fellenius, B.H., 1971. Negative skin friction on long piles in clay. Results from a full scale investigation and General views and design recommendations. Swedish Geotechnical Institute, Proceedings No. 25, 38 p. (Also in Royal Swedish Academy of Engineering Sciences, Commission on Pile Research, Bulletin No. 18).
- Fellenius, B.H., 1972. Downdrag on piles in clay due to negative skin friction. Canadian Geotechnical Journal, 9(4), 323-337.
- Fellenius, B.H., 1975. Reduction of negative skin friction with bitumen slip layers. Discussion. ASCE Journal of Geotechnical Engineering Division, 101(GT4) 412 - 414.
- Fellenius, B.H., 1979. Downdrag on bitumen coated piles. American Society of Civil Engineers, ASCE Journal of Geotechnical Engineering, 105(GT10) 1262-1265.
- Fellenius, B.H., 1984. Negative skin friction and settlement of piles. Proceedings of the Second International Seminar, Pile Foundations, Nanyang Technological Institute, Singapore, November 28 - 30, 12p.
- Fellenius, B.H., 1989. Tangent modulus of piles determined from strain data". 1989 Foundation Congress by F.H. Kulhawy, ASCE, 1, 500-510.
- Fellenius, B. H., 2002. Determining the true distributions of load in instrumented piles. Deep Foundations 2002: An International Perspective on Theory, Design, Construction, and Performance, pp. 1455-1470.
- Fellenius, B.H., 2006. Results from long-term measurement in piles of drag load and downdrag. Canadian Geotechnical Journal, 43(4) 409-430.
- Fellenius, B.H., Kim, S.R., and Chung, S.G., 2009. Long-term monitoring of strain in instrumented piles. ASCE Journal of Geotechnical and Geoenvironmental Engineering, 135(11), pp. 1583-1595.
-

- Fellenius, B.H., 2013. Capacity and load-movement of a CFA pile: A prediction event. GeoInstitute Geo Congress San Diego, March 3-6, 2013, Honoring Fred H. Kulhawy—Foundation Engineering in the Face of Uncertainty, ASCE, Reston, VA, James L. Withiam, Kwok-Kwang Phoon, and Mohamad H. Hussein, eds., Geotechnical Special Publication, GSP 229, pp. 707-719.
- Fellenius, B. H., 2015. Static tests on instrumented piles affected by residual load. DFI Journal - The Journal of the Deep Foundations Institute, 9(1), pp. 11-20.
- Fellenius, B.H., 2019. Basics of foundation design—a textbook. Electronic Edition, www.Fellenius.net, 484 p.
- Fellenius, B.H. and Nguyen, B.N., 2019. Common mistakes in static loading-test procedures and result analyses. Geotechnical Engineering Journal of the SEAGS & AGSSEA, 50(3), 20-31.
- Fellenius, B.H., 2020. Basics of foundation design—a textbook. Electronic Edition, www.Fellenius.net, 524 p.
- Fukuya, T., Todoroki, T., and Kasuga, M., 1982. Reduction of negative skin friction with steel tube NF pile. Proc. of the Seventh Southeast Asian Geotechnical Conference, Hong Kong, November 22-26, pp. 333-347.
- GEO, 2016. Viborg Banegårds Alle. Gymnasie i 6 etager uden kælder. Geoteknisk og miljøteknisk undersøgelse. Geo, Brabrand, 115 p.
- GEO, 2016. Esbjerg Strand, Laboratorieforsøg, 14 p.
- Goudreault, P.A. and Fellenius, B.H., 2011. UniSettle Version 4 tutorial with background and analysis examples. UniSoft Geotechnical Solutions Ltd. [www.UniSoftGS.com], 85 p.
- Goudreault, P.A. and Fellenius, B.H., 2014. UniPile Version 5, User and Examples Manual. UniSoft Geotechnical Solutions Ltd., [www.UniSoftGS.com], 120 p.
- Gwizdała, K., 1996. The analysis of pile settlement employing load-transfer functions (in Polish). Zeszyty Naukowe Politechniki Gdańskiej, Nr 532, Budownictwo Wodne, nr 41, Gdańsk, 192 p.
- Head, K.H. and Epps, R.J., 2011. Manual of Soil Laboratory Testing, Volume 2: Permeability, Shear Strength, and Compressibility Tests. Dunbeath, UK: Whittles Publishing.
- Holtz, R.D. and Broms, B.B., 1972. Embankments on soft ground. Proc. of the ASCE Specialty Conference on Performance of Earth and Earth-supported Structures. Purdue University, Lafayette, June 11-14, Vol. I, pp. 435-464.
-

-
- Hutchinson, J.N. and Jensen, E., 1968. Loading tests on piles driven into estuarine clays at the Port of Khorramshahr, Iran, and observations on the effect of bitumen coatings on shaft bearing capacity. Norwegian Geotechnical Institute Publ. 78, 12p.
- Inaudi, D. and Glisic, B., 2010. Long-range pipeline monitoring by distributed fiber optic sensing. *Journal of Pressure Vessel Technology*, 132, 011701.
- Indraratna, B., Balusubramanimam, A.S., Phamvan P., and Wong, Y. K., 1992. Development of negative skin friction on driven piles in soft Bangkok clay. *Canadian Geotechnical Journal*, 29(3), 393-404.
- Johannesen, I.J. and Bjerrum, L., 1965. Measurement of compression of a steel pile to Rock due to settlement of the surrounding clay. Proc. 6th ICSMFE, Montreal, September 8-15, Vol. 2, pp. 261-264.
- JyskGeoteknik. 2017. Geoteknisk Datarapporter, 57 p.
- Kania, J.G. and Sørensen, K.K., 2018. A static pile load test on a bored pile instrumented with distributed fibre optic sensors. 10th International Symposium on Field Measurements in Geomechanics. Rio de Janeiro.
- Kania, J.G. and Sørensen, K.K., 2019. A case study of soil-pile interaction in soft soils. XVII European Conference on Soil Mechanics and Geotechnical Engineering, Reykjavik, Iceland.
- Kania, J.G., Sørensen, K.K., and Fellenius, B.H., 2020. Application of distributed fibre optic cables in piles. *Geotechnical Engineering Journal of the SEAGS and AGSSEA*, March 2020, 51(1), 9 p.
- Kechavarzi, C., Soga, K.B., Battista, N.D., Pelecanos, L., Elshafie, M.Z.E.B., Mair, R.J., 2016. Distributed fibre optic strain sensing for monitoring civil infrastructure - a practical guide, ICE Publishing, London, UK, 264p.
- Kechavarzi, C., Pelecanos, L., and Soga, K., 2019. Distributed fibre optic sensing for monitoring reinforced concrete piles. *Geotechnical Engineering Journal of the SEAGS & AGSSEA*, 50(1).
- Kersey, A.D., Davis, M.A., Patrick, H.J., Leblanc, M., Koo, K., Asking, C., Putnam, M., and Friebele, E.J., 1997. Fiber grating sensors. *Journal of lightwave technology*, 15, pp. 1442-1463.
- Khare, M.G. and Gandhi, S.R., 2009. Skin resistance of bitumen-coated piles in sand. *Proceedings of the Institution of Civil Engineers-Geotechnical Engineering*, 162(6), pp. 303-310.
-

-
- Kim, S. R., Chung, S. G., Fellenius, B. H. 2011. Distribution of residual load and true shaft resistance for a driven instrumented test pile. *Canadian Geotechnical Journal* 48, 583-598.
- Klar, A., Bennett, P.J., Soga, K., Mair, R.J., Tester, P., Fernie, R., St John, H.D., and Torp-Peterson, G., 2006. Distributed strain measurement for pile foundations. *Proceedings of the Institution of Civil Engineers-Geotechnical Engineering*, 159, pp. 135-144.
- Knudsen, J., Sørensen, K.K., Steenfelt, T.J.S., and Trankjær, H., 2019. Design of bored piles in Denmark—a historical perspective. XVII European Conference on Soil Mechanics and Geotechnical Engineering, Reykjavik, Iceland.
- Kreger, S.T., Gifford, D.K., Froggatt, M.E., Soller, B.J., and Wolfe, M.S., 2006. High resolution distributed strain or temperature measurements in single-and multi-mode fiber using swept-wavelength interferometry. *Optical Fiber Sensors*. Optical Society of America, ThE42.
- Kulhawy, F.H., 1983. Transmission line structure foundation for uplift-compression loading. Report EL-2870, Electric Power Research. Institute.
- Lehane, B.M. and Jardine, R.J., 1992. Residual strength characteristics of Bothkennar clay. *Geotechnique*, 42(2), pp. 363-367.
- Lehane, B.M., Jardine, R.J., and McCabe, B.A., 2003. Pile group tension cyclic loading: field test programme at Kinnegar, Northern Ireland. Health and Safety Research Report RR101.
- Luna Inc., 2014. Distributed Fiber Optic Sensing: Temperature Compensation of Strain Measurement. Engineering note EN-FY1402, Roanoke, Virginia, United States, 7 p.
- Luna Inc., 2017. ODiSI B. Data sheet, 2 p.
- Lunne, T., Robertson, P., Powell, J. 1997. Cone penetration testing in geotechnical practice. Spon Press, Abingdon, 312 p.
- Martinez, A. and Stutz, H.H., 2019. Rate effect on the interface shear behaviour of normally and overconsolidated clay. *Geotechnique* 69(9), pp. 801-815.
- Mascarucci, Y., Mandolini, A. and Miliziano, S., 2013. Effects of residual stresses on shaft friction of bored cast in situ piles in sand. *Journal of Geo-Engineering Sciences*, 1(1), pp. 37-51.
- McCabe, B.A., 2002. Experimental investigations of driven pile group behaviour in Belfast soft clay. PhD thesis. Trinity College Dublin, 413 p.
-

-
- Mohamad, H., Bennett, P., Soga, K., Mair, R., and Bowers, K., 2010. Behaviour of an old masonry tunnel due to tunnelling-induced ground settlement. *Géotechnique*, 60(12), pp. 927-938.
- Mohamad, H., Soga, K., Pellew, A., and Bennett, P.J., 2011. Performance monitoring of a secant-piled wall using distributed fiber optic strain sensing. *ASCE Journal of Geotechnical and Geoenvironmental Engineering*, 137(12), pp. 1236-1243.
- Mohamad, H., Tee, B.P., Chong, M.F., and Ang, K.A., 2017. Investigation of shaft friction mechanisms of bored piles through distributed optical fibre strain sensing. 19th International Conference on Soil Mechanics and Geotechnical Engineering 2017, Seoul, pp. 2829-2832.
- Monsberger, C., Woschitz, H. and Hayden, M., 2016. Deformation measurement of a driven pile using distributed fibreoptic sensing. *Journal of Applied Geodesy*, 10(1), pp. 61-69.
- Nöther, N., Wosniok, A., Krebber, K., and Thiele, E., 2008. A distributed fiber optic sensor system for dike monitoring using Brillouin optical frequency domain analysis. *Smart Sensor Phenomena, Technology, Networks, and Systems 2008*. International Society for Optics and Photonics, 6933, pp. 69330T.
- Osterberg, J.O., 1957. Influence values for vertical stresses in semi-infinite mass due to embankment loading. *Proc. 4th ICSMFE, London, August 12-24, Vol. 1*, pp. 393 - 394.
- Ovesen, N.K., Fuglsang, L.D., Bagge, G., Krogsbøll, A., Sørensen, C.S., Hansen, J.B., Bødker, K., Thøgersen, L., Galsgaard, J., and Augustesen, A.H., 2012. *Lærebog i Geoteknik*, Polyteknisk Boghandel og Forlag (in Danish).
- Palmieri, L., Schenato, L. 2013. Distributed optical fiber sensing based on Rayleigh scattering. *The Open Optics Journal* 7, 104-127.
- Pelecanos, L., Soga, K., Elshafie, M.Z., De Battista, N., Kechavarzi, C., Gue, C.Y., Ouyang, Y., and Seo, H.J., 2018. Distributed fiber optic sensing of axially loaded bored piles. *ASCE Journal of Geotechnical and Geoenvironmental Engineering*, 144(3), pp. 04017122.
- Potyondy, J.G., 1961. Skin friction between various soils and construction materials. *Geotechnique* 11(4) 339-353.
- Poulos, H.G., 1973. Analysis of piles in soil undergoing lateral movement. *ASCE Journal of Soil Mechanics & Foundations Division*, 99(5), 391-406.
- Poulos, H. G., 1987. Analysis of residual stress effects in piles. *Journal of Geotechnical Engineering* 113, 216-229.
-

- Profound, 2018. SIT-series. Pile integrity testing. Data sheet, 2 p.
- Ravet, F., Niklès, M., and Rochat, E., 2017. A decade of pipeline geotechnical monitoring using distributed fiber optic monitoring technology. ASME 2017 International Pipeline Geotechnical Conference 2017. American Society of Mechanical Engineers.
- Savery, A.L., 2019. Gyttja deposits from Randers and Esbjerg – an investigation of composition and geotechnical properties. Department of Geoscience, Aarhus University, 46p.
- Siegel, T. C. and McGillivray, A., 2009. Interpreted residual load in an augered cast-in-place pile. Annual DFI Conference, Kansas City, 10 p.
- Soga, K., Kwan, V., Pelecanos, L., Rui, Y., Schwamb, T., Seo, H., and Wilcock, M., 2015. The role of distributed sensing in understanding the engineering performance of geotechnical structures. XVI European Conference on Soil Mechanics and Structures.
- Sørensen, K.K., 2015. Fuldskala pæleforsøg på Randers havn/Full-scale pile testing at Randers Harbour, presentation.
- Springman, S. and Bolton, M., 1990. The effect of surcharge loading adjacent to piles, Transport and Road Research Laboratory (TRRL), Wokingham, Berkshire, United Kingdom, 82 p.
- Tan, S.A. and Fellenius, B.H., 2016. Negative skin friction pile concepts with soil-structure interaction. ICE Geotechnical Research Journal, UK. Paper 16.00006. pp 1-11.
- Terzaghi, K., Peck, R.B, and Mesri, G., 1996. Soil mechanics in engineering practice. John Wiley & Sons, 592 p.
- Tika, T.E., Vaughan, P.R., and Lemos, L.J.L.J., 1996. Fast shearing of pre-existing shear zones in soil. Geotechnique 46(2), pp. 197-233.
- Tomlinson, M. and Woodward, J., 2008. Pile design and construction practice. Abingdon: Taylor & Francis.
- Tomlinson, M., 1957. The adhesion of piles driven in clay soils. Proc. 4th ICSMFE, London, August 12-24, Vol. 2, pp. 66-71.
- Van Essen Instruments, 2018. TD-Diver™ & Baro-Diver®. Product manual, 29 p.
- Walker, L.K., and Darvall, P.L.P., 1973. Dragdown on coated and uncoated piles. Proc. 8th ICSMFE, Moscow, August 12-19 1973, USSR National Society for SMFE, Vol. 2, Paper 3/41, pp. 257-262.
-

Zhang, H. and Wu, Z., 2008. Performance evaluation of BOTDR-based distributed fiber optic sensors for crack monitoring. *Structural Health Monitoring*, 7(2), pp. 143-156.